

LATTICE DISCRETISATION OF THE GREEN-SCHWARZ SUPERSTRING AND AdS/CFT

Masterarbeit

zur Erlangung des akademischen Grades
Master of Science (M. Sc.)
im Fach Physik



Humboldt-Universität zu Berlin
Mathematisch-Naturwissenschaftliche Fakultät I
Institut für Physik

eingereicht von: *Philipp Töpfer*
geboren am: *30.07.1990, Apolda*

Betreuung: *Dr. Valentina Forini*
Dr. Björn Leder

eingereicht am: *20. Dezember 2016*

Abstract

This thesis discusses the discretisation of an AdS -light-cone gauge-fixed action for the Type IIB GREEN-SCHWARZ superstring. We measure the masses of two bosonic excitations transverse to the classical null-cusp solution of the AdS LAGRANGIAN and investigate the cusp anomalous dimension of $\mathcal{N} = 4$ SYM from a string theory perspective via the AdS/CFT duality. For both observables we find a good agreement in the perturbative regime of the sigma-model at large 't HOOFT coupling. For smaller couplings we observe a quadratic divergence that we treat by non-perturbative subtraction. After taking the continuum limit we find a qualitative agreement with the predictions coming from the integrability of the model. We tamed a sign problem induced by the presence of a complex phase in the fermionic determinant by introducing an alternative fermionic linearisation. For small couplings we then face the problem of treating operators with small eigenvalues and potential sign flips, not effectively treatable via reweighting. All systematic effects are tried to be assessed and kept under control.

Zusammenfassung

Diese Arbeit beschreibt die Diskretisierung der Wirkung des Type IIB GREEN-SCHWARZ Superstrings unter AdS -Lichtkegelgleichfixierung. Es werden die Massen zweier bosonischer Anregungen transversal zur klassischen Lösung lichtartiger Spitzen (null-cusp) des AdS -LAGRANGIANS bestimmt. Das Hauptaugenmerk liegt bei der Ermittlung der anomalen Dimension lichtartiger Spitzen in $\mathcal{N} = 4$ SYM mittels einer stringtheoretischen Betrachtung unter Ausnutzung der AdS/CFT Korrespondenz. Für beide Observablen findet sich eine gute Übereinstimmung mit dem perturbativen Bereich bei starker 't HOOFT-Kopplung. Für kleinere Kopplungen treten quadratische Divergenzen auf, die einer nicht-perturbativen Subtraktion unterzogen werden. Nach der Kontinuumsextrapolation zeigt sich eine qualitative Übereinstimmung der Ergebnisse mit den Vorhersagen, welche aus der Integrabilität des zugrundeliegenden Modells gewonnen wurden. Es konnte erfolgreich in Vorzeichenproblem mittels einer alternativen Linearisierung der Fermionen eingedämmt werden. Für kleine Kopplungen werden jedoch Operatoren mit kleinen Eigenwerten und potentiellen Vorzeichenwechseln zum Problem, welche sich nicht effizient mit der Methode des „reweighting“ behandeln lassen. Es wird versucht alle systematischen Effekte abzuschätzen und zu kontrollieren.

Contents

Abstract	iii
1 Introduction	7
2 Basics on superstring theory	11
2.1 The bosonic string	11
2.2 Superstring theory	13
2.3 Strings in curved backgrounds	15
3 Preliminaries	17
3.1 AdS/CFT correspondence	17
3.2 Wilson loops	18
3.3 Wilson loops in AdS/CFT	19
3.4 The cusp anomalous dimension of $\mathcal{N} = 4$ SYM	21
3.5 The GS superstring action in AdS light-cone gauge	22
3.6 Symmetries of the fluctuation action	25
3.7 Perturbative 1-loop free energy	26
4 Lattice basics	29
4.1 Discretising the worldsheet	29
4.2 Bosons and fermions on the lattice	31
4.2.1 Bosonic propagator	31
4.2.2 Fermionic propagator and the doubling problem	32
4.3 Monte Carlo methods	34
4.3.1 Monte Carlo integration	35
4.3.2 Importance sampling and Markov chains	36
4.3.3 Fermions on the lattice and the HMC algorithm	38
4.3.4 The numerical sign problem	41
5 Towards the lattice simulation	43
5.1 Linearisation of fermionic contributions	43
5.1.1 Naive approach and sign problem	43
5.1.2 Alternative field redefinition	44
5.1.3 Matrix properties	46
5.1.4 Pseudofermionic weight function	47
5.2 Discretising the action	48
5.2.1 Bosonic action	48

5.2.2	Wilson term	49
5.2.3	Fermionic operator	51
5.3	Applying the RHMC algorithm	52
6	Simulations and observables	55
6.1	Implementation and the continuum limit	55
6.2	Simulation parameters	56
6.3	Observables	59
6.3.1	The $\langle xx^* \rangle$ correlator	60
6.3.2	The cusp action	62
7	Results	69
7.1	Mass of the x field	69
7.2	Cusp anomaly	69
7.3	Systematic errors and the Pfaffian sign	72
8	Conclusion and outlook	79
	Appendices	81
A	Grassmann numbers	83
A.1	Grassmann algebra	83
A.2	Grassmann analysis	84
A.3	Hubbard-Stratonovich transformation	86
B	$\text{AdS}_5 \times \text{S}^5$ spacetime	89
B.1	AdS_5 space	89
B.2	Poincaré patch	90
C	$\text{SO}(6)$ matrices	93
D	Discrete Fourier transform	95
E	Discretised fermion matrix	97
F	Simulation parameters	101
	Bibliography	105

1

Introduction

Towards our understanding of the underlying principles of nature, humanity has come a long way, covering the realm of subatomic particles up to the astronomic scale of stars and galaxies and even the universe as a whole. It has been a constant path of discovering and unifying knowledge to see a bigger picture. This path has led us to EINSTEIN'S theory of general relativity (GR), using the idea to manifest gravity via the curvature of the combined framework of space and time, known as spacetime. Many predictions of this theory proved to be correct, like the recent detection of gravitational waves by the LIGO and virgo collaborations [1, 2]. On the other hand there is quantum field theory (QFT) that emerged from a field theoretic generalisation of relativistic quantum mechanics and was elaborated via quantum electrodynamics (QED) and quantum chromodynamics (QCD) to the standard model (SM) which is the state of the art theory of elementary particle physics that has been completed by the recent discovery of the HIGGS boson [3, 4]. Nonetheless it was not possible to unify the three fundamental forces condensed in the standard model with the fourth elementary force - gravity. The current mathematical treatment of QFT requires renormalisation as a tool to extract finite physical observables. But this requirement also restricts a theory in its universality. Unfortunately GR is not renormalisable and therefore not ad hoc compatible to QFT.

A possible cure to this peculiarity might come from string theory which emerged from the study of hadrons and REGGE trajectories [5]. Further discoveries of superstring states with spin two, indicating the presence of gravitons and therefore gravity, made string theory a promising candidate for a unified theory. But string theory requires additional dimensions and a high energy scale for a phenomenological investigation which are both requirements that the abilities of modern detectors and accelerators still fail to realise. Therefore one is left to study string theory mainly in a theoretical framework which has made major progress in the last decades. One of the most remarkable discoveries is certainly the conjecture of the anti-DE SITTER / conformal field theory (*AdS/CFT*) correspondence made by MALDACENA [6]. It relates a maximally supersymmetric version of a non-ABELIAN gauge theory like QCD to a string theory and states their mathematical equivalence. This statement is remarkable in the sense that it relates a theory of quantum gravity to a gauge theory on a flat space that was thought to have no gravitational relation at all.

The aim of this thesis is to contribute to a deeper understanding of the *AdS/CFT* correspondence in a numerical study on the fundamental case where the conjecture relates $\mathcal{N} = 4$ *SU(N)* super YANG-MILLS (SYM) theory in four dimensions

to a Type IIB superstring theory on an $AdS_5 \times S^5$ background, supported by a RAMOND-RAMOND five-form flux.

As a non-ABELIAN gauge theory it is natural to approach $\mathcal{N} = 4$ SYM with the same numerical techniques known from lattice QCD, where an interesting program has been carried out by CATTERALL et. al. [7, 8]. Alternatively, one could discretise the worldsheet spanned by the GREEN-SCHWARZ string embedded in $AdS_5 \times S^5$. This route has been first explored in [9] where the observable of major concern - the cusp anomaly of $\mathcal{N} = 4$ SYM - has been investigated with lattice methods from a string theory point of view. The thesis at hand is mainly based on a proceeding of this lattice approach to the GREEN-SCHWARZ string proposed in [10, 11].

In $\mathcal{N} = 4$ SYM the renormalised vacuum expectation value (vev) of a WILSON loop along a light-like cusp is governed by the cusp anomaly (or “scaling function”) $f(g)$, a function of the coupling $g = \sqrt{\lambda}/4\pi$, where λ is the 't HOOFT coupling of the AdS/CFT dual gauge theory. The MALDACENA conjecture states an exact equivalence of the vev of any WILSON loop with the path integral of an open string ending on the boundary of AdS_5 , where the 4d gauge theory lives [12]. In the case of a cusped contour $\mathcal{C}_{\text{cusp}}$ for the WILSON loop we find

$$\langle \mathcal{W}[\mathcal{C}_{\text{cusp}}] \rangle \equiv Z_{\text{cusp}} = \int \mathcal{D}\delta X \mathcal{D}\delta \Psi e^{-S_{\text{cusp}}[X_{\text{cl}} + \delta X, \delta \Psi]} = e^{-\frac{1}{8}f(g)V_2}, \quad (1.0.1)$$

where S_{cusp} is the fluctuation action around a vacuum with the classical solution X_{cl} , describing a string worldsheet of an open string that ends on a null cusp [13]. The fields $X(s, t)$, $\Psi(s, t)$ are the bosonic and fermionic string coordinates, depending on the spatial and temporal worldsheet coordinates s and t , respectively. The factor $V_2 = \int ds dt$ is the worldsheet volume of the string. Approximations of the scaling function $f(g)$ can be obtained from the perturbative limits of either gauge theory [14] ($g \ll 1$) or string theory via sigma-model loop expansion [13, 15, 16] ($g \gg 1$). With help of a thermodynamic BETHE Ansatz it is also possible to derive an integral equation [17] that determines $f(g)$ exactly for any value of the coupling.

In lattice field theory it is common to investigate vevs of certain observables of interest. To study the scaling function in a lattice approach we need to find an observable vev that is related to $f(g)$. Such an observable is given by the “cusp” action

$$\langle S_{\text{cusp}} \rangle = \frac{\int \mathcal{D}\delta X \mathcal{D}\delta \Psi S_{\text{cusp}} e^{-S_{\text{cusp}}}}{\int \mathcal{D}\delta X \mathcal{D}\delta \Psi e^{-S_{\text{cusp}}}} = -g \frac{d \ln Z_{\text{cusp}}}{dg} \equiv g \frac{V_2}{2} f'(g), \quad (1.0.2)$$

where we are supposed to obtain information on the derivative of the scaling function.

This approach to a numerical treatment of the GREEN-SCHWARZ string might seem a bit restricted in its abilities at a first glance, due to the limitation to a certain gauge fixed vacuum. But this attempt is only a first step towards a new area of lattice field theory that might open a wide range of possibilities. The

model at hand is despite a highly non-trivial but two-dimensional one that only involves scalar fields which makes it computationally cheaper and more economical in the consumption of memory. In general, one merit of the analysis initiated in [9] and that is readdressed in [10, 11] and here is to explore another route via which lattice simulations could become a potentially efficient tool in numerical holography.

The thesis proceeds in the following way.

Chapter 2 gives a brief introduction of superstring theory and the non-linear sigma-model on curved backgrounds.

In chapter 3 we present the basic concepts of the *AdS/CFT* correspondence and other theoretical preliminaries to motivate the equivalence stated in (1.0.1). The chapter finishes with the derivation of the “cusp” fluctuation action motivated from [18, 19, 13].

Chapter 4 forges a bridge between the continuum model and its discretised version by providing the essential tools on discretising fields and operators and addresses a suitable algorithm to perform simulations.

In chapter 5 we use the methods from chapter 4 to construct a lattice version of the action derived in chapter 3. We study the properties of the resulting fermion matrix and present the full rational hybrid Monte Carlo algorithm that is used for the simulation.

Chapter 6 gives some technical details and lists of simulation parameters. We also present the observables of interest and how to conduct a continuum extrapolation from the observations on the lattice.

Chapter 7 illustrates the simulation results and the thesis finishes with a conclusion and an outlook on further research possibilities in chapter 8.

Details on several topics can be found in the appendices. We encourage the reader to consult them in parallel while reading the reading the main text.

2

Basics on superstring theory

In this chapter we want to give a brief introduction to the basic concepts of string theory, starting from its simplest possible form, the bosonic string, and further develop the subject to a supersymmetric version including fermions. Since we will work in the framework of the *AdS/CFT* correspondence (see chapter 3), we are mostly interested in strings propagating in *AdS* backgrounds. The following sections are mainly based on [20, 21, 22, 23].

2.1 The bosonic string

The basic idea of string theory is that the fundamental objects described by the model are one-dimensional strings, propagating through spacetime and sweeping out a $(1+1)$ -dimensional surface $\tilde{\Sigma}$ called the string worldsheet. The string can be parameterised by two coordinates, the proper time τ and the spatial extent σ of the string which we will also denote by $(\sigma^0, \sigma^1) = (\tau, \sigma)$. We can then apply a homeomorphism φ that maps the 2d sheet Σ into the target space, e.g. D -dimensional MINKOWSKI space¹ $\mathbb{R}^{D-1,1}$ with embedding coordinates $X^M(\tau, \sigma)$

$$\begin{aligned} \varphi : \quad \Sigma = (\tau_{\text{in}}, \tau_{\text{fin}}) \times (0, \sigma_0) &\longrightarrow \tilde{\Sigma} \\ (\tau, \sigma) &\longrightarrow X^M(\tau, \sigma). \end{aligned} \quad (2.1.1)$$

The simplest possible action of the string, the NAMBU-GOTO action, is proportional to the area of the surface $\tilde{\Sigma}$ and is given by

$$S_{\text{NG}} = -\frac{1}{2\pi\alpha'} \int_{\Sigma} d^2\sigma \sqrt{-\gamma}, \quad (2.1.2)$$

where γ is the GRAMIAN determinant of the embedding

$$\gamma = \det(\gamma_{\alpha\beta}), \quad \gamma_{\alpha\beta} = \partial_{\alpha} X^M \partial_{\beta} X^N \eta_{MN}, \quad \partial_{\alpha} \equiv \frac{\partial}{\partial \sigma^{\alpha}}, \quad \alpha = 0, 1, \quad (2.1.3)$$

and the induced metric $\gamma_{\alpha\beta}$ is the pull-back of η_{MN} . The parameter in front of the integral is the string tension, making the action dimensionless, with the REGGE slope α' being related to the string length l_s by $\alpha' = l_s^2$. We also defined $d^2\sigma = d\sigma^0 d\sigma^1$. Due to the square root this action is not very suitable for a path

¹We will use the metric $\eta_{MN} = \text{diag}(-, +, +, \dots, +)$ with $M, N = 0, 1, 2, \dots, D-1$.

integral quantisation. To get rid of the square root one can introduce an auxiliary metric² $h_{\alpha\beta}(\sigma)$ with $h_{\alpha\beta}h^{\beta\rho} = \delta_{\alpha}^{\rho}$ and define the POLYAKOV action

$$S_P = -\frac{1}{4\pi\alpha'} \int_{\Sigma} d^2\sigma \sqrt{-h} h^{\alpha\beta} \gamma_{\alpha\beta}. \quad (2.1.4)$$

This action is equivalent to the NAMBU-GOTO action at the classical level, as can be proved by deriving the equations of motion for $h_{\alpha\beta}$, $\delta S/\delta h^{\alpha\beta} = 0$. Defining the corresponding energy-momentum tensor $T_{\alpha\beta}$, such equations are the statement that $T_{\alpha\beta}$ has to vanish

$$T_{\alpha\beta} \equiv -4\pi\alpha' \frac{1}{\sqrt{-h}} \frac{\delta S}{\delta h^{\alpha\beta}} = \gamma_{\alpha\beta} - \frac{1}{2} h_{\alpha\beta} h^{\rho\sigma} \gamma_{\rho\sigma} = 0. \quad (2.1.5)$$

From this follows

$$\sqrt{-\gamma} = \frac{1}{2} \sqrt{-h} h^{\rho\sigma} \gamma_{\rho\sigma}, \quad (2.1.6)$$

and thus the classical equivalence of the actions S_{NG} and S_P . The symmetries of S_P are

- *Global D-dimensional Poincaré invariance*

$$X^M \rightarrow \widetilde{X}^M = \Lambda_N^M X^N + a^M, \quad \delta h_{\alpha\beta} = 0, \quad (2.1.7)$$

with Λ_N^M and a^M being D -dimensional LORENTZ transformations and space-time translations.

- *Reparametrisation (or diffeomorphism) invariance of the worldsheet*

We can choose a reparametrisation of the worldsheet coordinates $\sigma^\alpha \rightarrow \tilde{\sigma}^\alpha(\sigma)$, where the fields X^M and the 2d metric transform according

$$\begin{aligned} X^M(\sigma) &\rightarrow \widetilde{X}^M(\tilde{\sigma}) = X^M(\sigma), \\ h_{\alpha\beta}(\sigma) &\rightarrow \tilde{h}_{\alpha\beta}(\tilde{\sigma}) = \frac{\partial \sigma^\alpha}{\partial \tilde{\sigma}^\gamma} \frac{\partial \sigma^\beta}{\partial \tilde{\sigma}^\delta} h_{\gamma\delta}(\sigma). \end{aligned} \quad (2.1.8)$$

This is a gauge symmetry on the worldsheet.

- *Weyl invariance*

The action is invariant under the rescaling

$$\widetilde{X}^M(\sigma) = X^M(\sigma), \quad \tilde{h}_{\alpha\beta}(\sigma) = \Omega^2(\sigma) h_{\alpha\beta}(\sigma). \quad (2.1.9)$$

We also have to employ suitable boundary conditions. There are in fact two types of strings with different boundary conditions:

²With the dependence of σ we hereby actually mean a short form for $\sigma = (\sigma^0, \sigma^1)$ and by no means a single dependence on the string length only.

- *Open strings*

In this case we can set $\sigma_0 = \pi$ and thus $\sigma \in (0, \pi)$. These type of strings satisfy either NEUMANN boundary conditions

$$\partial_\sigma X^M(\tau, \sigma) \Big|_{\sigma=0, \pi} = 0 \quad (2.1.10)$$

or DIRICHLET boundary conditions

$$\delta X^M(\tau, \sigma) \Big|_{\sigma=0, \pi} = 0. \quad (2.1.11)$$

- *Closed strings*

Here we usually set $\sigma_0 = 2\pi$, leading to $\sigma \in [0, 2\pi)$. This type of string satisfies periodic boundary conditions

$$\begin{aligned} X^M(\tau, 0) &= X^M(\tau, 2\pi), & \partial_\sigma X^M(\tau, \sigma) \Big|_{\sigma=0} &= \partial_\sigma X^M(\tau, \sigma) \Big|_{\sigma=2\pi}, \\ h_{\alpha\beta}(\tau, 0) &= h_{\alpha\beta}(\tau, 2\pi). \end{aligned} \quad (2.1.12)$$

One can then exploit the symmetries of the POLYAKOV action to give the string equations of motion a rather simple form. For instance, one can use the local symmetries to choose a convenient gauge in which the worldsheet metric is conformally flat

$$h_{\alpha\beta} = \Omega^2(\sigma) \eta_{\alpha\beta}, \quad \text{with} \quad \eta_{\alpha\beta} = \text{diag}(-, +). \quad (2.1.13)$$

In this conformal gauge the POLYAKOV action takes the form

$$S_P = \frac{1}{4\pi\alpha'} \int d^2\sigma \left(\partial_\tau X^M \partial_\tau X^N - \partial_\sigma X^M \partial_\sigma X^N \right) \eta_{MN} \quad (2.1.14)$$

which is leading to the simple equations of motion

$$\left(\partial_\tau^2 - \partial_\sigma^2 \right) X^M = 0. \quad (2.1.15)$$

Their solutions are well known and can be derived by decomposition into FOURIER modes. If one analyses the mass spectrum of the free string, there will appear states of negative mass square

$$\alpha' M^2 = -1. \quad (2.1.16)$$

Such states are called tachyons. They are not very well understood and give rise to instabilities in the theory that need to be removed.

2.2 Superstring theory

The theory considered so far describes only bosons and also gives rise to unphysical tachyon states. To make predictions on the real world which also contains non-bosonic particles like quarks and leptons, we require string theory to include fermions as well. It turns out that for the presence of fermions, string theory requires supersymmetry, a symmetry that introduces a fermionic superpartner to every bosonic field. The resulting theories are then called superstring theories. Among others there are two basic approaches to incorporate supersymmetry into string theory [23] which are both equivalent

- The *Ramond-Neveu-Schwarz formalism* is supersymmetric on the worldsheet.
- The *Green-Schwarz (GS) formalism* is supersymmetric in the target space.

Depending on how one applies supersymmetry there arise different possibilities on what kinds of strings the model will describe. With regard to the *AdS/CFT* correspondence (see chapter 3) we want to focus on Type IIB superstring theory which requires $D = 10$ spacetime dimensions. Type II strings have both left and right moving fermions and the resulting spacetime theory has $\mathcal{N} = 2$ supersymmetry, whereas B refers to the property of additional background gauge fields. In the following we choose the GS formalism to apply supersymmetry in the target space.

Usually we map the worldsheet into spacetime, but for a supersymmetric generalisation in the GS formalism we consider mapping the worldsheet into superspace, where the basic target space fields are

$$X^M(\tau, \sigma) \quad \text{and} \quad \Theta^{Aa}(\tau, \sigma). \quad (2.2.1)$$

Here Θ^{Aa} are MAJORANA-WEYL (MW) spinors. The index A is running from 1 to the number of supersymmetries \mathcal{N} which is $\mathcal{N} = 2$ for the Type II string theories, whereas a labels the components of the spacetime spinor in D dimensions with $a = 1, \dots, 2^{D/2}$ if D is even. So in the ten-dimensional case of Type IIB string theory we have two anti-commuting spinors

$$\Theta^{1a}, \Theta^{2a} \quad \text{with} \quad a = 1, \dots, 32. \quad (2.2.2)$$

Due to the MW property there are only 16 independent real components for each spinor. To write a POLYAKOV-like supersymmetric action in MINKOWSKI space one can start by

$$S_1 = -\frac{1}{4\pi\alpha'} \int d^2\sigma \sqrt{-h} h^{\alpha\beta} \Pi_\alpha^M \Pi_\beta^N \eta_{MN}, \quad (2.2.3)$$

with the superfields

$$\Pi_\alpha^M \equiv \partial_\alpha X^M - \bar{\Theta}^A \Gamma^M_\alpha \partial_\alpha \Theta^A \quad (2.2.4)$$

and Γ^M are 10d DIRAC matrices and $\bar{\Theta} = \Theta^\dagger \Gamma_0$. By studying this kind of action for a point particle one finds that certain peculiarities arise when the particle is massless [23]. To circumvent this a WESS-ZUMINO (WZ) term S_2 is added which gives rise to a new symmetry in the full action $S = S_1 + S_2$. This so called κ -symmetry is a symmetry of the spinor fields

$$\delta \bar{\Theta}^1 = \bar{\kappa}^1 P_-, \quad \delta \bar{\Theta}^2 = \bar{\kappa}^2 P_+, \quad (2.2.5)$$

where κ^1 and κ^2 are arbitrary MW spinors with appropriate chirality and P_\pm are projection operators. This symmetry acts like an internal gauge symmetry for the fermionic spinor fields. By fixing κ -symmetry half of the components of the fermionic variables decouple from the theory which means we are left with 8 independent real components for each spinor. A natural and convenient gauge choice is

$$\Gamma^+ \Theta^A = 0, \quad \text{where} \quad \Gamma^+ = \frac{1}{\sqrt{2}} (\Gamma^0 + \Gamma^9). \quad (2.2.6)$$

2.3 Strings in curved backgrounds

For now we have only considered strings propagating in flat MINKOWSKI target space. To give string theory a more general application, one also has to take other backgrounds into account. Therefore we promote the target space metric $\eta_{MN} \rightarrow g_{MN}(X)$, leading to the bosonic POLYAKOV action

$$S_P = -\frac{1}{4\pi\alpha'} \int_{\Sigma} d^2\sigma \sqrt{-h} h^{\alpha\beta} g_{MN}(X) \partial_{\alpha} X^M \partial_{\beta} X^N. \quad (2.3.1)$$

This is called the *bosonic non-linear string sigma model*. Hereby, the process of incorporating supersymmetry is not so straightforward anymore. Next to the flat 10d MINKOWSKI spacetime there is also another maximally supersymmetric solution as a background for the Type IIB case which is the product $AdS_5 \times S^5$ of a five-dimensional anti-DE SITTER space AdS_5 and a five-sphere S^5 . This solution is supported by a self-dual RAMOND-RAMOND five-form flux. This is due to the presence of D-branes which can be seen as DIRICHLET-like boundary conditions or a higher-dimensional generalisation of strings. In this context an open string with DIRICHLET boundary conditions can be interpreted as an open string, ending on a hypersurface, called D-brane. Some of these D-branes can carry a conserved charge that ensures their stability. For an open string, ending on such charged branes, the spectrum is tachyon-free. In the following we consider three dimensional D3-branes which are required to formulate the AdS/CFT correspondence. In the language of forms we can compute the electric and magnetic³ charges μ_e and μ_m , using GAUSS'S law for Dp -branes⁴ in a generalised formulation of MAXWELL'S equations

$$\mu_e = \int_{S^{D-p-2}} \star F_{p+2}, \quad \mu_m = \int_{S^{p+2}} F_{p+2}, \quad (2.3.2)$$

where F_{p+2} is the field strength defined by

$$F_n = \frac{1}{n!} F_{\mu_1 \dots \mu_n} dx^{\mu_1} \wedge \dots \wedge dx^{\mu_n}, \quad (2.3.3)$$

and $\star F_{p+2}$ is its HODGE dual. For our case with D3-branes with $p = 3$ we find $F_{p+2} = F_5$ and in $D = 10$ dimensions that $F_5 = \star F_5$ is self-dual. Therefore both charges are computed via the flux supported by a self-dual five form through the sphere S^5 . To construct an action one has to incorporate the field strength to the kinetic part of the action

$$S_1 = -\frac{1}{4\pi\alpha'} \int d^2\sigma \sqrt{-h} h^{\alpha\beta} G_{\alpha\beta}, \quad (2.3.4)$$

where $G_{\alpha\beta}$ needs to contain contracted terms of Π_{α}^{μ} in (2.2.4) that respects the appropriate background and also a field strength $\mathcal{F}_{\alpha\beta} = F_{\alpha\beta} + b_{\alpha\beta}$, where $F_{\alpha\beta}$

³Here we assume the existence of magnetic monopoles.

⁴ Dp -branes refer to D-branes of dimension p .

represents the five-form field strength manifested on the worldsheet and $b_{\alpha\beta}$ is a term that makes it supersymmetric. To achieve κ -symmetry one needs to add a WZ term which is the integral of a three-form Ω_3 over a three-space M_3 that has the worldsheet as its boundary

$$S_2 = \int_{M_3} \Omega_3. \tag{2.3.5}$$

Remarkably this problem has been solved by Metsaev and Tseytlin in [24], but we will not present the full procedure here due to its complexity and requirement of sophisticated analytical tools. We therefore refer the reader to the original publication. What we will have to deal with in the following is a special solution to a gauge fixed version of this $AdS_5 \times S^5$ GS string developed in [24]. But before we come to that, we need to study the AdS/CFT correspondence and derive a possible extraction of our observable of interest - the cusp anomaly of $\mathcal{N} = 4$ SYM.

3.1 AdS/CFT correspondence

Among the most exciting breakthroughs in theoretical physics in the last decades there certainly is the famous conjecture made by MALDACENA in 1997 [6], now widely known as *AdS/CFT* correspondence which attracted many scientists to contribute their work to this field of study.

What makes this conjecture so promising is that it relates a quantum field theory (QFT) of gauge fields in flat spacetime with a string theory. The latter one is also a promising candidate for a theory of quantum gravity. Unifying gravity with the other fundamental forces condensed in the Standard Model would be one of the next big milestones in physics. By studying the predictions of the *AdS/CFT* correspondence scientists hope to get one step closer to this fundamental aim. The conjecture links two theories, very different in their physical content and interpretation, stating that they are mathematically equivalent. The *AdS* part refers to a gravity theory on asymptotically anti-DE SITTER spacetime, *CFT* stands for conformal field theory. In its primary form [22], the correspondence states that

Type IIB superstring theory

with string length $l_s = \sqrt{\alpha'}$ and coupling constant g_s on $AdS_5 \times S^5$ with
radius of curvature R and N units of $F_{(5)}$ flux on S^5

\uparrow *is dynamically equivalent to* \downarrow

$\mathcal{N} = 4$ Super Yang-Mills theory

with gauge group $SU(N)$ and YANG-MILLS coupling constant g_{YM} .

The free parameters on the field theory side g_{YM} and N are mapped to the free parameters g_s and $R/\sqrt{\alpha'}$ on the string theory side by

$$\frac{4\pi\lambda}{N} = g_s \quad \text{and} \quad \lambda \equiv g_{YM}^2 N = \frac{R^4}{\alpha'^2}. \quad (3.1.1)$$

In the second equation we defined the 't HOOFT coupling λ . String theory is yet best understood in the perturbative regime, therefore it is convenient to

restrict the coupling on the string theory side to $g_s \ll 1$, while keeping $R/\sqrt{\alpha'}$ constant. The *AdS* side reduces then, at leading order in g_s to classical string theory. The quantity R^2/α' is kept constant. Also the coupling on the *CFT* side is conveniently taken to be small, $g_{\text{YM}} \ll 1$, while $g_{\text{YM}}^2 N$ is kept finite. We therefore have to take the large N limit $N \rightarrow \infty$ with λ fixed, which is also known as the 't HOOFT limit. This corresponds to the planar limit of the gauge theory. We are then left with λ as the free parameter of the *AdS/CFT* system. In the limit of large λ , and therefore $\alpha'/R^2 \rightarrow 0$ or large radius R , the string does not feel the effect of the interaction created by the (now weakly curved) background. So for large λ one is in the perturbative regime of string theory, whereas the gauge theory side is perturbatively accessible for $\lambda \ll 1$. The fact that the perturbative (accessible) regimes of both models do not overlap - which is referred to as a weak-strong coupling duality - is on one side very fascinating, as it allows the exploration of the strong coupling regime of a theory via the study of the much simpler dual model. On the other side, it makes highly non-trivial any dynamical and direct check of the *AdS/CFT* correspondence. In this thesis we address the problem of realising such direct checks numerically within the string worldsheet model. In the latter, we control the large λ regime where we know analytical solutions. The lattice, numerical approach allows us to leave the perturbative regime and go to smaller λ , where comparison with the solutions of perturbative gauge theory is - once the difficulties peculiar to this approach are tamed - possible. In fact, in the case under study we can also attempt a comparison between string and gauge theory at finite values of λ , where together with the *AdS/CFT* hypothesis another powerful conjecture - the integrability of the underlying system - is available with its predictions.

3.2 Wilson loops

An important class of observables in gauge theories are non-local gauge invariant operators called WILSON loops. These operators are evaluated along a given closed path \mathcal{C} . For specific cusped paths one can (in a certain limit) extract a function, called cusp anomaly, from the WILSON loop. According to *AdS/CFT* the minimal surface of a string ending on a certain path gives (in a certain regime) the value of the corresponding WILSON loop. We therefore can extract information about the cusp anomaly function also from the string theory side. To make this remark more explicit, we first want to review some more details about WILSON loops.

For pure YANG-MILLS theory with the gauge group $SU(N)$ the WILSON loop $W[\mathcal{C}]$ is a path-ordered exponential of a gauge field A_μ along a closed contour \mathcal{C} , which in the fundamental representation of the gauge field is defined by

$$W[\mathcal{C}] = \frac{1}{N} \text{Tr} \left(\mathcal{P} \exp \left[i \oint_{\mathcal{C}} dx^\mu A_\mu \right] \right). \quad (3.2.1)$$

Here the trace is over the fundamental representation of the gauge group and \mathcal{P} is the path ordering operator. If we choose to parametrise the curve \mathcal{C} as $x^\mu(s)$

with $s \in [0, 1]$, we can write the exponent as

$$i \oint_{\mathcal{C}} dx^\mu A_\mu = i \int_0^1 ds \frac{dx^\mu}{ds} A_\mu(x(s)) . \quad (3.2.2)$$

Actually we have $A_\mu = A_\mu^a T_a$, where T_a is a generator of the Lie algebra $\mathfrak{su}(N)$ of the gauge group and therefore different fields A_μ do not commute in general. To avoid appearing ambiguities in the ordering of fields due to a TAYLOR expansion of the exponential, the operator \mathcal{P} is ordering them in the following sense

$$\mathcal{P}(A(x(s_1)) A(x(s_2))) = \begin{cases} A(x(s_1)) A(x(s_2)) & \text{for } s_1 > s_2, \\ A(x(s_2)) A(x(s_1)) & \text{for } s_2 > s_1. \end{cases} \quad (3.2.3)$$

3.3 Wilson loops in AdS/CFT

Since the action of four-dimensional $\mathcal{N} = 4$ SYM can be derived via dimensional reduction from $\mathcal{N} = 1$ SYM in ten dimensions [25] one can construct a WILSON loop there, starting from its definition in the ten dimensional gauge theory. By using the field theory content of the four-dimensional theory A_μ and x^μ and six additional scalar fields of $SU(N)$ the so called MALDACENA-WILSON loop proposed in [12] can be written as

$$\mathcal{W}[\mathcal{C}] = \frac{1}{N} \text{Tr} \mathcal{P} \exp \left(\int_{\mathcal{C}} ds \left(i A_\mu(x) \dot{x}^\mu + |\dot{x}| \phi_I(x) n^I \right) \right) . \quad (3.3.1)$$

Here $I = 1, \dots, 6$ and n^I might be considered coordinates in S^5 , satisfying $\delta_{IK} n^I n^K = 1$. The curve described by $n^I(s)$ in S^5 must not necessarily be closed. In the context of *AdS/CFT* the MALDACENA-WILSON loop also has a corresponding string theory description, which was first proposed in [12]. Thus the expectation value of the MALDACENA-WILSON loop operator is dual to a string partition function

$$\langle \mathcal{W}[\mathcal{C}] \rangle = Z_{\text{string}}[\mathcal{C}], \quad (3.3.2)$$

which is a path integral obeying suitable boundary conditions

$$Z_{\text{string}}[\mathcal{C}] = \int_{\partial X^\mu = \mathcal{C}} \mathcal{D} X^M \mathcal{D} h_{\alpha\beta} \exp(-S_{\text{string}}(X, h)) . \quad (3.3.3)$$

Here S_{string} is the action of the fundamental string in $AdS_5 \times S^5$, $h_{\alpha\beta}$ a 2d metric and $X^M = (X^\mu, X^{3+I})$ ($M = 0, \dots, 9$; $\mu = 0, \dots, 3$; $I = 1, \dots, 6$) are the embedding functions in the string target space, depending on the worldsheet coordinates $(\tau, \sigma) \in \Sigma$ where Σ is representing a map of the string worldsheet. By defining $\widetilde{X}^I = X^{3+I}$ and therefore $X^M = (X^\mu, \widetilde{X}^I)$ the partition function (3.3.3) needs to meet the following boundary conditions

$$X^\mu|_{\partial\Sigma} = x^\mu(s), \quad \left. \frac{\widetilde{X}^I}{|\widetilde{X}^I|} \right|_{\partial\Sigma} = n^I(s), \quad |\widetilde{X}^I|_{\partial\Sigma} = 0, \quad (3.3.4)$$

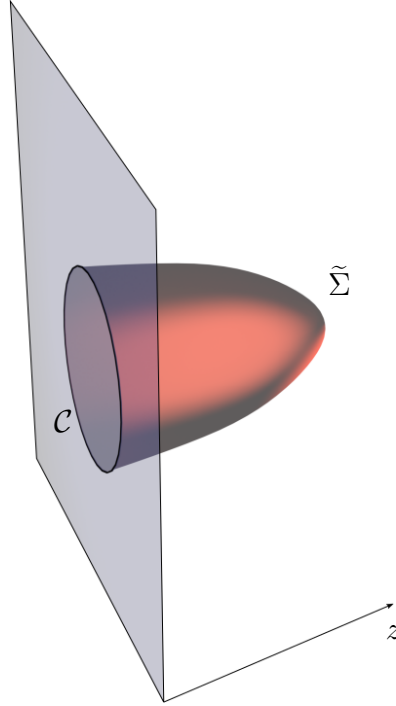


Figure 3.1 The embedding of the string worldsheet $\tilde{\Sigma}$ in $AdS_5 \times S^5$ is bounded by the contour \mathcal{C} as z approaches zero.

where $x^\mu(s)$ parametrises the curve \mathcal{C} . One can show that the conformal boundary of $AdS_5 \times S^5$ is 4d MINKOWSKI space¹. Therefore one can say that the embedding of the string worldsheet is bounded by the curve \mathcal{C} , see Figure 3.1. In the large 'T HOOFT coupling limit $\lambda \gg 1$, the path integral (3.3.3) can be evaluated with a saddle point approximation and results in the exponential of a minimal surface $\mathcal{A}_{\min}(\mathcal{C})$ bounded by \mathcal{C}

$$\langle \mathcal{W}[\mathcal{C}] \rangle \simeq \exp \left(\frac{\sqrt{\lambda}}{4\pi} \mathcal{A}_{\min}(\mathcal{C}) \right). \quad (3.3.5)$$

The dimensional scale $\sqrt{\lambda}/4\pi$ is set by the AdS/CFT mapping (3.1.1) which determines $1/\alpha' = \sqrt{\lambda}$ as it is common in the literature (e.g. [13]) to set the AdS radius to $R = 1$. From the pre factor of the action in the non-linear sigma model (2.3.1) we then find

$$\frac{1}{4\pi\alpha'} = \frac{\sqrt{\lambda}}{4\pi}. \quad (3.3.6)$$

In the following we will also make use of a new defined coupling $g \equiv \sqrt{\lambda}/4\pi$.

¹At the conformal boundary the five-sphere appears to have zero extent. See (B.1) for details on the conformal mapping of AdS_5 to flat 4d MINKOWSKI space.

3.4 The cusp anomalous dimension of $\mathcal{N} = 4$ SYM

To approach a numerical study of AdS/CFT it is important to consider an observable quantity that is widely known in different ranges of the 't HOOFT coupling λ , so its study may act as a guideline in discretising the theory. One such quantity is the cusp anomaly function (or scaling function). It was first studied as the anomalous dimension of twist two operators in $\mathcal{N} \geq 4$ SYM

$$\mathcal{O}_{\{\mu_1 \dots \mu_S\}} = \text{Tr } \phi \nabla_{\{\mu_1} \dots \nabla_{\mu_S\}} \phi, \quad (3.4.1)$$

where ϕ is a scalar field of SYM, ∇_μ is the covariant derivative with the indices $\{\mu_1 \dots \mu_S\}$ being symmetrised and the operator carries the spin S . The conformal dimension of such operators is $\Delta_S = S + 2 + \gamma_S(\lambda)$ with γ_S being the anomalous dimension and $\gamma_S \sim \ln S$ for $S \rightarrow \infty$. In [15] it was proposed that this conformal dimension corresponds to the energy of strings rotating in AdS , that for large S (and in the large λ regime) reads

$$E \simeq S + \frac{\sqrt{\lambda}}{\pi} \ln S, \quad (S \rightarrow \infty). \quad (3.4.2)$$

In [26], using previous knowledge in the context of QCD [27], it has been observed that $\gamma_S(\lambda)$ for large S is related to the anomalous dimension of cusped MALDACENA-WILSON loops. The expectation value of such a WILSON loop diverges if parts of it are light-like, thus it has to be regularised by introducing IR and UV cutoffs L and ϵ

$$\langle \mathcal{W}[\mathcal{C}_{\text{cusp}}] \rangle \sim e^{-\Gamma_{\text{cusp}}(\lambda, \gamma) \ln \frac{L}{\epsilon}} \xrightarrow{\gamma \rightarrow \infty} e^{-\frac{f(\lambda)|\gamma|}{2} \ln \frac{L}{\epsilon}}, \quad (3.4.3)$$

where γ is a boost angle in MINKOWSKI signature and $\Gamma_{\text{cusp}}(\gamma, \lambda)$ is the angle and coupling dependent cusp anomaly function. In the limit of large λ the function $f(\lambda)$ is obtained as the coefficient of the logarithmic divergence which in this context is also known as scaling function. It is related to the anomalous dimension of twist two operators via [26]

$$\gamma_S(\lambda) \simeq f(\lambda) \ln S, \quad (S \rightarrow \infty). \quad (3.4.4)$$

The correspondence (3.3.2) now tells us that it is possible to access the scaling function also via path integral calculations from the string theory side by considering fluctuations around a certain vacuum that acts as a minimal surface conformally bounded by a cusped contour $\mathcal{C}_{\text{cusp}}$. The remarks in [26, 28] suggest that the factor $|\gamma| \ln(L/\epsilon)$ in (3.4.3) corresponds to the regulated area of a cusped string worldsheet and is thus related to the world volume of the string $V_2 = \int d\tau d\sigma$, leading to

$$\langle \mathcal{W}[\mathcal{C}_{\text{cusp}}] \rangle = Z_{\text{string}}[\mathcal{C}_{\text{cusp}}] = e^{-\frac{f(\lambda)}{2} \frac{V_2}{4}}. \quad (3.4.5)$$

Semiclassical quantisation around such vacua allowed to compute the scaling function up to two loops in sigma-model perturbation theory (see e.g. [13])

$$f(g) = 4g - \frac{3 \ln 2}{\pi} - \frac{K}{4\pi^2 g} + \mathcal{O}(g^{-2}), \quad g \equiv \frac{\sqrt{\lambda}}{4\pi}, \quad (3.4.6)$$

where $K \approx 0.916$ is the CATALAN constant. As mentioned, the scaling function is also known relying on the assumption of the integrability of $\mathcal{N} \geq 4$ SYM (see e.g. [29]) where it can be derived from the BES^2 equation for any finite values of g . Our main aim is to reproduce the scaling function in numerical simulations for the string model with a path integral defined by (a suitable version of) (3.3.3).

3.5 The Green-Schwarz superstring action in AdS light-cone gauge

As mentioned in the previous section we can address the scaling function by considering fluctuations around suitable vacua with worldsheets bounded by a cusp. Therefore we chose to follow the approach presented in [13]. We hereby start from a GREEN-SCHWARZ type superstring in AdS light-cone gauge with fixed κ -symmetry, that was proposed in [19, 18]. This action contains terms quadratic and quartic in fermions and has a classical solution X_{cl} forming a null-cusp on the AdS boundary. Now one can consider fluctuations around this classical solution and use (3.3.2) and (3.3.3) to match the vacuum expectation value of a WILSON loop around a null-cusp which is related to the scaling function via (3.4.3)

$$\langle \mathcal{W}_{\text{cusp}} \rangle = Z_{\text{cusp}} = \int \mathcal{D}\delta X \mathcal{D}\delta \Psi e^{-S_{\text{cusp}}[X_{\text{cl}} + \delta X, \delta \Psi]} = e^{-\frac{f(\lambda)}{2} \frac{V_2}{4}}. \quad (3.5.1)$$

Hereby S_{cusp} refers to the action expanded around the null-cusp solution X_{cl} and $\Psi_{\text{cl}} = 0$, whereas Ψ is an abbreviated notation for the fermionic quantities and δX and $\delta \Psi$ are fluctuation fields. In the following we want to sketch shortly how to derive the action S_{cusp} . We will be using the $AdS_5 \times S^5$ metric in the POINCARÉ patch ($\mu = 0, \dots, 3$; $M = 1, \dots, 6$)

$$ds^2 = z^{-2} (dx^\mu dx_\mu + dz^M dz^M) = z^{-2} (dx^\mu dx_\mu + dz^2) + du^M du^M, \quad (3.5.2)$$

$$x^\mu x_\mu = x^+ x^- + x^* x, \quad x^\pm = x^3 \pm x^0, \quad x = x^1 + ix^2, \quad (3.5.3)$$

$$z^M = zu^M, \quad u^M u^M = 1, \quad z = (z^M z^M)^{\frac{1}{2}} \equiv e^\phi. \quad (3.5.4)$$

Here x^μ, z are the local coordinates in the POINCARÉ patch of AdS_5 (see Appendix B.2) and $u^M \in \mathbb{R}^6$ are EUCLIDEAN coordinates restricted to the S^5 sphere by (3.5.4). In this case AdS_5 and S^5 have the same constant curvature radius $R = 1$. Starting point is the action from [24], which is a covariant κ -symmetric superstring action for a Type IIB superstring on $AdS_5 \times S^5$ background. It is a 2d sigma-model on the coset superspace $\frac{SU(2,2|4)}{SO(4,1) \times SO(5)}$. Fixing κ -symmetry $\Gamma^+ \Theta^I = 0$ with ($I = 1, 2$) on the two 10d MAJORANA-WEYL GS spinors Θ^I and choosing the conformally analogue gauge on the 2d metric

$$\sqrt{-h} h^{\alpha\beta} = \text{diag}(-z^2, z^{-2}) \quad (3.5.5)$$

² BES stands for Beisert-Eden-Staudacher equation, which is an integral equation derived via a BETHE Ansatz in quantum integrability [17].

is leading to the light-cone gauge with a simple solution

$$x^+ = p^+ \tau \quad (3.5.6)$$

which can be imposed as an additional constraint to fix the 2d diffeomorphism invariance. The resulting action on $AdS_5 \times S^5$ is

$$\begin{aligned} S = g \int d\tau \int d\sigma \mathcal{L}, \quad g \equiv \frac{\sqrt{\lambda}}{4\pi}, \quad (3.5.7) \\ \mathcal{L} = \dot{x}^* \dot{x} + \left(\dot{z}^M + ip^+ z^{-2} z^N \eta_i (\rho^{MN})^i_j \eta^j \right)^2 + ip^+ (\theta^i \dot{\theta}_i + \eta^i \dot{\eta}_i + \theta_i \dot{\theta}^i + \eta_i \dot{\eta}^i) \\ - (p^+)^2 z^{-2} (\eta^2)^2 - z^{-4} (x'^* x' + z'^M z'^M) \\ - 2 \left[p^+ z^{-3} \eta^i \rho_{ij}^M z^M (\theta'^j - iz^{-1} \eta^j x') + p^+ z^{-3} \eta_i (\rho_M^\dagger)^{ij} z^M (\theta'_j + iz^{-1} \eta_j x'^*) \right], \end{aligned}$$

where we defined $\eta^2 \equiv \eta^i \eta_i$. The six 4×4 matrices ρ^M and their properties are stated in Appendix C. We also introduced the fields η_i, θ_i ($i = 1, \dots, 4$) which are complex GRASSMANN variables with $\eta^i \equiv (\eta_i)^\dagger, \theta^i \equiv (\theta_i)^\dagger$. They are the remnants of the original two 10d MAJORANA-WEYL GS spinors and transform in the fundamental representation of $SU(4)$. We will also refer to them as fermions due to their GRASSMANN-odd properties. The action is at most quartic in the fermions and the factors of p^+ can be absorbed by a rescaling of the selfsame and therefore we can set $p^+ = 1$. To get a real-valued BOLTZMANN factor e^{-S_E} in the path integral we perform a WICK rotation $\tau \rightarrow -i\tau, p^+ \rightarrow ip^+$ and after setting $p^+ = 1$ we obtain the EUCLIDEAN action

$$\begin{aligned} S_E = g \int d\tau \int d\sigma \mathcal{L}_E, \quad (3.5.8) \\ \mathcal{L}_E = \dot{x}^* \dot{x} + \left(\dot{z}^M + iz^{-2} z^N \eta_i (\rho^{MN})^i_j \eta^j \right)^2 + i (\theta^i \dot{\theta}_i + \eta^i \dot{\eta}_i + \theta_i \dot{\theta}^i + \eta_i \dot{\eta}^i) \\ - z^{-2} (\eta^2)^2 + z^{-4} (x'^* x' + z'^M z'^M) \\ + 2i \left[z^{-3} \eta^i \rho_{ij}^M z^M (\theta'^j - iz^{-1} \eta^j x') + z^{-3} \eta_i (\rho_M^\dagger)^{ij} z^M (\theta'_j + iz^{-1} \eta_j x'^*) \right], \end{aligned}$$

As mentioned, this EUCLIDEAN superstring action has the simple classical solution of a null-cusp, given by

$$\begin{aligned} x^+ = \tau, \quad x^- = -\frac{1}{2\sigma}, \quad x^1 = x^2 = 0, \quad z = \sqrt{-2x^+ x^-} = \sqrt{\frac{\tau}{\sigma}}, \quad (3.5.9) \\ \tau, \sigma \in (0, \infty). \end{aligned}$$

For $z \rightarrow 0$ we approach the AdS boundary and therefore the regime of $\mathcal{N} = 4$ SYM (see also Figure 3.2 for a visualisation for the cusped contour). The curve proceeding at the boundary can be parametrised by

$$\begin{aligned} \mathcal{C}_{\text{cusp}} : (-\infty, \infty) &\longrightarrow \mathbb{R}^{4,1} \\ s &\longrightarrow (x^1, x^2, x^3, x^4) \end{aligned} \quad (3.5.10)$$

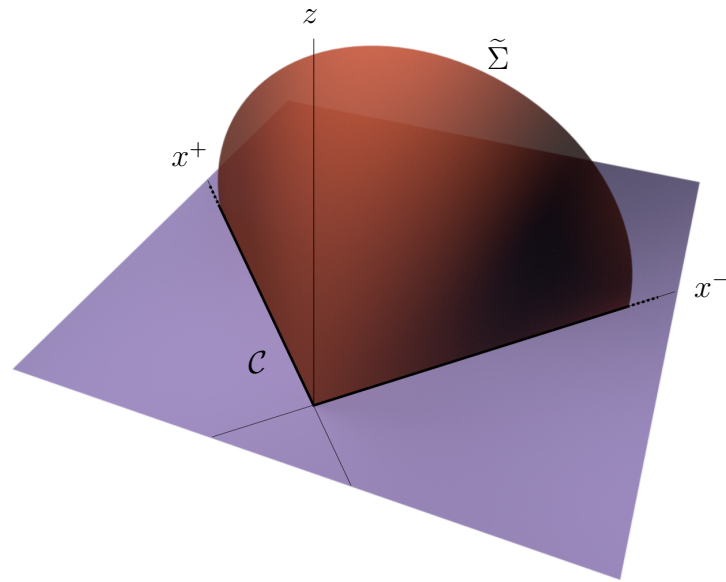


Figure 3.2 Visualisation of the string worldsheet in the AdS_3 subspace (which is orthogonal to the coordinates x, x^*). For $z \rightarrow 0$ the embedding of the string worldsheet $\tilde{\Sigma}$ is bounded by a cusped contour \mathcal{C} closed at infinity.

with

$$x^1 = x^2 = 0, \quad x^+ = \begin{cases} -s & s < 0, \\ 0 & \text{else,} \end{cases} \quad x^- = \begin{cases} s & s > 0, \\ 0 & \text{else.} \end{cases} \quad (3.5.11)$$

To arrive at the form of (3.5.1) with a fluctuation action S_{cusp} , we need to expand S_E around the null-cusp background (3.5.9). We therefore choose the field fluctuations to be

$$x = \sqrt{\frac{\tau}{\sigma}} \tilde{x}, \quad z^M = \sqrt{\frac{\tau}{\sigma}} \tilde{z}^M, \quad \theta_i = \frac{1}{\sqrt{\sigma}} \tilde{\theta}_i, \quad \eta_i = \frac{1}{\sqrt{\sigma}} \tilde{\eta}_i. \quad (3.5.12)$$

With a transition to the new worldsheet coordinates $(\tau, \sigma) \rightarrow (t, s) = (\ln \tau, \ln \sigma)$ the fluctuation action has no direct t or s dependence

$$S_{\text{cusp}} = g \int dt \int ds \mathcal{L}_{\text{cusp}} \quad (3.5.13)$$

$$\begin{aligned} \mathcal{L}_{\text{cusp}} = & \left| \partial_t \tilde{x} + \frac{1}{2} \tilde{x} \right|^2 + \frac{1}{\tilde{z}^4} \left| \partial_s \tilde{x} - \frac{1}{2} \tilde{x} \right|^2 + \left(\partial_t \tilde{z}^M + \frac{1}{2} \tilde{z}^M + \frac{i}{\tilde{z}^2} \tilde{z}_N \tilde{\eta}_i (\rho^{MN})^i_j \tilde{\eta}^j \right)^2 \\ & + \frac{1}{\tilde{z}^4} \left(\partial_s \tilde{z}^M - \frac{1}{2} \tilde{z}^M \right)^2 + i \left(\tilde{\theta}^i \partial_t \tilde{\theta}_i + \tilde{\eta}^i \partial_t \tilde{\eta}_i + \tilde{\theta}_i \partial_t \tilde{\theta}^i + \tilde{\eta}_i \partial_t \tilde{\eta}^i \right) - \frac{1}{\tilde{z}^2} (\tilde{\eta}^2)^2 \\ & + \frac{2i}{\tilde{z}^3} \tilde{z}^M \tilde{\eta}^i (\rho^M)_{ij} \left(\partial_s \tilde{\theta}^j - \frac{1}{2} \tilde{\theta}^j - \frac{i}{\tilde{z}} \tilde{\eta}^j \left(\partial_s \tilde{x} - \frac{1}{2} \tilde{x} \right) \right) \\ & + \frac{2i}{\tilde{z}^3} \tilde{z}^M \tilde{\eta}_i (\rho_M^\dagger)^{ij} \left(\partial_s \tilde{\theta}_j - \frac{1}{2} \tilde{\theta}_j + \frac{i}{\tilde{z}} \tilde{\eta}_j + \frac{i}{\tilde{z}} \tilde{\eta}^j \left(\partial_s \tilde{x} - \frac{1}{2} \tilde{x} \right)^* \right). \end{aligned}$$

In the following we will drop the tilde notation for convenience. We also want to remark that there has been no truncation applied and this is still the full fluctuation action and therefore perfectly valid for a further application on non-perturbative calculations. In a previous step we set the light-cone momentum $p^+ = 1$ for simplicity, but since p^+ will be a dimensionfull quantity in terms of a lattice spacing, when we discretise the model, we will insert a mass scale parameter m that will also be necessary for a later renormalisation on the lattice and we therefore change

$$\partial_t x + \frac{1}{2} x \rightarrow \partial_t x + \frac{m}{2} x, \quad \partial_t z^M + \frac{1}{2} z^M \rightarrow \partial_t z^M + \frac{m}{2} z^M \quad (3.5.14)$$

and in the same way also the terms with spacial derivatives.

3.6 Symmetries of the fluctuation action

In [18] it was presented, that the general κ -symmetry light-cone fixed action possesses several symmetries. Two fundamental ones, which are also inherited by the fluctuation action (3.5.13) in its gauge fixed status, are global symmetries.

- At first a $U(1) \sim SO(2)$ symmetry which rotates the x and x^* coordinate fields orthogonal to the other AdS_5 coordinates, which therefore does not affect the classical solution. In order for the action to be invariant, also

the fermions need to be shifted with the following transformations and the infinitesimal parameter ϵ

$$\begin{aligned} \delta x &= e^{i\epsilon} x, & \delta \eta_i &= e^{i\frac{\epsilon}{2}} \eta_i, & \delta \theta_i &= e^{-i\frac{\epsilon}{2}} \theta_i, \\ \delta x^* &= e^{-i\epsilon} x^*, & \delta \eta^i &= e^{-i\frac{\epsilon}{2}} \eta^i, & \delta \theta^i &= e^{i\frac{\epsilon}{2}} \theta^i. \end{aligned} \quad (3.6.1)$$

- The other symmetry is an $SU(4) \sim SO(6)$, which concerns the z^M fields and is inherited after gauge fixing due to the S^5 structure. By introducing an infinitesimal $SU(4)$ rotation ϵ^i_j the global symmetry transformations are given by

$$\begin{aligned} \delta z^M &= -\frac{1}{2} \epsilon^i_j (\rho^{MN})^j_i z^N \\ \delta \theta^i &= \epsilon^i_j \theta^j, \quad \delta \theta_i = -\theta_j \epsilon^j_i, \quad \delta \eta^i = \epsilon^i_j \eta^j, \quad \delta \eta_i = -\eta_j \epsilon^j_i. \end{aligned} \quad (3.6.2)$$

Hereby one can see that the z^M transform in the vector representation and the $\{\eta^i, \theta^i\}$ and $\{\eta_i, \theta_i\}$ in the fundamental and anti-fundamental representation of $SU(4)$, respectively.

3.7 Perturbative 1-loop free energy

Here we want to point out a quick check that fluctuations around the previously derived vacuum lead to the correct solution of (3.4.6). We thus want to reproduce the constant $3 \ln 2/\pi$ term in $f(g)$, knowing from (3.4.5) that we can write

$$Z_{\text{string}} = e^{-\frac{1}{8} f(\lambda) V_2} \equiv e^{-\Gamma(\lambda)}, \quad V_2 = \int dt \int ds, \quad (3.7.1)$$

where we define

$$\Gamma = \Gamma^{(0)} + \Gamma^{(1)} + \Gamma^{(2)} + \dots = \frac{1}{8} f(\lambda) V_2. \quad (3.7.2)$$

Thereby $\Gamma^{(0)} = S_E[X_{\text{cl}}, \Psi = 0]$ is the value of the classical action on the solution and $\Gamma^{(1)}, \Gamma^{(2)}, \dots$ are quantum corrections. The scaling function can be expanded in the following way

$$f(g) = g \left[a_0 + \frac{a_1}{g} + \frac{a_2}{g^2} + \dots \right]. \quad (3.7.3)$$

In [13] the 1-loop fluctuation coefficient a_1 has been calculated via $\Gamma^{(1)} = -\ln Z^{(1)}$, where $Z^{(1)}$ is the exponential of the truncated fluctuation action that has only quadratic field contributions. The LAGRANGIAN can therefore be written as a matrix-vector product with fermionic and bosonic matrix operators \hat{D}_F and \hat{D}_B . The 1-loop approximation of the path integral can then be written as³ (with

³With $\text{Det } \hat{O}$ we hereby mean the full infinite dimensional determinant in the sense of

$$\ln \text{Det } \hat{O} = \text{Tr } \ln \hat{O} = \int d^d s \langle s | \text{tr } \ln \hat{O} | s \rangle = \int d^d s \ln [\det O(s)],$$

where tr and \det refer to the regular trace and determinant if \hat{O} is a matrix of operators and here $|s\rangle$ is an eigenbase of the operator \hat{O} .

$$p^2 = (p_0)^2 + (p_1)^2$$

$$\begin{aligned} \Gamma^{(1)} &= \frac{1}{2} \ln \frac{\text{Det } \hat{D}_B}{\text{Det } \hat{D}_F} = \frac{V_2}{2} \int \frac{d^2 p}{(2\pi)^2} \ln \left[\frac{\det D_B(p)}{\det D_F(p)} \right] \\ &= \frac{V_2}{2} \int \frac{d^2 p}{(2\pi)^2} \ln \left[\frac{(p^2 + m^2) \left(p^2 + \frac{m^2}{2}\right)^2 (p^2)^5}{\left(p^2 + \frac{m^2}{4}\right)^8} \right] = -\frac{3 \ln 2}{\pi} \frac{V_2}{8} m^2, \end{aligned} \quad (3.7.4)$$

leading to the correct 1-loop coefficient for $f(g)$ with $m = 1$. In the UV limit divergences cancel due to the supersymmetric equivalence of boson and fermion numbers.

In order to discretise the derived model we will proceed with a chapter on lattice techniques that is of utmost importance for the further continuation.

4

Lattice basics

In this section we want to present the basic concepts of lattice field theory, which has developed to a highly sophisticated research area in the last decades especially in the regime of QCD. This approach to field theory is not only of major concern for performing numerical calculations. It even provides a natural attempt to regularisation, which makes it also an interesting topic for theorists in the field of gauge theories.

4.1 Discretising the worldsheet

A computer is not able to deal with continuous variables, since already a continuous real interval can contain an infinite amount of points, but a computer only has limited memory. Hence, we need to limit the amount of points that we consider to make calculations. Since all the target space coordinates¹ depend on the worldsheet coordinates τ and σ , it seems natural to discretise the worldsheet map. We therefore introduce a lattice spacing a and the lattice size in spacial direction L and in time direction T . Following the remarks in [30] we define the two-dimensional lattice Λ to be

$$\Lambda = \{(n_0, n_1) \mid n_0 = 0, 1, \dots, (T-1) ; n_1 = 0, 1, \dots, (L-1)\}. \quad (4.1.1)$$

With that we can express the worldsheet coordinates with the lattice coordinates (see Figure 4.1)

$$(\tau, \sigma) = (an_0, an_1). \quad (4.1.2)$$

And since the lattice spacing is overall constant we can abbreviatly refer to a field Φ in the theory as a function of the lattice variables $\Phi(n_0, n_1)$. We now further want to discretise differential operators and integrals. The differentiation can be discretised in various ways inspired by its mathematical definition via differential quotients. To see additionally which order of error is introduced compared to the exact derivative, we examine the TAYLOR expansion of a real function $f(x)$ with a small offset ϵ

$$f(x \pm \epsilon) = f(x) \pm \epsilon f'(x) + \frac{\epsilon^2}{2} f''(x) \pm \frac{\epsilon^3}{6} f'''(x) + \dots \quad (4.1.3)$$

Now we can define a forward derivative as the finite difference

$$\frac{f(x + \epsilon) - f(x)}{\epsilon} = f'(x) + \mathcal{O}(\epsilon) \quad (4.1.4)$$

¹which represent the fields in our two-dimensional QFT

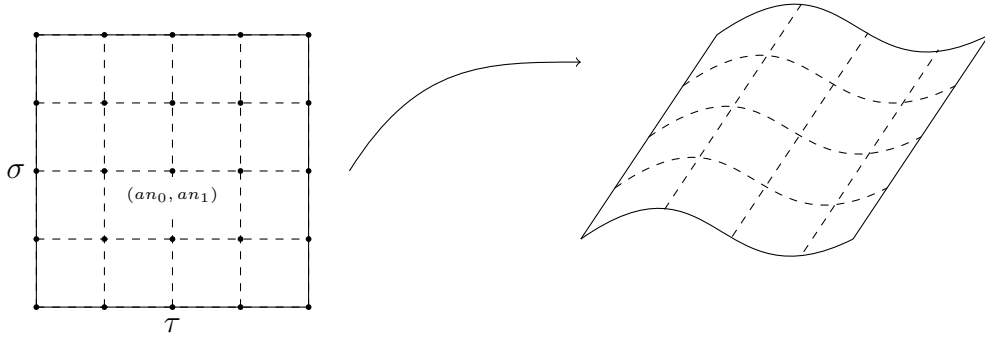


Figure 4.1 Mapping of the worldsheet grid into target space.

and in the same way also a backward derivative by using the $f(x - \epsilon)$ term. Combining both leads to the symmetric derivative with an error of higher order in ϵ

$$\frac{f(x - \epsilon) - f(x + \epsilon)}{2\epsilon} = f'(x) + \mathcal{O}(\epsilon^2). \quad (4.1.5)$$

It is more convenient to use the symmetric finite difference, because the error introduced by the finite lattice spacing is hereby reduced by one order. By adding additional terms of $f(x \pm 2\epsilon)$ it is possible to get a finite difference derivative which is exact up to an order of $\mathcal{O}(\epsilon^3)$ and so on. Depending on the demanded accuracy one is able to regulate the introduced error via this method. With ϵ being our lattice spacing a we find the derivative of our fields at $n = (n_0, n_1)$ to be²

$$\partial_\alpha \Phi(\tau, \sigma) = \hat{\partial}_\alpha \Phi(n) + \mathcal{O}(a^2) \equiv \frac{\Phi(n - \hat{\alpha}) - \Phi(n + \hat{\alpha})}{2a} + \mathcal{O}(a^2), \quad (4.1.6)$$

where $\hat{\alpha}$ is the unit vector in α -direction. For the integration over the worldsheet coordinates we replace the integral by a finite sum over all lattice points

$$\int d\tau d\sigma \longrightarrow a^2 \sum_{n \in \Lambda}. \quad (4.1.7)$$

For a better visualisation it is more convenient to use an abbreviated notation. In the following we will denote $\phi \equiv \phi(n)$ as a field which depends on the lattice coordinates n . The same is true for an operator $M \equiv M(m, n)$. A shorter expression of a matrix-vector like product is given by

$$\phi^T M \psi \equiv \sum_{m, n \in \Lambda} \phi(m) M(m, n) \psi(n). \quad (4.1.8)$$

²With $\hat{\partial}_\alpha$ being the symmetric finite difference in α -direction. We also define the forward and backward finite difference respectively by

$$\vec{\partial}_\alpha \Phi(n) = \frac{\Phi(n + \hat{\alpha}) - \Phi(n)}{a} \quad \text{and} \quad \check{\partial}_\alpha \Phi(n) = \frac{\Phi(n) - \Phi(n - \hat{\alpha})}{a}.$$

To implement the previous relation on a computer as an actual matrix-vector product it is necessary to map the grid index $n = (n_0, n_1)$ to a lexicographic vector index

$$l(n) = Ln_0 + n_1 \quad \text{with} \quad l = 0, 1, \dots, (V-1), \quad V = LT, \quad (4.1.9)$$

so that the according fields $\phi_{l(n)} \equiv \phi(n)$ are actual vectors and we can apply a matrix-vector notation

$$\phi^T M \phi \equiv \sum_{l,p=0}^{V-1} \phi_l M_{lp} \phi_p, \quad (4.1.10)$$

where then M is also an actual matrix. For the finite differences derivatives we also need to know the neighbouring relations. So if we want to move on the grid in direction $\pm\hat{\alpha}$, which lexicographic index corresponds to this movement? These relations are implemented into a *next neighbour* function (nb) which also takes into account the boundary conditions (toroidal in our case) and returns the corresponding vector index

$$l_{\pm\hat{\alpha}} = \text{nb}(l, \pm\hat{\alpha}). \quad (4.1.11)$$

We now want to define a symmetric finite difference without the factor $1/a$ for the lexicographic notation by

$$\bar{\Delta}_\alpha \phi_l \equiv \frac{1}{2} (\phi_{l+\hat{\alpha}} - \phi_{l-\hat{\alpha}}). \quad (4.1.12)$$

In consequence we can write $\bar{\Delta}_\alpha$ as a $V \times V$ matrix

$$(\bar{\Delta}_\alpha)_{lp} = \frac{\delta_{l+\hat{\alpha},p} - \delta_{l-\hat{\alpha},p}}{2}. \quad (4.1.13)$$

For other than periodic boundary conditions some of the signs have to be flipped according to the relation (D.9). In the same way we can define forward and backward finite differences by

$$(\Delta_\alpha)_{lp} = \delta_{l+\hat{\alpha},p} - \delta_{l,p}, \quad (\Delta_\alpha^*)_{lp} = \delta_{l,p} - \delta_{l-\hat{\alpha},p}. \quad (4.1.14)$$

We will come back to this notation in chapter 5. For now on we will presume using the grid notation for the further studies.

4.2 Bosons and fermions on the lattice

4.2.1 Bosonic propagator

In the examined theory bosons and fermions are both scalar fields of either real, or complex GRASSMANN type. The equations of motion of bosons are given by the KLEIN-GORDON equation, which contains only second order derivatives. To discretise the second order derivative we define the corresponding finite difference operator simply by applying a forward and a backward finite difference

$$\hat{\partial}_\alpha^2 \Phi(n) = \bar{\partial}_\alpha \vec{\partial}_\alpha \Phi(n) = \frac{\Phi(n + \hat{\alpha}) - 2\Phi(n) + \Phi(n - \hat{\alpha})}{a^2}. \quad (4.2.1)$$

In a Lagrangian we would find the differential operator enclosed by the fields, for instance like

$$\Phi(n) \left(\hat{\partial}_\alpha^2 \Phi \right)(n) = \sum_{m \in \Lambda} \Phi(n) \hat{\partial}_\alpha^2(n, m) \Phi(m), \quad (4.2.2)$$

where we use (4.2.1) to define

$$\hat{\partial}_\alpha^2(n, m) \equiv \frac{\delta_{m, n+\hat{\alpha}} - 2\delta_{m, n} + \delta_{m, n-\hat{\alpha}}}{a^2}. \quad (4.2.3)$$

To investigate the behaviour of bosons under the discretisation we are interested in the propagator (which is related to the inverse of the differential operator) in momentum space. We therefore perform a discrete FOURIER transform, which is discussed in Appendix D. Both indices m and n transform independently and in order to perform a unitary similarity transformation the second index is FOURIER transformed using the complex conjugated phase [30]

$$\begin{aligned} \tilde{\partial}_\alpha^2(p, q) &= \frac{1}{|\Lambda|} \sum_{m, n \in \Lambda} e^{-iq \cdot na} \hat{\partial}_\alpha^2(n, m) e^{ip \cdot ma} \\ &= \frac{1}{|\Lambda|} \sum_{n \in \Lambda} e^{-i(q-p) \cdot na} \frac{1}{a^2} \left[e^{ip_\alpha a} - 2 + e^{-ip_\alpha a} \right] \\ &= \delta(p - q) \tilde{\partial}_\alpha^2(p), \end{aligned} \quad (4.2.4)$$

where the FOURIER transform of the second derivative is defined by

$$\tilde{\partial}_\alpha^2(p) \equiv -\frac{4}{a^2} \sin^2 \left(\frac{p_\alpha a}{2} \right). \quad (4.2.5)$$

The EUCLIDEAN KLEIN-GORDON operator $\widetilde{D}(p)$ in momentum space with particle mass m reads

$$\widetilde{D}(p) = m^2 + \sum_{\alpha=0}^1 \tilde{\partial}_\alpha^2(p). \quad (4.2.6)$$

And so we find the propagator simply by inverting the previous relation. Of special interest is the massless case, where we want to investigate the continuum limit

$$\widetilde{D}^{-1}(p) \Big|_{m=0} = \frac{1}{-\frac{4}{a^2} \sum_{\alpha=0}^1 \sin^2 \left(\frac{p_\alpha a}{2} \right)} \xrightarrow{a \rightarrow 0} -\frac{1}{p^2}. \quad (4.2.7)$$

This is precisely what we expected for the EUCLIDEAN propagator in the continuum. Since we have $p_\alpha \in \left(-\frac{\pi}{a}, \frac{\pi}{a} \right]$, there are no additional poles within the sine function other than the physical one at $p = (0, 0)$.

4.2.2 Fermionic propagator and the doubling problem

In the case of fermions the equations of motion in four-dimensional QFT are given by the Dirac equation, which is a linearisation of the KLEIN-GORDON equation and only contains first order derivatives. To not explicitly break existing symmetries, we have to go with the symmetric derivative in this case. Now we can

follow the exact same steps as for the bosonic case to investigate the continuum limit of a DIRAC like operator in our two-dimensional space time. As mentioned we start from the symmetric finite difference

$$\hat{\partial}_\alpha(m, n) \equiv \frac{\delta_{m, n+\hat{\alpha}} - \delta_{m, n-\hat{\alpha}}}{2a} \quad (4.2.8)$$

and proceed with the FOURIER transform

$$\tilde{\partial}_\alpha(p, q) = \frac{1}{|\Lambda|} \sum_{m, n \in \Lambda} e^{-iq \cdot na} \hat{\partial}_\alpha(n, m) e^{ip \cdot ma} \quad (4.2.9)$$

$$= \frac{1}{|\Lambda|} \sum_{n \in \Lambda} e^{-i(q-p) \cdot na} \left[\frac{e^{ip_\alpha a} - e^{-ip_\alpha a}}{2a} \right] \quad (4.2.10)$$

$$= \delta(p - q) \tilde{\partial}_\alpha(p), \quad (4.2.11)$$

here we are left with the following differential operator in momentum space

$$\tilde{\partial}_\alpha(p) \equiv \frac{i}{a} \sin(p_\alpha a). \quad (4.2.12)$$

To construct an EUCLIDEAN DIRAC like operator in two dimensions we use the first two PAULI matrices³

$$\tilde{D}_D(p) = m\mathbf{1} + \sum_{\alpha=0}^1 \gamma_\alpha \tilde{\partial}_\alpha(p) = m\mathbf{1} + \frac{i}{a} \sum_{\alpha=0}^1 \gamma_\alpha \sin(p_\alpha a). \quad (4.2.13)$$

The inverse propagator follows from the properties of the PAULI matrices to be

$$\tilde{D}_D^{-1}(p) = \frac{m\mathbf{1} - \frac{i}{a} \sum_{\alpha=0}^1 \gamma_\alpha \sin(p_\alpha a)}{m^2 + a^{-2} \sum_{\alpha=0}^1 \sin^2(p_\alpha a)}. \quad (4.2.14)$$

Once more we want to study the continuum limit of the propagator for the massless case and find by setting $m = 0$

$$\tilde{D}_D^{-1}(p)|_{m=0} = \frac{-\frac{i}{a} \sum_{\alpha=0}^1 \gamma_\alpha \sin(p_\alpha a)}{a^{-2} \sum_{\alpha=0}^1 \sin^2(p_\alpha a)} \xrightarrow{a \rightarrow 0} \frac{-i \sum_{\alpha=0}^1 \gamma_\alpha p_\alpha}{p^2}. \quad (4.2.15)$$

Here again the propagator has the correct naive continuum limit, but this time we face another problem. Since again p_α is in the domain $\left(-\frac{\pi}{a}, \frac{\pi}{a}\right]$, there occur three other non-physical poles within the sine function at $p = (0, \pi/a)$, $p = (\pi/a, 0)$ and $p = (\pi/a, \pi/a)$. As a result in the numerical simulation it seems that there are in this case three additional fermions which emerge only from the method of discretisation and are non-physical. This is obviously leading to distorted calculations and needs to be circumvented. That particular problem is known as fermion doubling and has been investigated extensively by WILSON,

$$\gamma_0 = \sigma_1 = \begin{pmatrix} 0 & 1 \\ 1 & 0 \end{pmatrix} \quad \gamma_1 = \sigma_2 = \begin{pmatrix} 0 & -i \\ i & 0 \end{pmatrix}$$

who introduced a possible solution. He suggested to add a term proportional to the discretised LAPLACE operator[31], which is known as a WILSON term. We can express it in momentum space with the help of (4.2.5) and find⁴

$$W(p) \equiv -\mathbb{1} \frac{a}{2} \sum_{\alpha=0}^1 \tilde{\partial}_{\alpha}^2(p) = \mathbb{1} \frac{1}{a} \sum_{\alpha=0}^1 (1 - \cos(p_{\alpha}a)). \quad (4.2.16)$$

Since the LAPLACE operator is of order $\mathcal{O}(a^0)$, we see that the WILSON term vanishes in the continuum limit. It also vanishes for $p_{\alpha} = 0$ and therefore gives no contribution to the physical pole of the theory. If we now invert the new DIRAC-WILSON operator

$$\widetilde{D}_W(p) \equiv \widetilde{D}_D(p) + W(p), \quad (4.2.17)$$

we find the new massless momentum space propagator

$$\widetilde{D}_W^{-1}(p)|_{m=0} = \frac{\mathbb{1} \frac{1}{a} \sum_{\alpha=0}^1 (1 - \cos(p_{\alpha}a)) - \frac{i}{a} \sum_{\alpha=0}^1 \gamma_{\alpha} \sin(p_{\alpha}a)}{\left(\frac{1}{a} \sum_{\alpha=0}^1 (1 - \cos(p_{\alpha}a))\right)^2 + \frac{1}{a^2} \sum_{\alpha=0}^1 \sin^2(p_{\alpha}a)}. \quad (4.2.18)$$

Here we can convince ourselves, that there are no more additional poles in the domain of p_{α} , since for the points where $p_{\alpha} = \pi/a$ the denominator does not vanish like before. Actually for these points the WILSON-term behaves like an additional mass term that is growing infinitely in the continuum limit and consequently decouples from the theory.

4.3 Monte Carlo methods

Now after we know how to discretise differential operators and act with them on bosonic and fermionic quantities we are able to build a discretised Lagrangian as well. But what we really need is a method to perform the calculation of observables in the path integral formalism. In QFT in the continuum we calculate the expectation value of an observable O via [32]

$$\langle O \rangle = \frac{1}{Z} \int \mathcal{D}\phi O(\phi) \exp(-S[\phi]), \quad (4.3.1)$$

where S is the EUCLIDEAN action depending on the collection of fields ϕ and Z is the partition function

$$Z = \int \mathcal{D}\phi \exp(-S[\phi]). \quad (4.3.2)$$

In fact there is no rigorous mathematical definition for the path integral in the continuum. It is motivated from a discretised measure, which is then somehow

⁴using the identity

$$\begin{aligned} \cos(2x) &= \cos^2(x) - \sin^2(x) \\ \Leftrightarrow \sin^2(x) &= \frac{1}{2} (1 - \cos(2x)) \end{aligned}$$

said to be made continuous. This step is considered ill defined by most mathematicians, but since we stay on a discretised lattice, the path integral measure $\mathcal{D}\phi$ can be perfectly well defined and is represented by

$$\mathcal{D}\phi = \prod_{n \in \Lambda} d\phi(n). \quad (4.3.3)$$

This means, that for every lattice point a multi-dimensional integral needs to be calculated. Even for small lattices this task becomes tortuous and soon even supercomputers would not be able to do that calculation in reasonable time. Out of this reason other methods of calculation have been considered. The most favoured one is a statistical method going under the name of Monte Carlo simulation. With this type of calculation it is possible to obtain good statistical approximations of high-dimensional integrals in reasonable time. At this point we want to study some details of the Monte Carlo methods used in the scope of this thesis.

4.3.1 Monte Carlo integration

The easiest way to understand the idea behind any form of calculation with Monte Carlo methods is via the Monte Carlo integration. Suppose we want to calculate the following multi-dimensional integral

$$I = \int_{\Omega} f(x) dx, \quad (4.3.4)$$

where $\Omega \subset \mathbb{R}^n$ is a compact integration domain. Then probability theory tells us [33], that we can approximate the integral I with a set of random numbers $\{\bar{x}_1, \dots, \bar{x}_N\}$ uniformly distributed on Ω with

$$I_N = V \frac{1}{N} \sum_{i=1}^N f(\bar{x}_i). \quad (4.3.5)$$

Hereby $V = \int_{\Omega} dx$ denotes the integration volume. One can show that I_N approximates I up to an error of order $\mathcal{O}(1/\sqrt{N})$ and the law of large numbers tells us, that $\lim_{N \rightarrow \infty} I_N = I$. One can also write for the expectation value $\langle f \rangle$ of f , that

$$\langle f \rangle = \lim_{N \rightarrow \infty} \frac{1}{N} \sum_{i=1}^N f(\bar{x}_i) = \frac{\int_{\Omega} f(x) dx}{\int_{\Omega} dx}. \quad (4.3.6)$$

An instructive example is to calculate the value of π with the 2d integral $I = \int_{\Omega} H(x, y) dx dy$ over the domain $\Omega = [-1, 1] \times [-1, 1]$ with the function

$$H(x, y) = \begin{cases} 1 & \text{if } x^2 + y^2 \leq 1 \\ 0 & \text{else.} \end{cases} \quad (4.3.7)$$

Analytically we know that I corresponds to the area of the unit circle and has the value $I = \pi$. With the volume being $V = 4$ we can find an estimate

$$\pi \approx \frac{4}{N} \sum_{i=1}^N H(\bar{x}_i). \quad (4.3.8)$$

This means that we can estimate the value of $\pi/4$ by counting the number of points lying within the circle (see figure 4.2) and dividing by the total number of points.

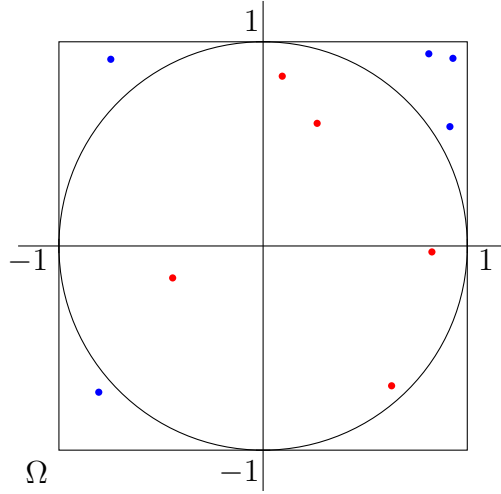


Figure 4.2 Graphic of random numbers uniform in Ω . $\pi/4$ can be estimated by the number of red points within the circle divided by the total number of points.

4.3.2 Importance sampling and Markov chains

More generally one can estimate integrals over a function $f(x)$ multiplied with a certain weight function $\rho(x)$ in the same way. We can write for the expectation value

$$\langle f \rangle_\rho \equiv \frac{\int_\Omega f(x) \rho(x) dx}{\int_\Omega \rho(x) dx} = \lim_{N \rightarrow \infty} \frac{1}{N} \sum_{i=1}^N f(\bar{x}_i). \quad (4.3.9)$$

But in this case the random numbers \bar{x}_i need to be distributed through the weight function $\rho(x)$. For this to be possible $\rho(x)$ needs to be a valid probability density function. Comparing with (4.3.1) we can convince ourselves, that this is the case for the discretised EUCLIDEAN path integral with measure (4.3.3). We can exploit this fact to make our calculation more efficient. In principle one could go with the simple Monte Carlo integration scheme, but since our integration domain is no bounded interval, but \mathbb{R}^n , we would produce a lot of configurations that would give no contribution to the path integral due to the weight factor and therefore introduce a large error. So if we produce random configurations distributed through a probability density given by the weight factor, we would generate mostly configurations with a non-vanishing contribution and the statistical error will be reduced. This procedure is called importance sampling. But to do the importance sampling one needs to be able to produce random configurations according to the given probability density. Since the action appearing in this probability density is in general a very complicated function, this task becomes highly non-trivial and there usually is no way to directly transform uniformly distributed random configurations into the favoured form. To make this

more explicit, consider the one-dimensional integral with normalised probability density function [34]

$$\langle f \rangle_\rho = \int_a^b f(x) \rho(x) dx, \quad \int_a^b \rho(x) dx = 1. \quad (4.3.10)$$

The distribution function $P(x)$ is given by

$$P(x) = \int_a^x \rho(t) dt. \quad (4.3.11)$$

If we perform the substitution

$$y(x) \equiv P(x), \quad \text{with} \quad \rho(x) = P'(x) = y'(x), \quad y \in [0, 1], \quad (4.3.12)$$

we are left with

$$\langle f \rangle_\rho = \int_a^b f(x) y'(x) dx = \int_0^1 f(x(y)) dy, \quad (4.3.13)$$

where $x(y) = P^{-1}(y)$. So if we generate uniformly distributed random numbers \bar{y} and use $\bar{x} = P^{-1}(\bar{y})$, which is now distributed according to $\rho(x)$, we can write

$$\langle f \rangle_\rho = \lim_{N \rightarrow \infty} \frac{1}{N} \sum_{i=1}^N f(\bar{x}_i). \quad (4.3.14)$$

For this to be true $P(x)$ needs to be strongly increasing and globally invertible. Extended to the higher-dimensional problem of path integrals this demand is met very unlikely, as said before.

To circumvent this issue one uses a statistical model called MARKOV chain to obtain configurations that are distributed according to the BOLTZMANN factor of the path integral. The idea is to start from an arbitrary configuration and generate a new one from the previous configuration via a pseudo random number generation process. Thereby new configurations are generated in a stochastic sequence that eventually follows an equilibrium distribution $P(\phi)$ [30]. The configurations in the chain can be numbered by an index, the so-called Monte Carlo time

$$\phi_0 \rightarrow \phi_1 \rightarrow \dots \rightarrow \phi_{N_{\text{th}}} \rightarrow \dots \quad (4.3.15)$$

The first configurations up to an index N_{th} should not be used for measurements since they are most certainly not properly distributed. The process needs a specific amount of time to reach its equilibrium distribution. Therefore this period is called equilibration or thermalisation phase. A MARKOV process is characterised by a conditional transition probability $T(\phi'|\phi)$ to move from a configuration ϕ to ϕ' . This probability depends only on the configurations ϕ and ϕ' and not any previous ones. It obeys the properties

$$0 \leq T(\phi'|\phi) \leq 1, \quad \sum_{\phi'} T(\phi'|\phi) = 1. \quad (4.3.16)$$

An important restriction is that the process must not get stuck at any configuration. It must always be possible to move between two specified configurations within a finite Monte Carlo time. This can be realised if the transition probability is strictly positive between all states which is called strong ergodicity. Furthermore the probability to move to ϕ' from any other state must be the same as to leave ϕ' to any other state which can be condensed to the following balance equation

$$\sum_{\phi} T(\phi'|\phi)P(\phi) = \sum_{\phi} T(\phi|\phi')P(\phi'). \quad (4.3.17)$$

A special solution to this equation will be obtained if one assumes that the equation holds for every term of the sum

$$T(\phi'|\phi)P(\phi) = T(\phi|\phi')P(\phi'). \quad (4.3.18)$$

This condition is called detailed balance and is used by most algorithms generating MARKOV chains.

4.3.3 Fermions on the lattice and the hybrid Monte Carlo algorithm

There are many possible algorithms to generate field configurations. The choice depends on the structure of the problem at hand. For the here presented case the algorithm of choice is called rational hybrid Monte Carlo (RHCM). The basic reason to use this algorithm is the presence of fermions in a specific manner. It is in general complicated to deal with fermions in numerical simulations due to the anti commuting properties of GRASSMANN variables. An efficient procedure is to integrate out fermions via GRASSMANN integration, presented in Appendix A.2, which results in our case in the PFAFFIAN of a fermionic operator $M[\phi]$ depending on the bosonic fields ϕ . We now want to include the PFAFFIAN as a probability weight factor in the process of generating MARKOV chain configurations. To act as a probability weight factor, $\text{Pf } M$ must be real and non-negative. If we consider this to be the case for the moment, we can write

$$\text{Pf } M = (\det M)^{\frac{1}{2}} = \left(\det MM^{\dagger}\right)^{\frac{1}{4}}. \quad (4.3.19)$$

In general one could have to deal with an arbitrary fraction α in the exponent on the right side of (4.3.19). If we restrict $\text{Pf } M$ to be also non-zero and therefore entirely positive using that MM^{\dagger} is positive definite, one can rewrite the determinant as a bosonic path integral with pseudofermions ξ

$$\left(\det MM^{\dagger}\right)^{\alpha} = \frac{1}{\det (MM^{\dagger})^{-\alpha}} \sim \int \mathcal{D}\eta \mathcal{D}\eta^{\dagger} e^{-\xi^{\dagger}(MM^{\dagger})^{-\alpha}\xi}. \quad (4.3.20)$$

Since there is an inversion included, the operator in the exponent is highly non-local in the bosonic fields ϕ . So even a small change in the fields could cause a large difference in the weight factor. Ergo one needs an algorithm that ensures that the generated configurations are part of the contributing regime of the

weight factor. In a case like that it proved efficient to use a hybrid Monte Carlo (HMC) algorithm when $\alpha = 1$, which uses HAMILTONIAN dynamics trajectories along some fictitious time to generate new configurations. For non-integer α one can use a rational approximation of $(MM^\dagger)^{-\alpha}$. Combined with the HMC this is called the rational hybrid Monte Carlo (RHMC) algorithm.

At this point we want to introduce the HMC algorithm which has been proposed in [35]. A more detailed explanation is presented in [30, 31] which serves as a guideline for the following. The HMC is referred to as hybrid because it combines a molecular dynamic (MD) evolution with random noise patterns to simulate quantum fluctuations, an additional METROPOLIS acceptance step lets it result into an exact MC algorithm. The field update is separated into two phases. Pseudofermions are updated first with an exact heat bath, while the bosons are kept constant. Therefore, a configuration ϑ is generated from a GAUSSIAN distribution $P(\vartheta) \sim e^{-\vartheta^\dagger \vartheta}$ and we set $\xi = M\vartheta$.

In the second phase a molecular dynamic evolution is used to update the bosonic fields while the pseudofermions are kept constant. We can now think of the effective action $S_{\text{eff}}[\phi] = S_B[\phi] + \xi^\dagger (MM^\dagger)^{-1} \xi$ as only dependent on the bosonic fields ϕ . Now for each field ϕ_i a conjugate momentum π_i is introduced and we expand the path integral with $\int \mathcal{D}\pi \exp(-1/2 \pi^2)$ to obtain

$$\langle O \rangle = \frac{\int \mathcal{D}\phi \mathcal{D}\eta \mathcal{D}\pi O(\phi) e^{-H[\phi, \pi]}}{\int \mathcal{D}\phi \mathcal{D}\eta \mathcal{D}\pi e^{-H[\phi, \pi]}}, \quad (4.3.21)$$

where we have introduced the HAMILTONIAN

$$H[\phi, \pi] = \frac{1}{2} \pi^2 + S_{\text{eff}}[\phi], \quad \pi^2 = \sum_i \sum_{n \in \Lambda} \pi_i^2(n). \quad (4.3.22)$$

The evolution of the fields follows according to the classical equations of motion along a fictitious MC time τ

$$\begin{aligned} \dot{\pi}_i &= -\frac{\partial H}{\partial \phi_i} = -\frac{\partial S_{\text{eff}}}{\partial \phi_i}, \\ \dot{\phi}_i &= \frac{\partial H}{\partial \pi_i} = \pi_i. \end{aligned} \quad (4.3.23)$$

A numerical implementation of (4.3.23) introduces a discrete step size $\epsilon \equiv \delta\tau$ and errors of order $\mathcal{O}(\epsilon^2)$. An additional METROPOLIS acceptance step can correct these errors. First the momenta π are randomly generated from a GAUSSIAN distribution $P_G(\pi) = \exp(-1/2 \pi^2)$. Then a numerical integration scheme is used to change the configuration $\{\phi, \pi\}$ along a discretised trajectory in phase space to the new point $\{\phi', \pi'\}$. The transition probability $T_{\text{MD}}(\phi', \pi' | \phi, \pi)$ of the MD evolution depends on the integration scheme. The latter needs to be reversible and area preserving for the algorithm to obey detailed balance. Thus, a *leapfrog integration* scheme is used. For one trajectory the fields ϕ are evolved in n steps of length ϵ . The momenta start with half a step of length $\epsilon/2$, then $(n - 1)$ full

steps are performed and again a half-step. The first half-step is given by

$$\begin{aligned}\pi_i\left(\frac{\epsilon}{2}\right) &= \pi_i(0) - \frac{\partial S_{\text{eff}}(\phi(0))}{\partial \phi_i} \frac{\epsilon}{2}, \\ \phi_i(\epsilon) &= \phi_i(0) + \pi_i\left(\frac{\epsilon}{2}\right)\epsilon.\end{aligned}\tag{4.3.24}$$

The next steps for $j = 1, \dots, n-1$ are

$$\begin{aligned}\pi_i\left(\left(j + \frac{1}{2}\right)\epsilon\right) &= \pi_i\left(\left(j - \frac{1}{2}\right)\epsilon\right) - \frac{\partial S_{\text{eff}}(\phi(j\epsilon))}{\partial \phi_i} \epsilon, \\ \phi_i((j+1)\epsilon) &= \phi_i(j\epsilon) + \pi_i\left(\left(j + \frac{1}{2}\right)\epsilon\right)\epsilon.\end{aligned}\tag{4.3.25}$$

With the last half-step we arrive at the final momentum

$$\pi_i(n\epsilon) = \pi_i\left(\left(n - \frac{1}{2}\right)\epsilon\right) - \frac{\partial S_{\text{eff}}(\phi(n\epsilon))}{\partial \phi_i} \frac{\epsilon}{2}.\tag{4.3.26}$$

With an additional METROPOLIS acceptance step

$$T_A(\phi', \pi' | \phi, \pi) = \min(1, \exp(H[\phi, \pi] - H[\phi', \pi']))\tag{4.3.27}$$

the total transition probability to move from ϕ to ϕ' is given by

$$T(\phi' | \phi) = \int \mathcal{D}\pi' \mathcal{D}\pi T_A(\phi', \pi' | \phi, \pi) T_{\text{MD}}(\phi', \pi' | \phi, \pi) P_G(\pi).\tag{4.3.28}$$

This has been proved to obey detailed balance in [35]. Concluding one can summarise the HMC algorithm in the following steps:

- **Pseudofermions**

Generate the pseudofermion field $\xi = M\vartheta$, where ϑ is distributed according to $\exp(-\vartheta^\dagger \vartheta)$.

- **Conjugate fields**

For an initial boson configuration $\phi^{(0)}$ generate $\pi^{(0)}$ according to the GAUSSIAN distribution $\exp(-\frac{1}{2}\pi^2)$.

- **Initial step**

$$\pi_i^{(\frac{1}{2})} = \pi_i^{(0)} - \frac{\epsilon}{2} F_i[\phi] \Big|_{\phi^{(0)}}.$$

- **Intermediate steps**

Full steps for $j = 1, \dots, n-1$

$$\phi_i^{(j)} = \phi_i^{(j-1)} + \pi_i^{(j-\frac{1}{2})}, \quad \pi_i^{(j+\frac{1}{2})} = \pi_i^{(j-\frac{1}{2})} - \epsilon F_i[\phi] \Big|_{\phi^{(j)}}.$$

- **Final step**

$$\phi'_i = \phi_i^{(n)} = \phi_i^{(n-1)} + \pi_i^{(n-\frac{1}{2})}, \quad \pi'_i = \pi_i^{(n)} = \pi_i^{(n-\frac{1}{2})} - \frac{\epsilon}{2} F_i[\phi] \Big|_{\phi^{(n)}}.$$

- **Monte Carlo step**

Accept new configuration ϕ' if a random number $r \in [0, 1)$ is smaller than

$$\exp\left(\frac{1}{2}(\pi^2 - \pi'^2) + S_B[\phi] - S_B[\phi'] + \vartheta^\dagger \vartheta - \xi^\dagger (M' M'^\dagger)^{-1} \xi\right).$$

Here we used $\phi_i^{(j)} \equiv \phi_i(j\epsilon)$ and the driving forces are denoted by

$$F_i[\phi] = \frac{\partial}{\partial \phi_i} \left[S_B[\phi] + \xi^\dagger (MM^\dagger)^{-1} \xi \right]. \quad (4.3.29)$$

4.3.4 The numerical sign problem

As discussed previously we want to calculate expectation values of observables $O(\phi)$, depending on bosonic fields ϕ which are distributed according to a certain probability weight function $\rho(\phi)$

$$\langle O \rangle_\rho = \frac{\int \mathcal{D}\phi O(\phi) \rho(\phi)}{\int \mathcal{D}\phi \rho(\phi)}. \quad (4.3.30)$$

The feasibility of calculations like that via Monte Carlo methods is only guaranteed if the weight function $\rho(\phi)$ is non-negative. In the process of dealing with fermions it is sometimes necessary to introduce bosonic auxiliary fields by a HUBBARD-STRATONOVICH (HS) transformation⁵ which might lead to a complex phase in the weight function. For fluctuations of this phase that are very close to the purely real spectrum, this can be corrected by a reweighting procedure. If nonetheless the phase is distributed on the whole complex spectrum where the reweighting tends to fail, then one is talking of a *sign problem*. There are several approaches to fix this issue but none of them works as a general method to cure the sign problem.

With this set of basic methods we are able to attempt the continuum model action from the previous chapter and apply a discretisation on the fields and operators. This process will be the subject of the next chapter.

⁵See Appendix A.3 for further details on the HS transformation.

5

Towards the lattice simulation

With the current status of the action (3.5.13) we could almost start to discretise the operators and fields, at least for the bosonic part this is not a problem. For the fermions, however, this is not so straightforward. In order to include the fermionic contribution into the weight factor of the path integral like explained in section 4.3.3 one needs to integrate out the GRASSMANN variables to result into a PFAFFIAN or determinant of a fermionic operator. As presented in Appendix A.2 this is only possible if the fermions appearing are of quadratic order. But in the fluctuation action (3.5.13) also quartic contributions of fermions emerge, which have to be linearised first with help of a HUBBARD-STRATONOVICH transformation¹.

5.1 Linearisation of fermionic contributions

5.1.1 Naive approach and sign problem

The only quartic interactions are coming from the η fields and we can write this part of the action as

$$S_4^F[\eta_i, \eta^i] = g \int dt ds \left[-\frac{1}{z^2} (\eta^2)^2 + \left(\frac{i}{z^2} z_N \eta_i (\rho^{MN})^i_j \eta^j \right)^2 \right]. \quad (5.1.1)$$

In the path integral representation the EUCLIDEAN action contributes within an exponential e^{-S_E} . By performing a naive HUBBARD-STRATONOVICH transformation on this exponential we can reduce the four-fermion contributions to quadratic YUKAWA terms whereas we have to introduce 7 bosonic real auxiliary fields ϕ and ϕ^N

$$\begin{aligned} & \exp \left\{ -g \int dt ds \left[-\frac{1}{z^2} (\eta^2)^2 + \left(\frac{i}{z^2} z_N \eta_i (\rho^{MN})^i_j \eta^j \right)^2 \right] \right\} \\ & \sim \int \mathcal{D}\phi \mathcal{D}\phi^M \exp \left\{ -g \int dt ds \left[\frac{1}{2} \phi^2 + \frac{\sqrt{2}}{z} \phi \eta^2 + \frac{1}{2} (\phi^M)^2 \right. \right. \\ & \quad \left. \left. - i \frac{\sqrt{2}}{z^4} \phi_M \left(i \eta_i (\rho^{MN})^i_j \eta^j \right) z_N \right] \right\}. \end{aligned} \quad (5.1.2)$$

¹See Appendix A.2 for details

Here we can notice that the second term appears to be complex, since the $SO(6)$ matrix in parenthesis is HERMITIAN (with respect to the indices M, N)

$$\left(i \eta_i (\rho^{MN})^i_j \eta^j\right)^\dagger = i \eta_j (\rho^{MN})^j_i \eta^i, \quad (5.1.3)$$

where we have used (C.6). As discussed in section 4.3.4 this complex phase in the weight function is potentially leading to a non-treatable sign problem. We therefore choose to make a field redefinition that circumvents the appearance of a complex phase during the HS transformation.

5.1.2 Alternative field redefinition

By using the identities for the $SO(6)$ matrices stated in Appendix C we can rewrite the second term in the LAGRANGIAN of (5.1.1) as

$$\left(i \eta_i (\rho^{MN})^i_j n^N \eta^j\right)^2 = -3(\eta^2)^2 + 2\eta_i (\rho^N)^{ik} n_N \eta_k \eta^j (\rho^L)_{jl} n_L \eta^l, \quad (5.1.4)$$

where we defined $n^N = \frac{z^N}{z}$. This leads to the LAGRANGIAN

$$\mathcal{L}_4 = \frac{1}{z^2} \left(-4(\eta^2)^2 + 2 \left| \eta_i (\rho^N)^{ik} n_N \eta_k \right|^2 \right). \quad (5.1.5)$$

In order to circumvent the sign problem the second term needs to be negative. To achieve this we define new fields²

$$\Sigma_i^j = \eta_i \eta^j \quad \tilde{\Sigma}_j^i = (\rho^N)^{ik} n_N (\rho^L)_{jl} n_L \eta_k \eta^l. \quad (5.1.6)$$

with this new definitions it is simple to check that

$$\Sigma_i^j \Sigma_j^i = -(\eta^2)^2 \quad \tilde{\Sigma}_i^j \tilde{\Sigma}_j^i = -(\eta^2)^2 \quad \Sigma_j^i \tilde{\Sigma}_i^j = - \left| \eta_i (\rho^N)^{ik} n_N \eta_k \right|^2. \quad (5.1.7)$$

With this we then define

$$\Sigma_{\pm i}^j = \Sigma_i^j \pm \tilde{\Sigma}_i^j \quad (5.1.8)$$

and find

$$\Sigma_{\pm i}^j \Sigma_{\pm j}^i = -2(\eta^2)^2 \mp 2 \left| \eta_i (\rho^N)^{ik} n_N \eta_k \right|^2. \quad (5.1.9)$$

We can thus substitute the new fields into the LAGRANGIAN and obtain

$$\mathcal{L}_4 = \frac{1}{z^2} \left(-4(\eta^2)^2 \mp 2(\eta^2)^2 \mp \Sigma_{\pm i}^j \Sigma_{\pm j}^i \right), \quad (5.1.10)$$

where we only need to select the right sign in the field definition to overcome the sign problem, which is leading to

$$\mathcal{L}_4 = \frac{1}{z^2} \left(-6(\eta^2)^2 - \Sigma_{+i}^j \Sigma_{+j}^i \right). \quad (5.1.11)$$

²Where we actually set $\Sigma_i^j = \eta_i \eta^j$, then defined $\Sigma_j^i \equiv (\Sigma_i^j)^* = \Sigma_j^i$ to emphasise the notation Σ_i^j and equivalent for $\tilde{\Sigma}$.

If we then perform a HS transformation there will be no complex phase. The HS transformation yields

$$-\frac{6}{z^2}(\eta^2)^2 \rightarrow \frac{12}{z}\eta^2\phi + 6\phi^2, \quad (5.1.12)$$

where a single bosonic field was introduced like in the naive case. And further

$$-\frac{1}{z^2}\Sigma_{+j}^i\Sigma_{+i}^j \rightarrow \frac{2}{z}\Sigma_{+j}^i\phi_i^j + \phi_j^i\phi_i^j \quad \text{with} \quad (\phi_j^i)^* = \phi_i^j. \quad (5.1.13)$$

Here the collection of fields ϕ_j^i can be thought of as a complex HERMITIAN matrix with 16 real free parameters. We find it convenient to rescale the field $\phi \rightarrow \phi/\sqrt{6}$, to get rid of the pre factor of 6 in (5.1.12). After reinserting the old fields for Σ_+ we can conclude that

$$\mathcal{L}_4 \rightarrow \frac{2\sqrt{6}}{z}\eta^2\phi + \phi^2 + \frac{2}{z}\eta_j\phi_i^j\eta^i + \frac{2}{z}(\rho^N)^{ik}n_N\eta_k\phi_i^j(\rho^L)_{jl}n_L\eta^l + \phi_j^i\phi_i^j, \quad (5.1.14)$$

and we can write the full LAGRANGIAN as

$$\begin{aligned} \mathcal{L}_{\text{cusp}} = & \left| \partial_t x + \frac{m}{2}x \right|^2 + \frac{1}{z^4} \left| \partial_s x - \frac{m}{2}x \right|^2 + \left(\partial_t z^M + \frac{m}{2}z^M \right)^2 \\ & + \frac{1}{z^4} \left(\partial_s z^M - \frac{m}{2}z^M \right)^2 + \phi^2 + \text{tr}(\tilde{\phi}\tilde{\phi}^\dagger) + \Psi^T \mathcal{O}_F \Psi. \end{aligned} \quad (5.1.15)$$

Hereby we defined the fermionic vector $\Psi \equiv (\theta^i, \theta_i, \eta^i, \eta_i)$ as well as the auxiliary matrix $\tilde{\phi} = (\tilde{\phi}_{ij}) \equiv \phi_j^i$. We used partial integration and the properties of the GRASSMANN numbers and $SO(6)$ matrices to write the fermionic contribution in a matrix-vector notation. The 16×16 fermionic operator is hereby represented as 4×4 block matrix

$$\mathcal{O}_F = \begin{pmatrix} 0 & i\mathbb{1}_4\partial_t & -i\rho^M(\partial_s + \frac{m}{2})\frac{z^M}{z^3} & 0 \\ i\mathbb{1}_4\partial_t & 0 & 0 & -i\rho_M^\dagger(\partial_s + \frac{m}{2})\frac{z^M}{z^3} \\ i\frac{z^M}{z^3}\rho^M(\partial_s - \frac{m}{2}) & 0 & 2\frac{z^M}{z^4}\rho^M(\partial_s x - m\frac{x}{2}) & i\mathbb{1}_4\partial_t - A^T \\ 0 & i\frac{z^M}{z^3}\rho_M^\dagger(\partial_s - \frac{m}{2}) & i\mathbb{1}_4\partial_t + A & -2\frac{z^M}{z^4}\rho_M^\dagger(\partial_s x^* - m\frac{x^*}{2}) \end{pmatrix}, \quad (5.1.16)$$

where

$$A = -\frac{\sqrt{6}}{z}\phi\mathbb{1}_4 + \frac{1}{z}\tilde{\phi} + \frac{1}{z^3}\rho_N^*\tilde{\phi}^T\rho^L z^N z^L + i\frac{z^N}{z^2}\rho^{MN}\partial_t z^M. \quad (5.1.17)$$

The auxiliary matrix $\tilde{\phi}$ is constructed from 16 real auxiliary fields ϕ_I ($I = 1, \dots, 16$) in the following way

$$\tilde{\phi} = \frac{1}{\sqrt{2}} \begin{pmatrix} \sqrt{2}\phi_{13} & \phi_1 + i\phi_2 & \phi_3 + i\phi_4 & \phi_5 + i\phi_6 \\ \phi_1 - i\phi_2 & \sqrt{2}\phi_{14} & \phi_7 + i\phi_8 & \phi_9 + i\phi_{10} \\ \phi_3 - i\phi_4 & \phi_7 - i\phi_8 & \sqrt{2}\phi_{15} & \phi_{11} + i\phi_{12} \\ \phi_5 - i\phi_6 & \phi_9 - i\phi_{10} & \phi_{11} - i\phi_{12} & \sqrt{2}\phi_{16} \end{pmatrix}, \quad (5.1.18)$$

so that we have the simple expression

$$\text{tr}(\tilde{\phi}\tilde{\phi}^\dagger) = \sum_{I=1}^{16}(\phi_I)^2 \equiv (\phi_I)^2. \quad (5.1.19)$$

5.1.3 Matrix properties

The fermion matrix obeys some fundamental symmetries that shall be summarised in this section. Since \mathcal{O}_F is acting as a bilinear together with the anti-commuting GRASSMANN fields, it is clear that the matrix representation of \mathcal{O}_F needs to be skew-symmetric

$$\mathcal{O}_F^T = -\mathcal{O}_F. \quad (5.1.20)$$

It further possesses a global $U(1)$ and $SO(6)$ symmetry. The $U(1)$ symmetry manifests itself through the fact that certain blocks of \mathcal{O}_F are zero. As we saw from (3.6.1) fermions transform under $U(1)$ according to a certain charge q

$$\psi \rightarrow e^{iq\alpha}\psi. \quad (5.1.21)$$

Therefore only fermions with complementary charges are allowed to couple in order to respect the $U(1)$ symmetry, and the blocks that lead to other couplings need to be zero. The $SO(6)$ symmetry requires the 4×4 block structure and that each block is built from the $SO(6)$ invariant structures: $\mathbb{1}_4, \rho^M u^M, \rho_M^\dagger u^M$. The fermion matrix obeys also another constraint which is reminiscent of the γ_5 -HERMITICITY in lattice QCD [31]

$$\mathcal{O}_F^\dagger = \Gamma_5 \mathcal{O}_F \Gamma_5, \quad (5.1.22)$$

where Γ_5 is the following unitary, anti-HERMITIAN matrix

$$\Gamma_5 = \begin{pmatrix} 0 & \mathbb{1}_4 & 0 & 0 \\ -\mathbb{1}_4 & 0 & 0 & 0 \\ 0 & 0 & 0 & \mathbb{1}_4 \\ 0 & 0 & -\mathbb{1}_4 & 0 \end{pmatrix}, \quad \Gamma_5^\dagger \Gamma_5 = \mathbb{1}_{16}, \quad \Gamma_5^\dagger = -\Gamma_5. \quad (5.1.23)$$

A general skew-symmetric block matrix M that is Γ_5 -HERMITIAN needs to have the structure

$$M = \begin{pmatrix} d_1 & a & b & c \\ -a^T & -d_1^\dagger & -c^* & b^* \\ -b^T & c^\dagger & d_2 & f \\ -c^T & -b^\dagger & -f^T & -d_2^\dagger \end{pmatrix}, \quad d_i = -d_i^T, \quad a = a^\dagger, \quad f = f^\dagger. \quad (5.1.24)$$

We can use the two properties (5.1.20) and (5.1.22) to ensure the absence of a complex phase in the determinant

$$\begin{aligned} \det(\mathcal{O}_F)^* &= \det(\mathcal{O}_F^\dagger) = \det(\Gamma_5 \mathcal{O}_F \Gamma_5) \\ &= \det(\Gamma_5)^2 \det(\mathcal{O}_F) \\ &= \det(\mathcal{O}_F) \end{aligned} \quad (5.1.25)$$

and thereby follows that $\det \mathcal{O}_F \in \mathbb{R}$. For the PFAFFIAN of \mathcal{O}_F to be non-negative we require that $\det \mathcal{O}_F$ is positive and factorisable into two equivalent terms, so that

$$\det \mathcal{O}_F = \text{Pf}(\mathcal{O}_F)^2. \quad (5.1.26)$$

Therefore we want to examine the spectrum of \mathcal{O}_F . Assuming that λ is an eigenvalue of \mathcal{O}_F and $P(\lambda)$ is the characteristic polynomial we can prove

$$\begin{aligned} P(\lambda) &= \det(\mathcal{O}_F - \lambda \mathbf{1}) = \det(\Gamma_5(\mathcal{O}_F - \lambda \mathbf{1})\Gamma_5) \\ &= \det(\mathcal{O}_F^\dagger + \lambda \mathbf{1}) = \det(\mathcal{O}_F + \lambda^* \mathbf{1})^* \\ &= P(-\lambda^*)^*, \end{aligned} \quad (5.1.27)$$

and thereby see that if λ is an eigenvalue, then also $-\lambda^*$ is an eigenvalue. Since \mathcal{O}_F is skew-symmetric also $-\lambda$ and λ^* must be eigenvalues. So if for a discretised version $\hat{\mathcal{O}}_F$ all these eigenvalues would be complex with non-vanishing real and imaginary part we could write the determinant as

$$\det \hat{\mathcal{O}}_F = \prod_{i=1}^N |\lambda_i|^2 |\lambda_i|^2 \quad (5.1.28)$$

and therefore

$$\text{Pf } \hat{\mathcal{O}}_F = \pm \prod_{i=1}^N |\lambda_i|^2, \quad (5.1.29)$$

where $N = |\Lambda|/4$. Since the eigenvalues should behave like continuous functions along a HMC trajectory it should not be possible for the PFAFFIAN to change its sign throughout a trajectory. So if one chooses a starting configuration with positive PFAFFIAN it should remain non-negative during the whole simulation and the PFAFFIAN should be a valid probability distribution. Yet it is not quite clear what happens if there are also purely real or imaginary eigenvalues appearing. If they come in the same kind of quartets then there should not be a problem, otherwise the sign of the PFAFFIAN can change if an odd number of these purely real or imaginary eigenvalues make a transition through zero. We therefore need to keep track of the PFAFFIAN during simulation and check that the eigenvalues of $\hat{\mathcal{O}}_F$ are clearly separated from zero to legitimate its status as a valid probability density.

5.1.4 Pseudofermionic weight function

Now since we have linearised fermionic contributions to quadratic order, we are able to integrate over the GRASSMANN fields in the partition function

$$Z = \int \mathcal{D}x \mathcal{D}x^* \mathcal{D}z^N \mathcal{D}\phi \mathcal{D}\phi_I \mathcal{D}\Psi e^{-S}, \quad (5.1.30)$$

where we will split $S = S_B + S_F$ into its bosonic (S_B) and fermionic (S_F) contributions with

$$\begin{aligned} S_B &= g \int dt ds \left(\left| \partial_t x + \frac{m}{2} x \right|^2 + \frac{1}{z^4} \left| \partial_s x - \frac{m}{2} x \right|^2 + \left(\partial_t z^M + \frac{m}{2} z^M \right)^2 \right. \\ &\quad \left. + \frac{1}{z^4} \left(\partial_s z^M - \frac{m}{2} z^M \right)^2 + \phi^2 + (\phi_I)^2 \right), \end{aligned} \quad (5.1.31)$$

$$S_F = g \int dt ds \Psi^T \mathcal{O}_F \Psi.$$

As motivated in section A.2 the GRASSMANN integral over Ψ will result in a PFAFFIAN $\text{Pf } \mathcal{O}_F$. To include the PFAFFIAN into the weight function we have to rewrite it in terms of pseudofermions ξ as emphasised in section 4.3.3. To legitimately apply this procedure we need the PFAFFIAN to be real and non-negative. By our alternative approach to linearisation we made sure to exclude any potential phase ambiguities. As we could see from the previous section we are convinced that the PFAFFIAN can be treated as a positive real quantity which we will assume to be true in the following. For this reason, we proceed as in [9] and introduce pseudofermions ξ via

$$\int \mathcal{D}\Psi e^{-S_F} = \text{Pf } \mathcal{O}_F = \left(\det \mathcal{O}_F \mathcal{O}_F^\dagger \right)^{\frac{1}{4}} = \int \mathcal{D}\xi \mathcal{D}\xi^\dagger e^{-S_\xi}, \quad (5.1.32)$$

where

$$S_\xi = g \int dt ds \xi^\dagger \left(\mathcal{O}_F \mathcal{O}_F^\dagger \right)^{-\frac{1}{4}} \xi, \quad (5.1.33)$$

and ξ is a collection of 16 complex bosonic scalar fields. But before we can go any further we need to discretise the action with help of the methods introduced in section 4.1.

5.2 Discretising the action

In the previous steps we have constructed a LAGRANGIAN fitting to our problem and modified terms to be able to apply a RHMC algorithm. To proceed with this task we need a discretised version of the bosonic action and the fermionic operator \mathcal{O}_F .

5.2.1 Bosonic action

For the bosonic term this is quite easy. First we need to do a dimensional analysis of the fields in the action. In the simulation we can only deal with dimensionless fields. Since the action also needs to be dimensionless we can see that the fields x, x^* and z^M are dimensionless as preferred but the auxiliary fields are of dimension $[\phi] = 1/[a]$. We therefore do a redefinition of the discretised fields

$$a\phi(n) \rightarrow \phi(n), \quad a\phi_I(n) \rightarrow \phi_I(n) \quad (5.2.1)$$

in order to have dimensionless quantities as well. We can now write the discretised version of the bosonic action in (5.1.31) as

$$\begin{aligned} \hat{S}_B = g \sum_{n \in \Lambda} & \left[\left| x(n + \hat{0}) + \left(\frac{M}{2} - 1 \right) x(n) \right|^2 + \frac{1}{[z(n)]^4} \left| x(n + \hat{1}) - \left(\frac{M}{2} + 1 \right) x(n) \right|^2 \right. \\ & + \sum_{M=1}^6 \left\{ \left(z^M(n + \hat{0}) + \left(\frac{M}{2} - 1 \right) z^M(n) \right)^2 \right. \\ & \quad \left. + \frac{1}{[z(n)]^4} \left(z^M(n + \hat{1}) - \left(\frac{M}{2} + 1 \right) z^M(n) \right)^2 \right\} \\ & \left. + \phi^2(n) + \sum_{I=1}^{16} [\phi_I(n)]^2 \right], \end{aligned} \quad (5.2.2)$$

where we applied a simple forward derivative to the x, x^* and z^M fields and introduced the dimensionless lattice mass parameter $M = ma$.

5.2.2 Wilson term

Before discretising the fermionic operator we have to think about the doubling problem arising through naively discretised first order derivatives, discussed in subsection 4.2.2. The free fermionic operator (evaluated in the bosonic vacuum) represented in a momentum basis reads

$$K_F = \begin{pmatrix} 0 & -p_0 \mathbb{1}_4 & (p_1 - i \frac{m}{2}) \rho^M u^M & 0 \\ -p_0 \mathbb{1}_4 & 0 & 0 & (p_1 - i \frac{m}{2}) \rho_M^\dagger u^M \\ - (p_1 + i \frac{m}{2}) \rho^M u^M & 0 & 0 & -p_0 \mathbb{1}_4 \\ 0 & - (p_1 + i \frac{m}{2}) \rho_M^\dagger u^M & -p_0 \mathbb{1}_4 & 0 \end{pmatrix}, \quad (5.2.3)$$

and has determinant

$$\det K_F = \left(p_0^2 + p_1^2 + \frac{m^2}{4} \right)^8. \quad (5.2.4)$$

The fermionic propagators are proportional to the inverse of dynamic operators. It is therefore reasonable that the naive discretisation (like in (4.2.12))

$$p_i \rightarrow \mathring{p}_i \equiv \frac{1}{a} \sin(p_i a) \quad (5.2.5)$$

will give rise to doublers. For this reason we would like to introduce a WILSON-like term that cancels the additional poles in the fermionic propagator. It should obey the following conditions:

- preserve the maximal amount of symmetries and relevant matrix properties,
- give the correct continuum limit for $a \rightarrow 0$,
- should not give rise to a complex phase.

Due to the properties of \mathcal{O}_F presented in subsection 5.1.3 we can see that there is only a small margin of variations that we can apply to the fermion matrix as a WILSON term and that respects the $U(1)$ and $SO(6)$ symmetries. In fact it was not possible to construct such an operator that also preserves relevant matrix properties like skew- and Γ_5 -symmetry and also leads to the correct perturbative 1-loop coefficient in (3.4.6).

We therefore chose to explicitly break the $U(1)$ symmetry and introduce a WILSON-like operator on the diagonal blocks of \mathcal{O}_F . In terms of the free fermion operator in momentum space this takes the form

$$\hat{K}_F = \begin{pmatrix} W_+ & -\hat{p}_0 \mathbb{1}_4 & (\hat{p}_1 - i\frac{m}{2}) \rho^M u^M & 0 \\ -\hat{p}_0 \mathbb{1}_4 & -W_+^\dagger & 0 & (\hat{p}_1 - i\frac{m}{2}) \rho_M^\dagger u^M \\ -(\hat{p}_1 + i\frac{m}{2}) \rho^M u^M & 0 & W_- & -\hat{p}_0 \mathbb{1}_4 \\ 0 & -(\hat{p}_1 + i\frac{m}{2}) \rho_M^\dagger u^M & -\hat{p}_0 \mathbb{1}_4 & -W_-^\dagger \end{pmatrix}, \quad (5.2.6)$$

where

$$W_\pm = \frac{ra}{2} (\hat{p}_0^2 \pm i\hat{p}_1^2) \rho^M u^M, \quad |r| = 1, \quad (5.2.7)$$

and similar to (4.2.16)

$$\hat{p}_i \equiv \frac{2}{a} \sin \frac{p_i a}{2}. \quad (5.2.8)$$

This leads to the analogue expression of (5.2.4)

$$\det \hat{K}_F = \left(\hat{p}_0^2 + \hat{p}_1^2 + \frac{r^2 a^2}{4} (\hat{p}_0^4 + \hat{p}_1^4) + \frac{m^2}{4} \right)^8. \quad (5.2.9)$$

If we substitute this into the denominator of (3.7.4) and apply the replacement $p_i^2 \rightarrow \hat{p}_i^2$ in the numerator, the discretised equivalent of the 1-loop free energy can be defined by

$$\Gamma_{\text{LAT}}^{(1)} = -\ln Z_{\text{LAT}}^{(1)} \equiv \mathcal{I}(a). \quad (5.2.10)$$

With $r = 1$ and rescaled momentum integration over the first BRILLOUINE zone this results in

$$\begin{aligned} \mathcal{I}(a) = \frac{V_2}{2a^2} \int_{-\pi}^{\pi} \frac{d^2 p}{(2\pi)^2} & \left\{ 5 \ln \left[4 \left(\sin^2 \frac{p_0}{2} + \sin^2 \frac{p_1}{2} \right) \right] \right. \\ & + 2 \ln \left[4 \left(\sin^2 \frac{p_0}{2} + \sin^2 \frac{p_1}{2} + \frac{M^2}{8} \right) \right] \\ & + \ln \left[4 \left(\sin^2 \frac{p_0}{2} + \sin^2 \frac{p_1}{2} + \frac{M^2}{4} \right) \right] \\ & \left. - 8 \ln \left[4 \sin^4 \frac{p_0}{2} + \sin^2 p_0 + 4 \sin^4 \frac{p_1}{2} + \sin^2 p_1 + \frac{M^2}{4} \right] \right\}. \end{aligned} \quad (5.2.11)$$

For a consistent discretisation this should lead to the same result as (3.7.4) in the $a \rightarrow 0$ limit. And indeed a numerical integration of (5.2.11) yields

$$\Gamma^{(1)} = -\ln Z^{(1)} = \lim_{a \rightarrow 0} \mathcal{I}(a) = -\frac{3 \ln 2}{8\pi} |A| M^2, \quad (5.2.12)$$

where we used that $V_2 = a^2|A| = a^2LT$ and we are left with the expected result. Given the structure of the WILSON term in the vacuum it is quite natural to generalise it to the interacting case. The discretised momentum space operator therefore reads

$$\tilde{\mathcal{O}}_F = \begin{pmatrix} W_+ & -\dot{p}_0 \mathbb{1}_4 & (\dot{p}_1 - i\frac{m}{2}) \rho^M u^M & 0 \\ -\dot{p}_0 \mathbb{1}_4 & -W_+^\dagger & 0 & (\dot{p}_1 - i\frac{m}{2}) \rho_M^\dagger u^M \\ -(\dot{p}_1 + i\frac{m}{2}) \rho^M u^M & 0 & 2\frac{z^M}{z^4} \rho^M (\partial_s x - \frac{m}{2} x) + W_- & -\dot{p}_0 \mathbb{1}_4 \\ 0 & -(\dot{p}_1 + i\frac{m}{2}) \rho_M^\dagger u^M & -\dot{p}_0 \mathbb{1}_4 & -2\frac{z^M}{z^4} \rho_M^\dagger (\partial_s x^* - \frac{m}{2} x^*) - W_-^\dagger \end{pmatrix}, \quad (5.2.13)$$

with

$$W_\pm = \frac{ra}{2z^2} (\hat{p}_0^2 \pm i\hat{p}_1^2) \rho^M z^M, \quad (5.2.14)$$

where an additional $1/z$ factor is present for the purpose of improved stability during simulations. From (5.1.24) one can see that the added WILSON term respects the Γ_5 -HERMITICITY and skew-symmetry which ensures the determinant to be real and positive.

5.2.3 Fermionic operator

By knowing the structure of the WILSON term we can finally discretise the fermionic operator and write it in terms of a single matrix by using the lexicographic index notation introduced in section 4.1. The discretised fermion matrix $\hat{\mathcal{O}}_F$ is of size $16V \times 16V$ and we are going to subdivide it into 4 by 4 blocks of size $4V \times 4V$ as

$$(\hat{\mathcal{O}}_F)_{16V \times 16V} = \begin{pmatrix} \hat{\mathcal{O}}_{4V \times 4V} & \cdots & \cdots & \cdots \\ \vdots & \ddots & & \\ \vdots & & \ddots & \\ \vdots & & & \ddots \end{pmatrix}. \quad (5.2.15)$$

To build the block matrices we assume that for every lattice index $l, p = 0, \dots, (V-1)$ we have a 4×4 matrix with indices $i, j = 1, \dots, 4$ and emphasise the structure

$$\hat{\mathcal{O}}_{4 \times 4}(V \times V) \longleftrightarrow \hat{\mathcal{O}}_{ij}(l, p). \quad (5.2.16)$$

One can map this to a $4V \times 4V$ matrix with global indices like

$$\hat{\mathcal{O}}_{4V \times 4V} \longleftrightarrow \hat{\mathcal{O}}_{AB}, \quad A = 4l + i, \quad B = 4p + j. \quad (5.2.17)$$

The discretised fermion matrix is now given by

$$\hat{\mathcal{O}}_F = \begin{pmatrix} \hat{W}_+ & i\bar{\Delta}_0^A & -i(\vec{\Delta}_1^Z + \frac{M}{2}\bar{Z}) & 0 \\ i\bar{\Delta}_0^A & -\hat{W}_+^\dagger & 0 & -i(\vec{\Delta}_1^{Z^\dagger} + \frac{M}{2}\bar{Z}^\dagger) \\ i(\vec{\Delta}_1^Z - \frac{M}{2}\bar{Z}) & 0 & 2(\bar{\Delta}_1^x - \frac{M}{2}\bar{Z}^x) + \hat{W}_- & i\bar{\Delta}_0^A - \hat{A}^T \\ 0 & i(\vec{\Delta}_1^{Z^\dagger} - \frac{M}{2}\bar{Z}^\dagger) & i\bar{\Delta}_0^A + \hat{A} & 2(\bar{\Delta}_1^{x^*} - \frac{M}{2}\bar{Z}^{x^*}) - \hat{W}_-^\dagger \end{pmatrix}, \quad (5.2.18)$$

where we refer the reader to Appendix E for a detailed derivation of the single terms.

5.3 Applying the RHMC algorithm

Since the current status is a realisation of discretised operators and fields that are also dimensionless, we can return to a discretised version of the equations (5.1.30-5.1.33) and implement a RHMC algorithm based on HMC algorithm introduced in section 4.3.3. There we described the algorithm by means of an inverse HERMITIAN operator in the pseudofermionic action

$$\hat{S}_\xi = g\xi^\dagger \left(\hat{M}^\dagger \hat{M} \right)^{-1} \xi, \quad (5.3.1)$$

where we applied a matrix-vector notation in the sense of (4.1.10). In our present case we are instead faced with

$$\hat{S}_\xi = g\xi^\dagger \left(\hat{\mathcal{O}}_F^\dagger \hat{\mathcal{O}}_F \right)^{-\frac{1}{4}} \xi. \quad (5.3.2)$$

To treat this kind of matrix valued function one uses a rational approximation

$$\left(\hat{M}^\dagger \hat{M} \right)^\rho = \alpha_0 + \sum_{i=1}^P \frac{\alpha_i}{\hat{M}^\dagger \hat{M} + \beta_i \mathbb{1}}, \quad (5.3.3)$$

where α_i and β_i are constant coefficients. For predicted limits of the eigenvalues λ_{\min} and λ_{\max} of a matrix and of course a given exponent ρ one can use a REMEZ algorithm to obtain the coefficients α_i and β_i up to some order P of accuracy of the approximation, valid for any matrix satisfying the spectral bounds.

For the implementation of the RHMC we need two sets of coefficients for two different approximations with $\rho = 1/8$ and $\rho = -1/4$, respectively. The requirement of $\rho = -1/4$ should be clear, but we also need an approximation with $\rho = 1/8$ to generate pseudofermionic fields³

$$\xi = \left(\hat{\mathcal{O}}_F^\dagger \hat{\mathcal{O}}_F \right)^{\frac{1}{8}} \vartheta \quad (5.3.4)$$

distributed according to

$$\exp \left(-\vartheta^\dagger \vartheta \right) = \exp \left(-\xi^\dagger \left(\hat{\mathcal{O}}_F^\dagger \hat{\mathcal{O}}_F \right)^{-\frac{1}{4}} \xi \right). \quad (5.3.5)$$

We use an order $P = 15$ approximation and the utilised values α_i and β_i can be found in Table 6.1. In order to state the full RHMC procedure we want to take a closer look at the pseudofermionic contribution to the bosonic force

$$F_m^\xi[\Phi] = \frac{\partial}{\partial \Phi_m} \left[\xi^\dagger \left(\hat{\mathcal{O}}_F^\dagger \hat{\mathcal{O}}_F \right)^{-\frac{1}{4}} \xi \right], \quad \Phi_m = (x, x^*, z^N, \phi, \phi^I), \quad (5.3.6)$$

with $m = 1, \dots, 25$. Inserting the rational approximation yields⁴

$$\begin{aligned} F_m^\xi[\Phi] &= - \sum_{i=1}^P \alpha_i \left(\frac{1}{\hat{\mathcal{O}}_F^\dagger \hat{\mathcal{O}}_F + \beta_i \mathbb{1}} \xi \right)^\dagger \frac{\partial}{\partial \Phi_m} \left(\hat{\mathcal{O}}_F^\dagger \hat{\mathcal{O}}_F \right) \left(\frac{1}{\hat{\mathcal{O}}_F^\dagger \hat{\mathcal{O}}_F + \beta_i \mathbb{1}} \xi \right) \\ &= - \sum_{i=1}^P \alpha_i \left[\left(\hat{\mathcal{O}}_F s_i \right)^\dagger \frac{\partial \hat{\mathcal{O}}_F}{\partial \Phi_m} s_i + s_i^\dagger \frac{\partial \hat{\mathcal{O}}_F^\dagger}{\partial \Phi_m} \hat{\mathcal{O}}_F s_i \right], \end{aligned} \quad (5.3.7)$$

³Compare to the list of items in section 4.3.3.

⁴With help of the matrix-scalar derivative $\frac{\partial U^{-1}(x)}{\partial x} = -U^{-1} \frac{\partial U}{\partial x} U^{-1}$.

where $s_i = \left(\hat{\mathcal{O}}_F^\dagger \hat{\mathcal{O}}_F + \beta_i \mathbb{1} \right)^{-1} \xi$ are interpreted as the solutions to the matrix equation

$$\left(\hat{\mathcal{O}}_F^\dagger \hat{\mathcal{O}}_F + \beta_i \mathbb{1} \right) s^i = \xi, \quad i = 1, \dots, P. \quad (5.3.8)$$

To obtain all P solutions at once, we employ a *multi-shift conjugate gradient solver* adapted from the `openQCD` package⁵ by Martin Lüscher. The single steps for the RHMC are therefore:

- **Pseudofermions**

Generate the $16V$ -dimensional pseudofermionic field $\xi = \left(\hat{\mathcal{O}}_F^\dagger \hat{\mathcal{O}}_F[\Phi] \right)^{\frac{1}{8}} \vartheta$, where ϑ is distributed according $\exp(-\vartheta^\dagger \vartheta)$.

- **Conjugate fields**

For the initial boson configuration $\Phi = \Phi^{(0)}$ generate $\Pi = \Pi^{(0)}$ according to the GAUSSIAN distribution $\exp\left(-\frac{1}{2}\Pi^2\right)$.

- **Initial step**

$$\Pi_m^{(\frac{1}{2})} = \Pi_m^{(0)} - \frac{\epsilon}{2} F_m[\Phi] \Big|_{\Phi^{(0)}}.$$

- **Intermediate step**

Full steps for $j = 1, \dots, n-1$

$$\Phi_m^{(j)} = \Phi_m^{(j-1)} + \Pi_m^{(j-\frac{1}{2})}, \quad \Pi_m^{(j+\frac{1}{2})} = \Pi_m^{(j-\frac{1}{2})} - \epsilon F_m[\Phi] \Big|_{\Phi^{(j)}}.$$

- **Final step**

$$\Phi'_m = \Phi_m^{(n)} = \Phi_m^{(n-1)} + \Pi_m^{(n-\frac{1}{2})}, \quad \Pi'_m = \Pi_m^{(n)} = \Pi_m^{(n-\frac{1}{2})} - \frac{\epsilon}{2} F_m[\Phi] \Big|_{\Phi^{(n)}}.$$

- **Monte Carlo step**

Accept new configuration Φ' if a random number $r \in [0, 1)$ is smaller than

$$\exp\left(\frac{1}{2}(\Pi^2 - \Pi'^2) + S_B[\Phi] - S_B[\Phi'] + \vartheta^\dagger \vartheta - \xi^\dagger \left(\hat{\mathcal{O}}_F^\dagger \hat{\mathcal{O}}_F[\Phi'] \right)^{-\frac{1}{4}} \xi\right).$$

Hereby we have used

$$F_m[\Phi] = \frac{\partial S_B[\Phi]}{\partial \Phi_m} + F_m^\xi[\Phi]. \quad (5.3.9)$$

⁵<http://luscher.web.cern.ch/luscher/openQCD/>

6

Simulations and observables

In this chapter we will present some basic information on the implementation of the previously discussed algorithm and state the utilised parameters of the conducted simulations. Furthermore we need to discuss how to take the continuum limit of the observables of interest.

6.1 Implementation and the continuum limit

The executables for the Monte Carlo simulation are built from an implementation in the FORTRAN 95 standard and are compiled with an Intel[®] `ifort` compiler¹. For the lattice we deploy several sizes for the spatial extent $L = 8, 10, 12, 16, 24, 32$, whereas the temporal extent is always twice of the spatial one $T = 2L$ for an improved accuracy of the bosonic correlators. Thus we have a world volume of $V_2 = 2a^2L^2$. In the continuum model there are two "bare" parameters that determine its behaviour, the dimensionless coupling $g = \sqrt{\lambda}/4\pi$ and the mass scale m . To take the continuum limit it is necessary to set a line of constant physics when $a \rightarrow 0$ which is said to be the squared physical mass of the field excitations rescaled with the world volume

$$V_2 m_x^2 = \text{const.} \quad (6.1.1)$$

From a dimensional regularisation scheme it is possible to find the corrections to the masses of the bosonic fields x, x^* which read [36]

$$m_x^2(g) = \frac{m^2}{2} \left(1 - \frac{1}{8g} + \mathcal{O}(g^{-2}) \right). \quad (6.1.2)$$

Together with (6.1.1) and for a fixed value of g this leads to

$$\frac{V_2 m^2}{2} = (LM)^2 = \text{const}, \quad (6.1.3)$$

where $M = ma$ is the dimensionless lattice mass scale. The equality (6.1.3) relies on the hypothesis that g is not (infinitely) renormalised². Further the validity of

¹From the Intel[®] Parallel Studio XE 2015.

²This argument can be substantiated by our perturbative knowledge of the scaling function. One could define $f(g)/4 = g + \text{const.} + \mathcal{O}(g^{-1})$ as a renormalised coupling. Since it is linear in g up to first order and does not depend on a renormalisation scale, the β -function is zero and g needs no renormalisation.

(6.1.2) in the discretised model needs to be verified in order the physical masses undergo only a finite renormalisation. This claim is supported by studying x, x^* correlators where indeed no presence of $(1/a)$ divergences in the m_x^2/m^2 ratios can be found. Also for the large g region they reach their expected continuum value of $1/2$. Having this in mind and also the result of the perturbative 1-loop free energy (3.7.4), we assume no further presence of a scale in the discretised model other than the lattice spacing a . Therefore any expectation value of an observable $\langle F_{\text{LAT}} \rangle$ is a function of the "bare" input parameters g, L and M

$$\langle F_{\text{LAT}} \rangle = \langle F_{\text{LAT}}(g, L, M) \rangle = \langle F(g) \rangle + \mathcal{O}(L^{-1}) + \mathcal{O}(e^{-LM}). \quad (6.1.4)$$

For fixed g one chooses a fixed LM , large enough to keep finite volume effects $\mathcal{O}(e^{-LM})$ small. For each finite value L there will be a difference of $\langle F_{\text{LAT}} \rangle$ and its continuum equivalent by means of lattice artefacts $\mathcal{O}(L^{-1})$. The continuum limit $\langle F(g) \rangle$ is obtained via an extrapolation to infinite L .

6.2 Simulation parameters

As mentioned we employ different lattice sizes varying between $L = 8$ and $L = 32$. In the HMC simulation the MD equations of motion are evaluated along a fictitious MC time τ . For one trajectory we utilise a MC time of $\tau = 0.5$ with by default 100 integrator steps and therefore $\epsilon = \delta\tau = 0.005$. For the fractional powers of the fermion matrix we use a rational approximation (5.3.3) of degree $P = 15$ with the two sets of parameters stated in Table 6.1. We checked for a subset of the configurations that its accuracy is always better than 10^{-3} for $\xi^\dagger (\mathcal{O}_F^\dagger \mathcal{O}_F)^{-\frac{1}{4}} \xi$.

ρ	i	α_i	β_i
1/8	0	3.2148873149863206	-
	1	$-2.2977600408751347 \cdot 10^{-9}$	$5.5367335615411457 \cdot 10^{-8}$
	2	$-1.6898103706901084 \cdot 10^{-8}$	$4.6910257304582898 \cdot 10^{-7}$
	3	$-1.1099658368596436 \cdot 10^{-7}$	$2.6768223190551614 \cdot 10^{-6}$
	4	$-7.2162146587729939 \cdot 10^{-7}$	$1.4319657256375662 \cdot 10^{-5}$
	5	$-4.6841070484595924 \cdot 10^{-6}$	$7.5694473187855338 \cdot 10^{-5}$
	6	$-3.0396303865820389 \cdot 10^{-5}$	$3.9922490005559548 \cdot 10^{-4}$
	7	$-1.9723870959636086 \cdot 10^{-4}$	$2.1046795395127538 \cdot 10^{-3}$
	8	$-1.2798599250624023 \cdot 10^{-3}$	$1.1094832053548640 \cdot 10^{-2}$
	9	$-8.3051856063983548 \cdot 10^{-3}$	$5.8486687698920667 \cdot 10^{-2}$
	10	$-5.3904877281192094 \cdot 10^{-2}$	$3.0834388405073770 \cdot 10^{-1}$
	11	$-3.5026088217184553 \cdot 10^{-1}$	1.6264534005778293
	12	-2.2893521967679966	8.6030459456576764
	13	$-1.5436668340425719 \cdot 10$	$4.6179583183155444 \cdot 10$
	14	$-1.2297861076048798 \cdot 10^2$	$2.6854965277696181 \cdot 10^2$
	15	$-2.6252652966414048 \cdot 10^3$	$2.6004158696112045 \cdot 10^3$
	0	$9.5797060554725838 \cdot 10^{-2}$	-

	1	$1.7701746700099842 \cdot 10^{-6}$	$3.1085594175442315 \cdot 10^{-8}$
	2	$5.8705983656937455 \cdot 10^{-6}$	$3.2994455960441383 \cdot 10^{-7}$
	3	$1.9961158693570120 \cdot 10^{-5}$	$1.9424842756552213 \cdot 10^{-6}$
	4	$6.9125367600088173 \cdot 10^{-5}$	$1.0453359626231250 \cdot 10^{-5}$
	5	$2.4032965323696816 \cdot 10^{-4}$	$5.5337819905761986 \cdot 10^{-5}$
	6	$8.3620125835371663 \cdot 10^{-4}$	$2.9204178440857227 \cdot 10^{-4}$
-1/4	7	$2.9099006745502945 \cdot 10^{-3}$	$1.5403300046437174 \cdot 10^{-3}$
	8	$1.0126504714418652 \cdot 10^{-2}$	$8.1233558140562465 \cdot 10^{-3}$
	9	$3.5241454044660878 \cdot 10^{-2}$	$4.2840454273820550 \cdot 10^{-2}$
	10	$1.2266034741624667 \cdot 10^{-1}$	$2.2594500626442715 \cdot 10^{-1}$
	11	$4.2721681852328125 \cdot 10^{-1}$	1.1921171782283737
	12	1.4932820692676758	6.3026182343759860
	13	5.3188766358452595	$3.3683411978650057 \cdot 10$
	14	$2.0944763089672641 \cdot 10^1$	$1.9083658214156412 \cdot 10^2$
	15	$1.4525770103354523 \cdot 10^2$	$1.5386784635765257 \cdot 10^3$

Table 6.1 Two sets of coefficients used for the rational approximation (5.3.3) sufficient for the exponents $\rho = 1/8$ and $\rho = -1/4$, respectively.

In Table F.1 we list the parameters of the simulations presented in this thesis. For each set of parameters we collected a certain amount of data points. Their total number would cover a trajectory of the length of the corresponding MDU value stated in the table. In most cases data has been collected along independent trajectories, launched from different start configurations which are referred to as replica. These can be used to improve statistics. We also determined auto-correlation times of the main observables, the correlator $\langle x^*x \rangle$ and the action $\langle S_{\text{cusp}} \rangle$ (which will be subject of the next section), and included their effect in the error analysis [37]. The meaning of the Q-value, given in the table, is defined in [37]. It reveals information about the quality of an observable with respect to their replica. One derives the mean value for each replicum and analyses the distribution of these means in comparison to the total mean of all replica. The Q-value is of course more meaningful if there is a high number of replica.

Additional simulations have been conducted for fixed $LM = 6$ to check for the influence of finite volume effects and with $r = 0$ which means without the presence of a WILSON term to check its influence on the observables.

We can observe that for lower g values the simulations become more involved. For too small values of g the conjugate gradient method to solve (5.3.8) does not converge. This is due to the eigenvalue spectrum of the fermion matrix $\hat{\mathcal{O}}_F$ shown in Figure 6.1. For small g the condition number of $\hat{\mathcal{O}}_F$ (which is basically the ratio of the largest and smallest eigenvalue) becomes very bad. The smallest eigenvalues are so close to zero that they might leave the regime of accuracy of the rational approximation (5.3.3) and are within the range of errors of the conjugate gradient solver which could cause a phase transition of the PFAFFIAN. During our simulation with $LM = 4$ and a present WILSON term this behaviour occurred for the first time for $g = 5$. We tried to cure this peculiarity with help of a reweighting procedure which was introduced first in [38] (see also [39, 40]).

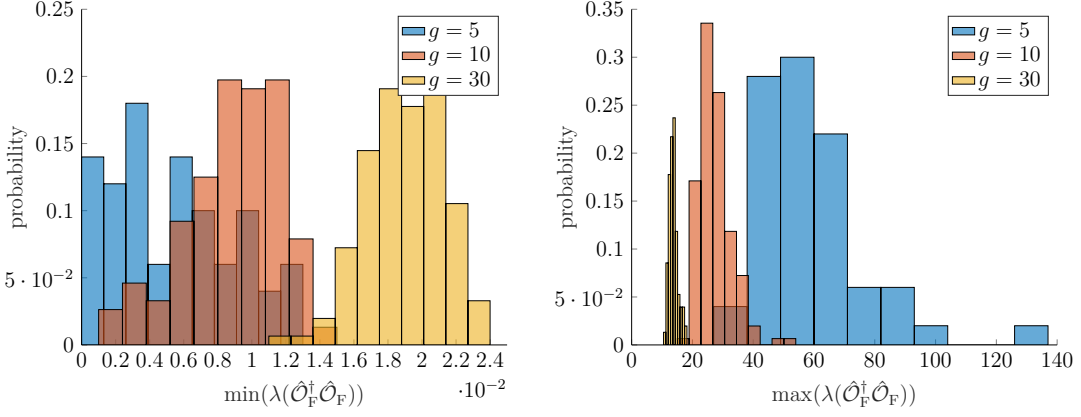


Figure 6.1 Histogram plot of the distribution of the minimal and maximal eigenvalue of the operator $\hat{O}_F \hat{O}_F^\dagger$ for one replicum with 400 field configurations for $L = 12$ and $g = 5, 10, 30$. For high values of g the smallest eigenvalues are clearly separated from zero which ensures the stability of the simulation. With decreasing g the smallest eigenvalues come arbitrarily close to zero whereas the largest eigenvalues increase at the same time which leads to high condition numbers of the fermionic operator and threatens the stability of the simulation.

Therefore we add a twisted mass term to the fermionic matrix to obtain

$$\tilde{\mathcal{O}}_F = \hat{\mathcal{O}}_F + i\mu\Gamma_5, \quad \tilde{\mathcal{O}}_F \tilde{\mathcal{O}}_F^\dagger = \hat{\mathcal{O}}_F \hat{\mathcal{O}}_F^\dagger + \mu^2 \mathbf{1}, \quad (6.2.1)$$

where μ is the reweighting mass parameter. The term $\mu^2 \mathbf{1}$ will shift the eigenvalues of $\tilde{\mathcal{O}}_F \tilde{\mathcal{O}}_F^\dagger$ apart from zero and ensures the stability of the simulation. Hereby the crucial term in measuring an observable is the PFAFFIAN which is included in the probability distribution in the RHMC. We want to estimate observables generated from a distribution without an additional mass term by actually doing simulations with a twisted mass. While assuming the PFAFFIAN to be positive we can write

$$\begin{aligned} \text{Pf}(\hat{\mathcal{O}}_F) &= \left(\frac{\det(\hat{\mathcal{O}}_F \hat{\mathcal{O}}_F^\dagger)}{\det(\tilde{\mathcal{O}}_F \tilde{\mathcal{O}}_F^\dagger)} \right)^{\frac{1}{4}} \text{Pf}(\tilde{\mathcal{O}}_F) \\ &\equiv W \text{Pf}(\tilde{\mathcal{O}}_F). \end{aligned} \quad (6.2.2)$$

For a small reweighting mass μ we can thus compute an estimate of the observable vev without the twisted mass $\langle O \rangle_0$ via

$$\langle O \rangle_0 = \frac{\langle OW \rangle_\mu}{\langle W \rangle_\mu}. \quad (6.2.3)$$

The vev $\langle O \rangle_\mu$ represents the value obtained from a RHMC simulation with twisted mass term and W is the reweighting factor defined in (6.2.2). It can be expressed in terms of $\tilde{W} = W^4$ which can be rewritten to

$$\tilde{W} = \frac{\det(\hat{\mathcal{O}}_F \hat{\mathcal{O}}_F^\dagger)}{\det(\hat{\mathcal{O}}_F \hat{\mathcal{O}}_F^\dagger + \mu^2)} = \frac{1}{\det\left(\mathbf{1} + \frac{\mu^2}{\hat{\mathcal{O}}_F \hat{\mathcal{O}}_F^\dagger}\right)} \equiv \frac{1}{\det M}. \quad (6.2.4)$$

In a separate MC integration we estimate \widetilde{W} by using

$$\frac{1}{\det M} = \int \mathcal{D}\xi \, e^{-\xi^\dagger M \xi} = \int \mathcal{D}\xi \, \left(\frac{e^{-\xi^\dagger M \xi}}{\rho(\xi)} \right) \rho(\xi), \quad (6.2.5)$$

where the complex fields ξ are distributed according to $\rho(\xi)$ so that by (4.3.14) we can write

$$\frac{1}{\det M} = \left\langle \frac{e^{-\xi^\dagger M \xi}}{\rho(\xi)} \right\rangle_\rho. \quad (6.2.6)$$

With a GAUSSIAN distribution $\rho(\xi) = \exp(-\xi^\dagger \xi)$ we find the stochastic estimation

$$\begin{aligned} \widetilde{W} &= \left\langle \exp \left[-\xi^\dagger \left(\frac{\mu^2}{\hat{\mathcal{O}}_F \hat{\mathcal{O}}_F^\dagger} \right) \xi \right] \right\rangle_\rho \\ &= \frac{1}{N_\xi} \sum_{k=1}^{N_\xi} \exp \left[-\xi_k^\dagger \left(\frac{\mu^2}{\hat{\mathcal{O}}_F \hat{\mathcal{O}}_F^\dagger} \right) \xi_k \right] + \mathcal{O} \left(\frac{1}{\sqrt{N_\xi}} \right). \end{aligned} \quad (6.2.7)$$

The reweighting procedure is of course also limited in its application and is only valid for small shifts μ . We therefore choose μ as small as possible, but large enough to ensure the stability of the simulation. Reweighting has only been applied for the collection of data with $g = 5$. A plot of the reweighting factors for a collection of field configurations is given in Figure 6.2.

6.3 Observables

As pointed out earlier we are utmost interested in obtaining information on the scaling function $f(g)$. In our numerical simulation we are basically restricted to calculate observable vevs and therefore need to find a suitable observable providing a connection to $f(g)$. By recapitulating (3.5.1) we can write

$$-\ln Z_{\text{cusp}} = \frac{1}{8} f(g) V_2. \quad (6.3.1)$$

With $Z_{\text{cusp}} = \int \mathcal{D}\delta X \mathcal{D}\delta \Psi \, e^{-S_{\text{cusp}}}$ and the structure of the action

$$S_{\text{cusp}} = g \int dt ds \, \mathcal{L}_{\text{cusp}} \quad (6.3.2)$$

we find

$$\langle S_{\text{cusp}} \rangle = \frac{\int \mathcal{D}\delta X \mathcal{D}\delta \Psi \, S_{\text{cusp}} e^{-S_{\text{cusp}}}}{\int \mathcal{D}\delta X \mathcal{D}\delta \Psi \, e^{-S_{\text{cusp}}}} = -g \frac{d \ln Z_{\text{cusp}}}{dg} \equiv g \frac{V_2}{2} f'(g). \quad (6.3.3)$$

We can therefore obtain information on the derivative of the scaling function from the vev of the action.

To motivate our line of constant physics, we investigate the mass of the bosonic fluctuation field x around the string vacuum which can be obtained from the correlation function $\langle xx^* \rangle$.

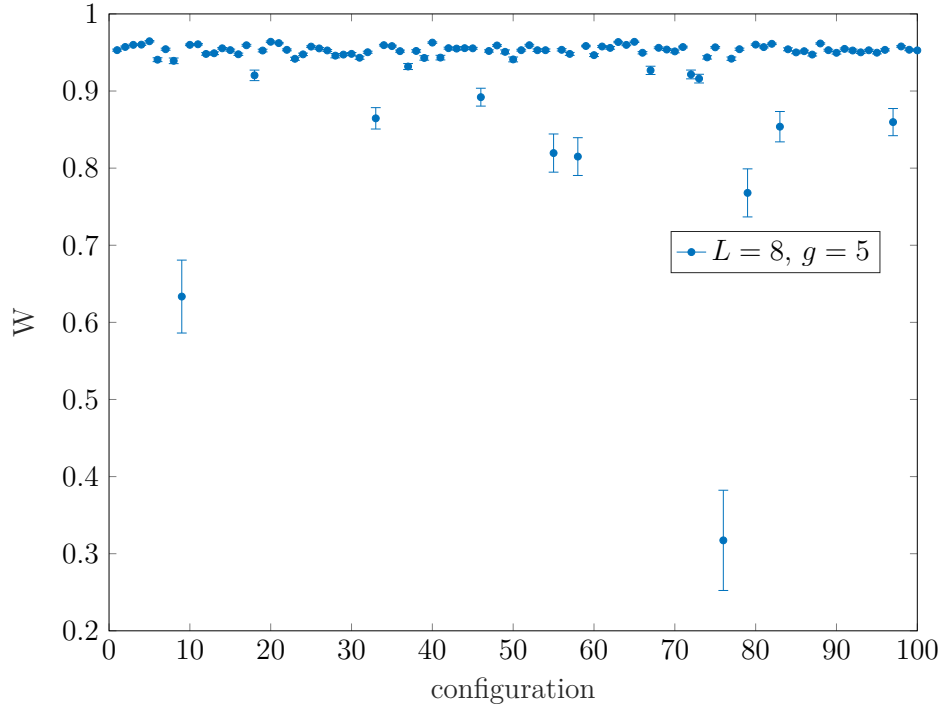


Figure 6.2 The reweighting factor W for a collection of 100 field configurations for $L = 8$ and $g = 5$. Most values are very close to one, pointing out a good estimate in this region, but there are also a few much lower values that might indicate a transition of the PFAFFIAN phase and therefore a too small μ .

6.3.1 The $\langle x x^* \rangle$ correlator

We define the physical masses of the x, x^* fields as the values of the energy at vanishing momentum. In the large coupling limit the mass can be read off from a quadratic expansion of the LAGRANGIAN [10] to

$$\frac{m_x^2}{m^2} \stackrel{g \gg 1}{=} \frac{1}{2}. \quad (6.3.4)$$

The leading quantum corrections to the dispersion limit of the regarding fields have been computed in [36], leading to (6.1.2). We can determine the mass for different values of the coupling to estimate a dependence of m_x^2 of g . For a fixed value of g one can calculate the physical mass on the lattice with timeslice correlation functions derived from the connected two-point functions

$$G_x(t_1, s_1; t_2, s_2) = \langle x(t_1, s_1) x^*(t_2, s_2) \rangle_c, \quad (6.3.5)$$

which coincide with the regular two-point functions in the case of a present $SO(2)$ symmetry. A FOURIER transform in the spatial components results in the *timeslice correlator*

$$C_x(t, k) = \frac{1}{L} \sum_{s_1, s_2} e^{-ik(s_1 - s_2)} G_x(t, s_1; 0, s_2). \quad (6.3.6)$$

Thinking in terms of particle eigenstates $|k\rangle = |k, \alpha\rangle$, where k corresponds to the spatial momentum and α to different energy states, one would find for a

momentum and energy operator P and H

$$P|k, \alpha\rangle = k|k, \alpha\rangle, \quad (6.3.7)$$

$$H|k, \alpha\rangle = E(k, \alpha)|k, \alpha\rangle. \quad (6.3.8)$$

We can therefore think in general of $C(t, k)$ representing (see [31])

$$C(t, k) = \langle k|e^{-tH}|k\rangle = \sum_{\alpha} |c_{\alpha}|^2 e^{-tE(k, \alpha)}. \quad (6.3.9)$$

For large t the lowest energy $E(k, 0)$ dominates the timeslice correlator. It can be recognised as the energy of a one-particle state and we can identify a physical mass with the energy at vanishing momentum

$$m \equiv E(0, 0). \quad (6.3.10)$$

For the x fields we can therefore make the same assumptions and identify

$$C_x(t) \equiv C_x(t, 0) \stackrel{t \gg 1}{\sim} e^{-tm_{x\text{LAT}}}, \quad m_{x\text{LAT}} = E_x(k=0). \quad (6.3.11)$$

The temporal boundary conditions on the lattice require to respect also a left moving part, since

$$C_x(t) = C_x(T-t) \quad (6.3.12)$$

and thus

$$C_x(t) \stackrel{t \gg 1}{\sim} e^{-tm_{x\text{LAT}}} + e^{-(T-t)m_{x\text{LAT}}} \sim \cosh\left(\left(\frac{T}{2} - t\right)m_{x\text{LAT}}\right). \quad (6.3.13)$$

On the lattice we can determine $m_{x\text{LAT}}$ as a limit of an *effective mass* m_x^{eff} . For fixed values of g and T we can estimate $m_x^{\text{eff}}(g, T)$ by a fit of the timeslice correlator $C_x(t)$ to the curve (see Figure 6.3)

$$A \cdot e^{-Tm_x^{\text{eff}}/2} \cdot \cosh\left(\left(\frac{T}{2} - t\right)m_x^{\text{eff}}\right). \quad (6.3.14)$$

We usually omit the points close to $T/2$ from the fit since they are afflicted with large errors. To obtain the continuum value, we extrapolate $m_x^{\text{eff}}(g, T)$ for different lattice sizes (see Figure 6.4) to find

$$m_{x\text{LAT}}(g) = \lim_{T \rightarrow \infty} m_x^{\text{eff}}(g, T). \quad (6.3.15)$$

To improve the fit that estimates m_x^{eff} we chose the temporal lattice extent to be twice the spatial one. There is in fact another issue we need to consider. A present WILSON term breaks the $SO(2)$ symmetry and the connected correlators do not coincide with the disconnected ones. With the spatially FOURIER transformed fields at zero momentum

$$\tilde{x}(t) \equiv \frac{1}{\sqrt{L}} \sum_s x(t, s) \quad (6.3.16)$$

we can rewrite the timeslice correlators in the following way

$$C_x(t) = \langle \tilde{x}(t) \tilde{x}^*(0) \rangle_c, \quad (6.3.17)$$

where the connected correlator is defined as

$$\langle \tilde{x}(t) \tilde{x}^*(0) \rangle_c \equiv \langle \tilde{x}(t) \tilde{x}^*(0) \rangle - \langle \tilde{x} \rangle \langle \tilde{x}^* \rangle \quad (6.3.18)$$

In the lattice simulation we implement the x field as its real and imaginary part x_R and x_I and thus want to write the correlator in terms of these components

$$\begin{aligned} \langle \tilde{x}(t) \tilde{x}^*(0) \rangle_c &= \langle \tilde{x}_R(t) \tilde{x}_R(0) \rangle + \langle \tilde{x}_I(t) \tilde{x}_I(0) \rangle \\ &\quad + i (\langle \tilde{x}_I(t) \tilde{x}_R(0) \rangle - \langle \tilde{x}_R(t) \tilde{x}_I(0) \rangle) \\ &\quad - \langle \tilde{x}_R \rangle^2 - \langle \tilde{x}_I \rangle^2. \end{aligned} \quad (6.3.19)$$

The second line will vanish according to translational invariance and time reversal. We can thus calculate the connected timeslice correlators as

$$C_x(t) = \langle \tilde{x}_R(t) \tilde{x}_R(0) \rangle + \langle \tilde{x}_I(t) \tilde{x}_I(0) \rangle - \langle \tilde{x}_R \rangle^2 - \langle \tilde{x}_I \rangle^2. \quad (6.3.20)$$

Numerically we checked the two conditions

$$\begin{aligned} \langle \tilde{x}_k(t) \tilde{x}_i(0) \rangle_c &= 0 \quad \text{for } k \neq i, \quad k, i \in \{R, I\}, \\ \langle \tilde{x}_R \rangle &= -\langle \tilde{x}_I \rangle. \end{aligned} \quad (6.3.21)$$

Applying these we can calculate the connected timeslice correlator via

$$C_x(t) = \langle \tilde{x}_R(t) \tilde{x}_R(0) + \tilde{x}_I(t) \tilde{x}_I(0) + \tilde{x}_R(t) \tilde{x}_I(0) + \tilde{x}_I(t) \tilde{x}_R(0) \rangle. \quad (6.3.22)$$

We want to emphasise here that we can subtract the non-connected part for every configuration and then do the average. This reduces the statistical errors compared to the previous method.

6.3.2 The cusp action

To measure the action (6.3.3) we first explore the regime of large g . With fixed $LM = 4$ which we think is large enough to omit finite volume effects we recover, according to (6.1.4), the following lattice observable, behaving linear in g and containing a quadratic divergence in L in the continuum limit

$$\langle S_{\text{LAT}} \rangle = S_0 + \frac{c}{2} (2L^2) + \mathcal{O}(L^{-1}), \quad g \gg 1. \quad (6.3.23)$$

In the continuum we would find

$$\langle S_{\text{cusp}} \rangle = g \frac{V_2}{8} f'(g) \stackrel{g \gg 1}{\approx} \frac{V_2}{2} g \equiv S_0, \quad (6.3.24)$$

leading to a possible description of $f'(g)$ given by

$$\frac{\langle S_{\text{cusp}} \rangle}{S_0} = \frac{f'(g)}{4}. \quad (6.3.25)$$

For a discretised version nonetheless we have to include the mass scale for the action to be dimensionless with respect to the lattice spacing

$$S_0 = \frac{V_2}{2} m^2 g = \frac{1}{2} (2L^2) M^2 g. \quad (6.3.26)$$

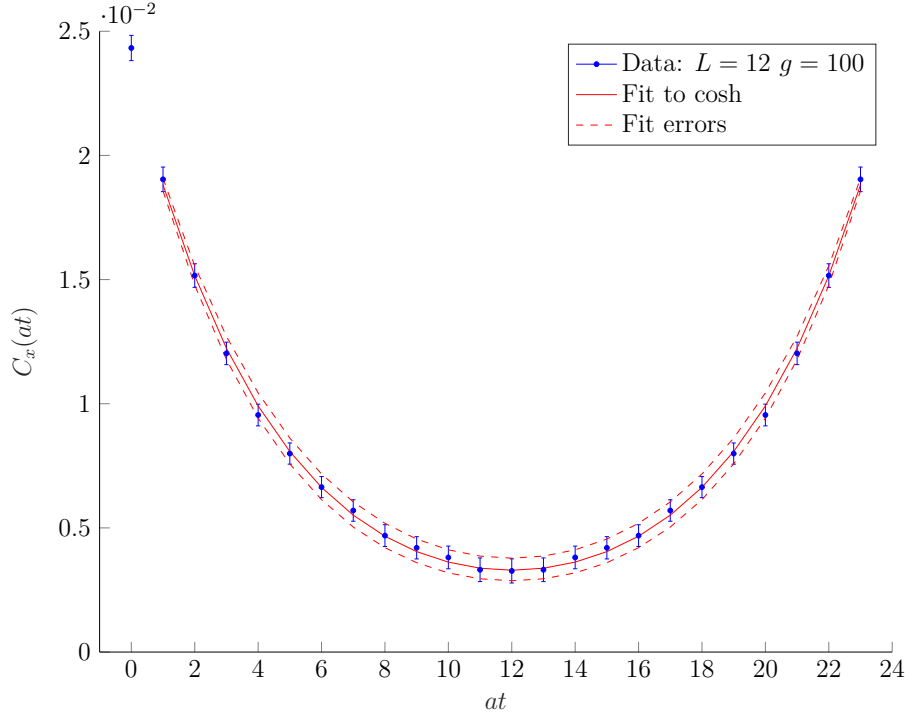


Figure 6.3 Plot of the timeslice correlator $C_x(t)$ for a measurement of 400 field configurations with $L = 12$ and $g = 100$ without a WILSON term (blue dots). The parameters A and m_x^{eff} have been determined by a fit and the corresponding curve (6.3.14) is given in red with the errors of the effective mass as dashed lines.

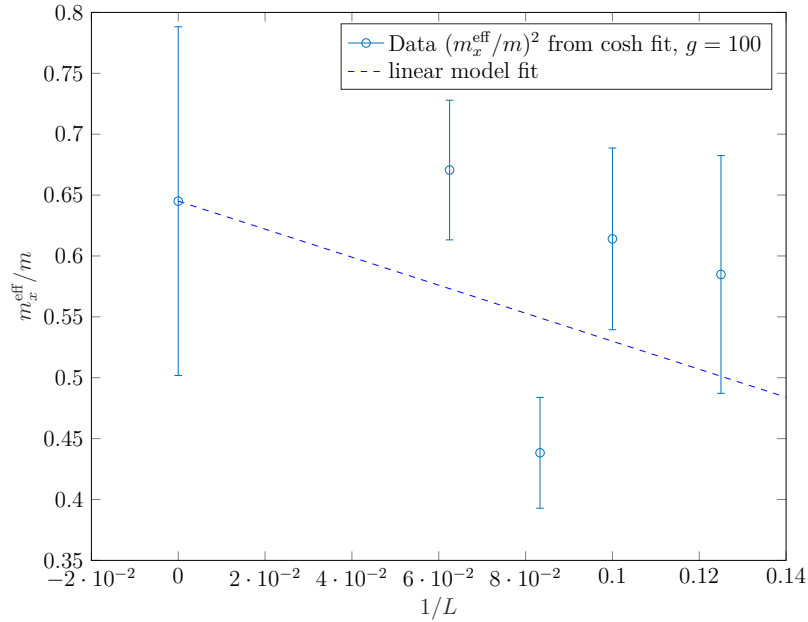


Figure 6.4 This plot shows a simple example of a continuum extrapolation for $m_{x\text{LAT}}$ with $g = 100$ in absence of a WILSON term. Every point represents a value $m_x^{\text{eff}}(T)$ generated from one replicum with 400 field configurations each. The result of the linear regression is added as a point with errorbars at zero.

Furthermore we recall the behaviour $f(g) = 4g + \text{const.} + \mathcal{O}(g^{-1})$ from (3.4.6) and insert $V_2 = a^2(TL) = a^2(2L^2)$, since we always use $T = 2L$. S_0 is the discretised classical action and its value is fixed in each simulation for given g and LM . In (6.3.23) we observe a term quadratically divergent in L in the continuum limit. To motivate the appearance of such behaviour let us recall that we calculate the vev of the cusp action via

$$\langle S_{\text{cusp}} \rangle = -g \frac{d \ln Z_{\text{cusp}}}{dg}. \quad (6.3.27)$$

and focus especially on any contribution to the partition function that is of quadratic order in the bosonic and fermionic fields $Z_{\text{cusp}}^{(2)} = Z_{\text{B}}^{(2)} Z_{\text{F}}^{(2)}$. For these contributions we can schematically write

$$\begin{aligned} Z_{\text{B}}^{(2)} &= \int \prod_{n=1}^{N_{\text{B}}} \mathcal{D}\phi_n e^{-g \sum_{i=1}^{N_{\text{B}}} \int dt ds \phi_i \mathcal{O}_i \phi_i} \\ &\stackrel{\text{LAT}}{=} \int \prod_{n=1}^{N_{\text{B}}} \left(\prod_{k=1}^{|A|} d\phi_n^{(k)} \right) e^{-g \sum_{i=1}^{N_{\text{B}}} \phi_i^T \hat{\mathcal{O}}_i \phi_i} \\ &= \prod_{i=1}^{N_{\text{B}}} \frac{1}{\sqrt{\det(g \hat{\mathcal{O}}_i)}} = g^{-N_{\text{B}} \frac{V}{2}} \prod_{i=1}^{N_{\text{B}}} \frac{1}{\sqrt{\det \hat{\mathcal{O}}_i}}, \end{aligned} \quad (6.3.28)$$

where $V = |A|$ and N_{B} is the number of bosonic fields ϕ_i . In the same manner we find (with the number of fermions N_{F})

$$Z_{\text{F}}^{(2)} = g^{N_{\text{F}} \frac{V}{2}} \text{Pf}(\hat{\mathcal{O}}_{\text{F}}) \quad (6.3.29)$$

and thus

$$\begin{aligned} \langle S_{\text{cusp}}^{(2)} \rangle &= -g \frac{d}{dg} \left(-\frac{V}{2} N_{\text{B}} \ln g - \frac{1}{2} \sum_{i=1}^{N_{\text{B}}} \ln(\det \hat{\mathcal{O}}_i) + \frac{V}{2} N_{\text{F}} \ln g + \ln(\text{Pf} \hat{\mathcal{O}}_{\text{F}}) \right) \\ &= \frac{V}{2} (N_{\text{B}} - N_{\text{F}}). \end{aligned} \quad (6.3.30)$$

This divergence with respect to the lattice volume is arising from all quadratic field contributions due to the non-equality of boson and fermion numbers. After the HS transformation we have an additional amount of 17 auxiliary fields and in total 25 bosonic fields in contrast to 16 independent fermionic quantities.

The fermionic contribution to (6.3.3) is solely of quadratic order and will result in a divergent term only and is thus not relevant to measure $f'(g)$. Out of this reason it is conventional to omit the coupling from the (pseudo) fermionic part of the action. In the observable $\langle S_{\text{LAT}} \rangle$ therefore only contributes a measurement of the bosonic part of the action and thus a divergence that should be proportional to the number of bosonic fields in the large g region

$$c \stackrel{g \gg 1}{=} N_{\text{B}}. \quad (6.3.31)$$

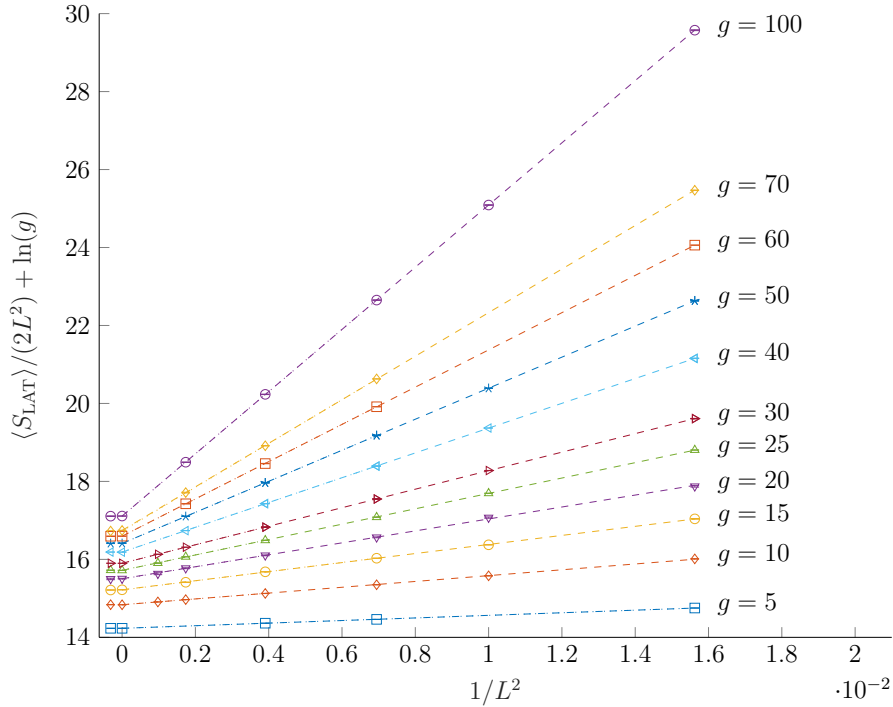


Figure 6.5 Plots of $\frac{\langle S_{\text{LAT}} \rangle}{2L^2}$, where fits (dashed lines) to data points are linear in $1/L^2$. To ensure better visibility of the fits at different g values, $\ln g$ has been added. The extrapolation to the continuum limit (symbol at infinite L) determines the coefficient $c/2$ of the divergent ($\sim L^2$) contribution in (6.3.23).

To prove this, c can be determined numerically by an extrapolation with a fit linear in $1/L^2$ from data points for $\frac{\langle S_{\text{LAT}} \rangle}{2L^2} = \frac{c}{2} + \frac{S_0}{2L^2}$ (see Figures 6.5, 6.6). We hereby find a value of $\frac{c}{2} = 12.5(0)$ (with a discrepancy of 0.01) for $g = 30, \dots, 100$. This extrapolation thus supports the previous claim that the coefficient of the divergence corresponds to half the number of bosons appearing in the path integral which is $N_B = 25$. Having determined the value of c with good precision, we can proceed first by fixing it to be exact $c = 25$ and subtract the contributing divergence from $\langle S_{\text{LAT}} \rangle$. We apply (6.3.25) on the lattice

$$\frac{\langle S_{\text{LAT}} \rangle - \frac{c}{2}(2L^2)}{S_0} \equiv \frac{f'(g)}{4}, \quad (6.3.32)$$

in order to perform simulations for finite g and determine values for $f'(g)$ which is the main aim of our study. Data points with $g = 100, \dots, 30$ in Figure 6.7 show a good agreement with the perturbative predictions at leading order of (3.4.6). For lower values of g we observe deviations that obstruct the continuum limit and signal the presence of a further quadratic ($\sim L^2$) divergence increasing in its amplitude for decreasing g . From Figure 6.6 we observe that the coefficient of the subtracted divergence is not overall constant, but possesses a g dependence

$$c(g) = N_B + \mathcal{O}(g^{-1}). \quad (6.3.33)$$

We therefore must not only subtract the constant, but the full contribution of $c(g)$

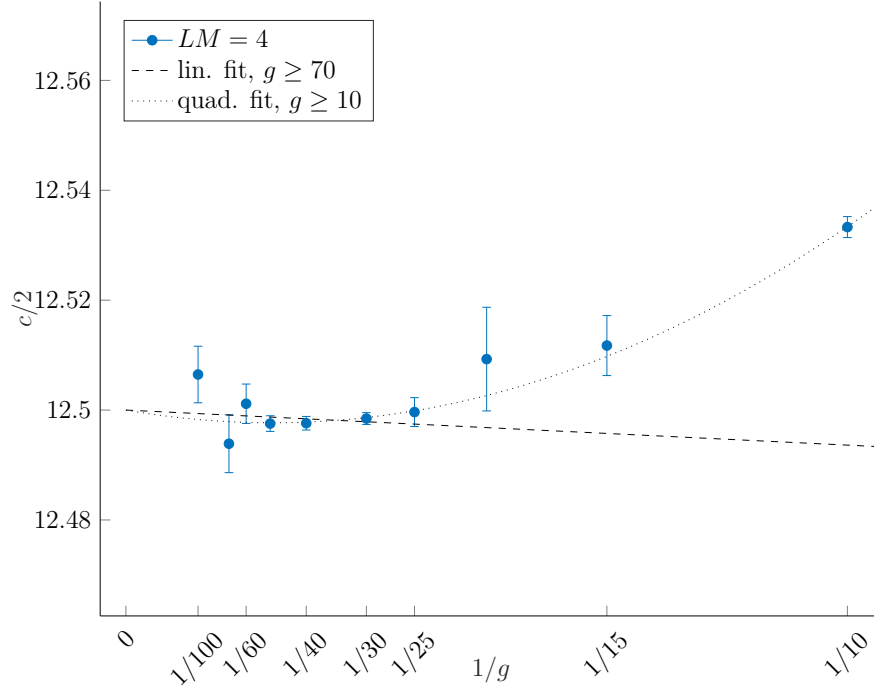


Figure 6.6 Data points estimate the value of $c/2$ as from the extrapolations of the linear fits in Figure 6.5. Dashed and dotted lines are the results of, respectively, a linear fit in $1/g$ and a fit to a polynomial of degree two. For better visibility we omitted the data point for $g = 5$ which is $c/2 = 12.62(2)$.

which we do not know exactly. Hence we subtract the continuum extrapolation of $c(g)/2$ (times the number of lattice points, $2L^2$), as obtained in Figure 6.6. The result is shown in Figure 6.8 and the divergences appear to be removed completely. Due to the flatness of the data points, which indicates small lattice artefacts, they are fitted to a constant. Since we do not observe further divergences, we thus use the continuum extrapolation $L \rightarrow \infty$ of Figure 6.8 to obtain the continuum limit of (6.3.32) and therefore a measure of $f'(g)/4$.

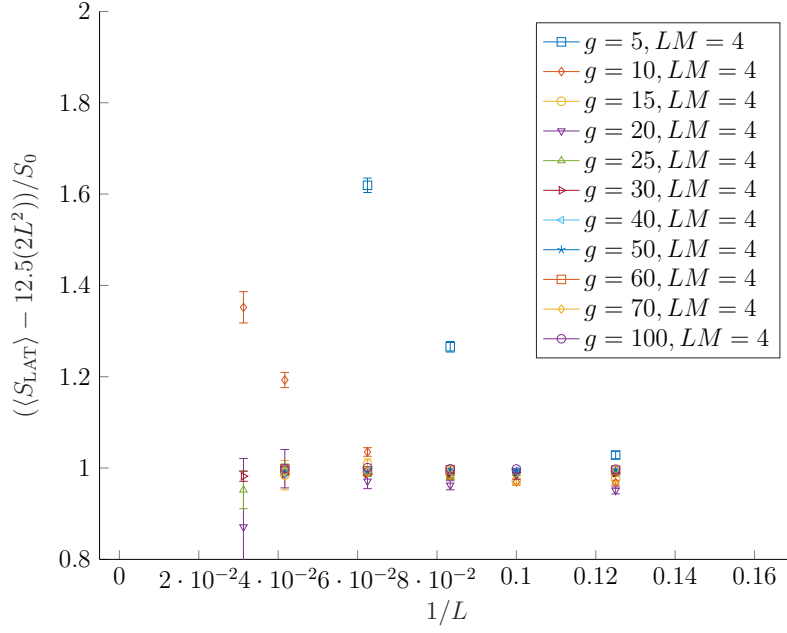


Figure 6.7 Plot of the ratio $\frac{\langle S_{\text{LAT}} \rangle - \frac{c}{2}(2L^2)}{S_0} \equiv \frac{f'(g)}{4}$, where its coefficient of the divergent contribution c has been fixed to the value $c = 15$ and $S_0 = \frac{1}{2}M^2(2L^2)g$. For very large g , there is agreement with the continuum prediction $f'(g) = 4$ in (3.4.6). For smaller values ($g = 10, 5$) strong deviations appear.

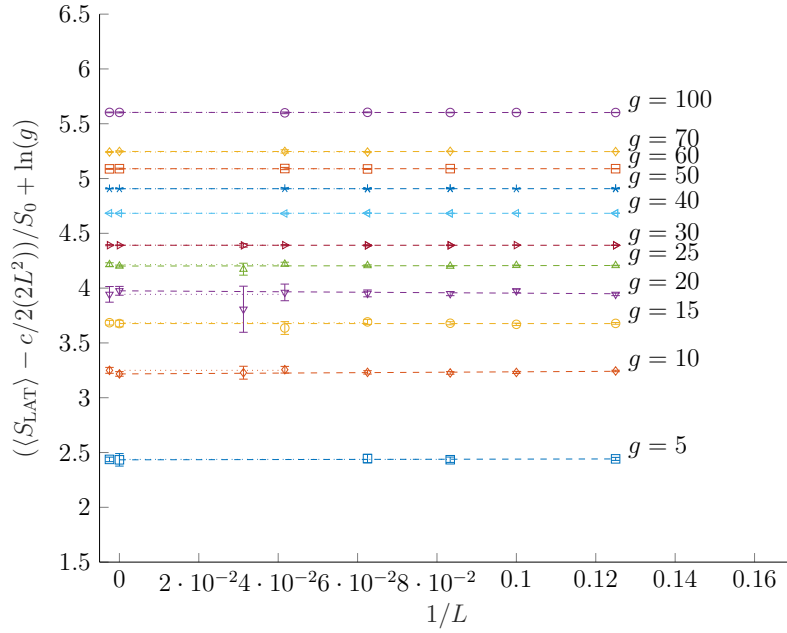


Figure 6.8 Plots for the ratio $\frac{\langle S_{\text{LAT}} \rangle - \frac{c}{2}(2L^2)}{S_0} + \ln g$ as a function of $1/L$, where the divergent contribution $c(g)L^2/2$ is now the continuum extrapolation determined in Figure 6.6. To ensure better visibility of the fits at different g values, $\ln g$ as been added. Dashed lines represent a linear fit to all the data points for one value of g , while for dotted lines the fit is to a constant and only includes the two smallest lattice spacings. Symbols at zero are extrapolations from the constant in $1/L$.

7

Results

In the end of the previous chapter we introduced the two observables that we explore in our lattice simulation and demonstrated the methods that lead to their continuum extrapolation. We now present the results from measuring the mass of the x field and the derivative of the cusp anomaly. We further expose the data for additional simulations performed for $LM = 6$ and without a WILSON term, respectively, to check for finite volume effects and the influence of fermion doublers.

7.1 Mass of the x field

To estimate the mass of the x field we proceed as presented in section 6.3.1 by calculating the effective masses for the various lattice sizes under consideration. For every fixed g we do a continuum extrapolation (Figure 7.1) and plot m_x^2/m^2 over g in Figure 7.2. The data points are afflicted with large errorbars. This is because the correlation functions are highly fluctuating and the mass therefore is a challenging observable with a lot of statistical noise that needs a high amount of replica to give good estimates. Nonetheless we observe for $10 < g < 70$ ($0.4 < g_c < 2.8$) a very good agreement with the perturbative large g prediction ((6.1.2) and dotted line in Figure 7.2) within errorbars and we see that the data almost perfectly follows the predicted bending down. In this regime we collected a high amount of replica, whereas for the other points at $g = 5, 10$ and $g = 70, 100$ our simulations suffer from a sufficient amount of statistics to make valid predictions, due to the highly fluctuative nature of the correlators. A look at Figure 7.1 reveals that for some of these points also cutoff effects play a role. The quality of the linear fit decreases if there are only too few or too tiny lattices involved. The number of replica and considered lattice sizes can be found in Table F.1. For the point at $g = 5$ also the reweighting could conflict with the mass measurement.

7.2 Cusp anomaly

The main aim of the study at hand is to predict values of the derivative of the cusp anomaly function for fine g , where our estimate for $f'(g)/4$ is governed by the continuum extrapolation in Figure 6.8, leading to Figure 7.3. Data points from the simulation can be directly compared to the derivative of the perturbative prediction (3.4.6), depicted as a dashed line and to a prediction obtained via the

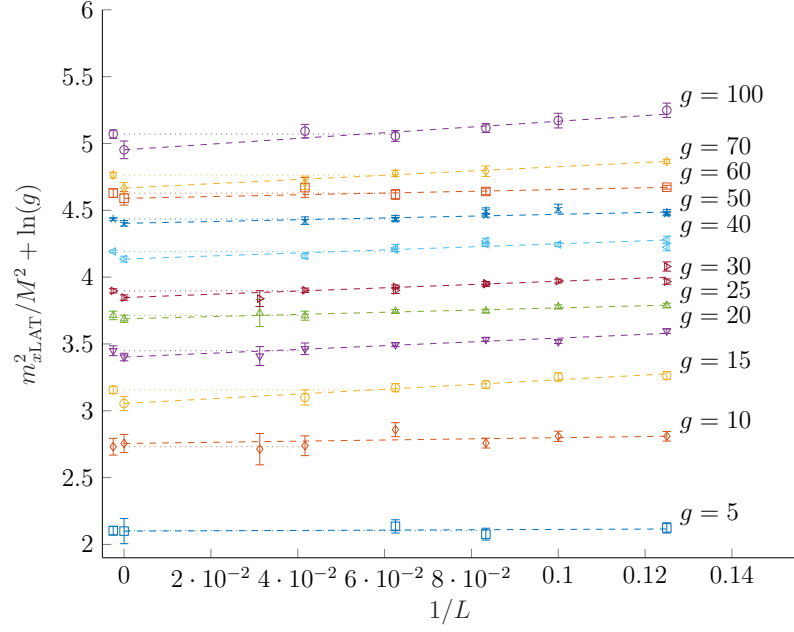


Figure 7.1 Plot of $m_{xLAT}^2(L, g)/M^2 = m_x^2(g)/m^2 + \mathcal{O}(1/L)$, as from fits to connected correlators discussed in section 6.3.1. To ensure better visibility of the fits at different g values, $\ln g$ has been added. Dashed lines represent a linear fit to all the data points for one value of g , while for dotted lines the fit is to a constant and only contains the two smallest lattice spacings. Multiple points at the same value of g and L indicate multiple replica.

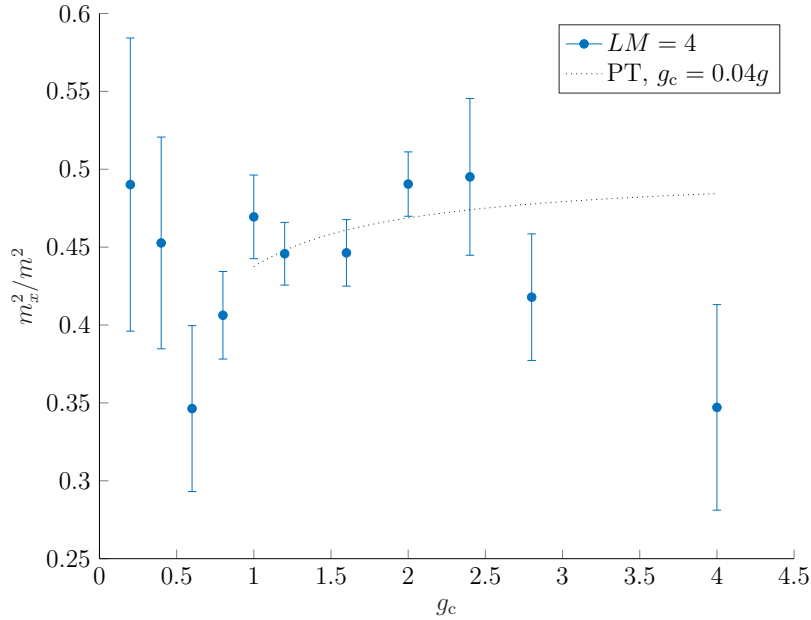


Figure 7.2 Continuum extrapolation corresponding to the linear fits in Figure 7.1. The extrapolation is plotted as a function of the continuum coupling $g_c = 0.04g$ to facilitate the comparison with the prediction coming from the perturbative expectation (PT) (6.1.2), and uses the matching procedure performed for the observable action. The latter is described in section 7.2.

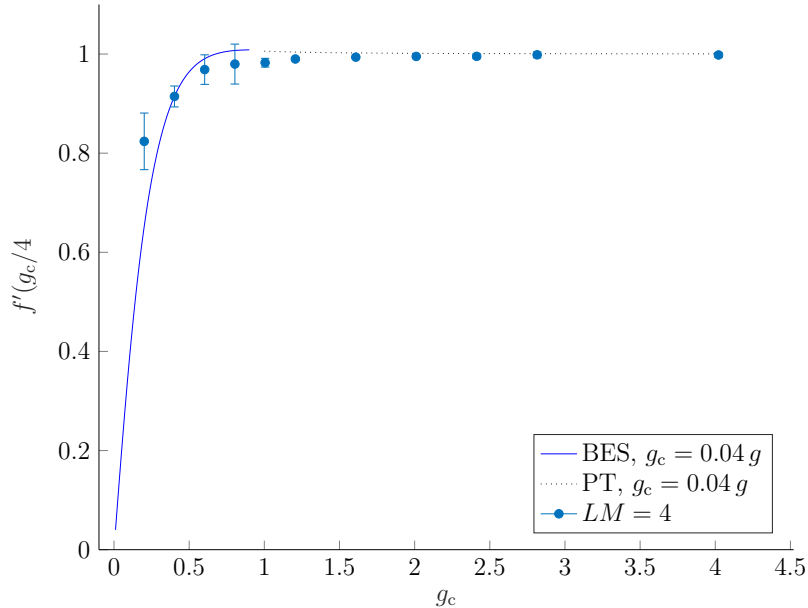


Figure 7.3 Plot for $f'(g)/4$ as determined from the $L \rightarrow \infty$ extrapolation of (6.3.32), exposed as the extrapolations of the fits in Figure 6.8, and plotted as a function of the bare continuum coupling g_c under the assumption that it is related to the bare coupling on the lattice g via a finite rescaling ($g_c = 0.04 g$). The dashed line represents the derivative of the first few terms of the perturbative series (3.4.6), the continuous line is obtained from a numerical solution to the *BES* equation.

integrability of the model (first derivative of the cusp anomaly obtained from a numerical solution to the *BES* equation [17], depicted as a continuous line). To compare our results from the simulation $f'(g)$ with the continuum prediction $f'(g_c)_c$, we have to match our data points to the continuum curve, since it is not clear that the bare continuum coupling g_c is equivalent to the one on the lattice. We assume that we can achieve the matching by a simple rescaling with a factor $g_c = b \cdot g$. We then choose a data point where we want to apply the matching and obtain the rescaling parameter b from $f'(g) = f'(g_c)_c$. This matching point is chosen to be at $g = 10$, since it is far enough from the substantially flat regime of the observable and still in a region where no reweighting has to be applied and thus errors are still acceptably small. It therefore lies exactly in the continuous curve in Figure 7.3 and we derive $g_c = 0.04 g$. In the perturbative regime of large g our data points are in good agreement with the perturbative prediction. For decreasing g the perturbative series (3.4.6) predicts an increase of $f'(g)$, governed by the term proportional to the CATALAN constant K . In this regime we have increased the statistics of our simulation, compared to [10], to reduce errors, but our data in Figure 7.3 still does not catch the predicted upward trend. But notice that the data (still under the hypothesis of a simple scaling relation between the couplings) is following the predicted decrease of values of g which are below the perturbative region. The non-perturbative regime begins with $g_c = 1$ or $g = 25$, respectively, implying that our simulations at $g = 15, 10, 5$ are already testing a fully non-perturbative regime of the string sigma-model under investigation. The point at $g = 5$ ($g_c = 0.2$) does not match the predicted curve within its

errorbars which could be the effect of several different causes. It might be that the relation between continuum and lattice coupling is more complex than the assumed rescaling. Further the reweighting might have caused a systematic error, and there has not been so many simulation data conducted at this specific value of $g = 5$, also not for finer lattices than $L = 16$, since for such small g simulations are very involved and take more time. Another conspicuous point at $g = 20$ ($g_c = 0.8$) is afflicted with large errorbars as well. The behaviour there is quite peculiar, since the produced configurations are strongly correlated, noticeable from very high autocorrelation times in Table F.1 (similar response occurs for simulations at $g = 80$ and $r = 0$). This behaviour might be some intrinsic problem of the algorithm, that is not determined yet, but is most certainly not related to the underlying theory. In the following we investigate further possible influences of systematic errors like finite volume effects or fermion doubling and check for the reliability of the PFAFFIAN as a valid probability density for the RHMC.

7.3 Systematic errors and the Pfaffian sign

Finite volume effects

According to (6.1.4) finite volume effects can be decreased by increasing the value of LM . To check for the influence of these effects we performed simulations with $LM = 6$. The results for the cusp anomaly are illustrated in Figure 7.4 (red) together with the values of the $LM = 4$ simulation (blue). Both results are in very good agreement with each other within their respective errors which suggests that finite volume effects do not play a dominating role in our conducted simulations. The mass is presented in Figure 7.5 together with the $LM = 4$ values. Here the data points deviate more due to the high statistical noise involved in this observable. According to Table F.1 we do not have a high number of replica for the $LM = 6$ simulations. We also had to omit many simulation results for lattice sizes $L = 8, 10$. For larger values of LM smaller lattices tend to behave unstable. There the simulations get stuck at some configuration and do not change any more. This also deteriorates the statistics for the mass measurement. Therefore the mass derived from the $LM = 6$ simulations is not very representative. But the received data points are in the same regime as those for the $LM = 4$ simulations which also indicates no influence of finite volume effects.

Wilson term

To check for the possible influence of fermion doubling or the breaking of symmetry induced by the WILSON term we perform simulations for $LM = 4$ at $r = 0$, i.e. without the presence of a WILSON term. We observe that the instabilities due to small eigenvalues of the fermionic operator occur at much higher values of g than before. A reweighting procedure has not been applied in this case and we are thus only able to conduct simulations for $g \geq 25$. This indicates that the WILSON term already contributes to the shift of the eigenvalues and allows simulations at lower g , at the cost of breaking the $SO(2)$ symmetry which leads

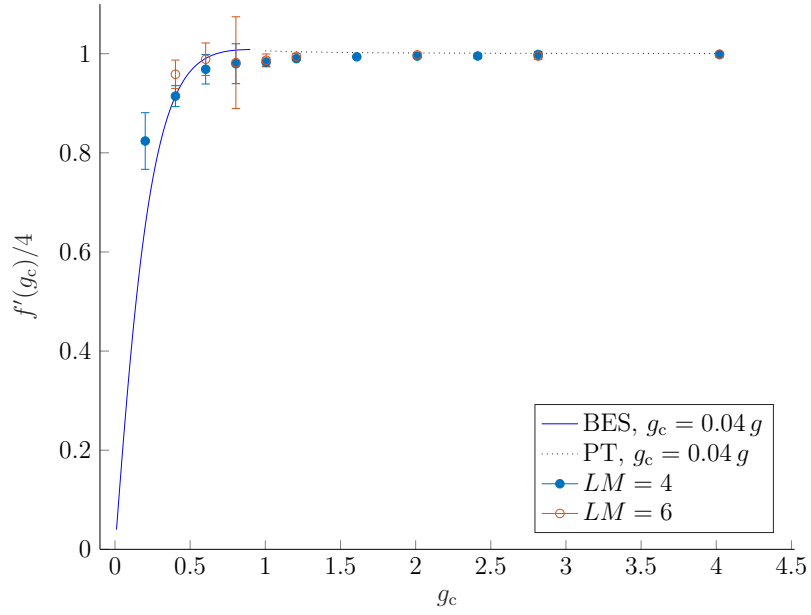


Figure 7.4 Plot for $f'(g)/4$ as a function of the bare continuum coupling $g_c = 0.04g$. Data points from simulations with $LM = 6$ (red) are added to those with $LM = 4$ (blue). The matching is again made for the $LM = 4$ point at $g = 10$.

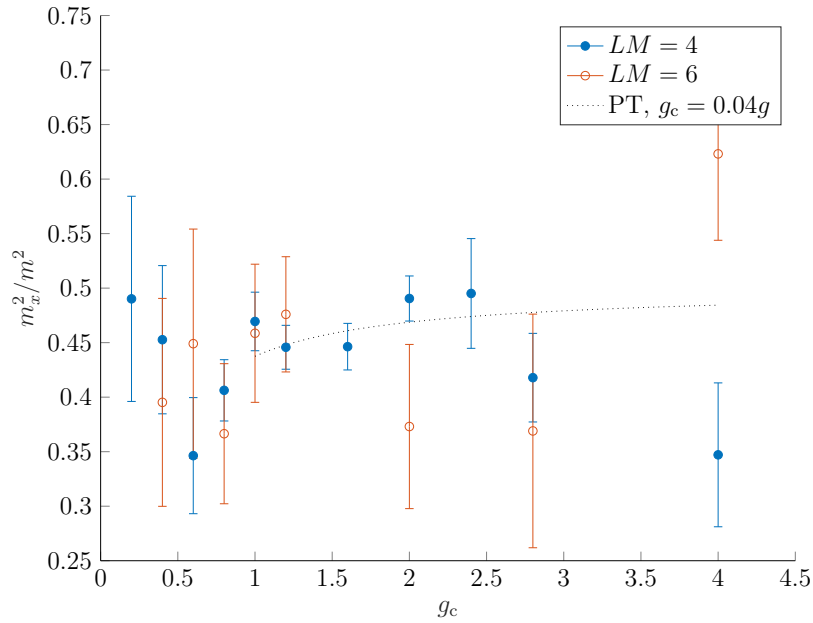


Figure 7.5 Continuum extrapolation for the x field mass as a function of the bare continuum coupling $g_c = 0.04g$. Data points for the $LM = 6$ simulations (red) are added to those with $LM = 4$ (blue).

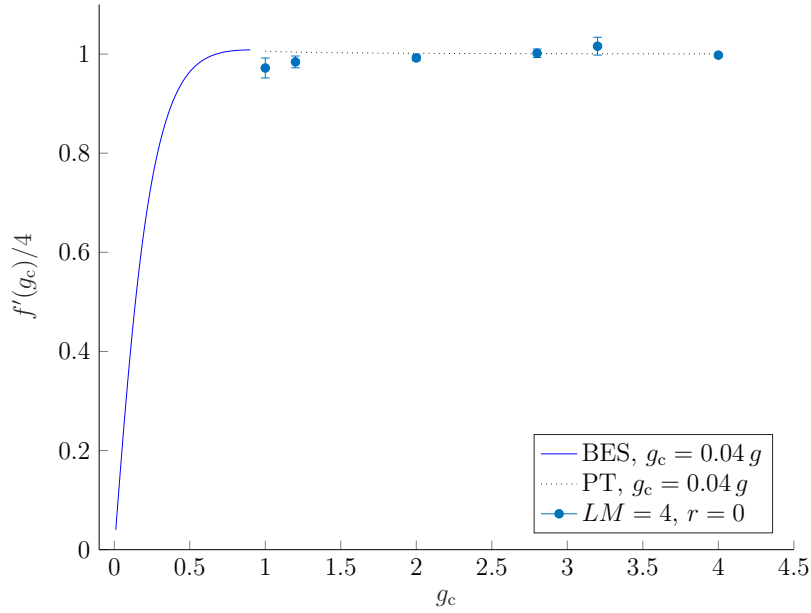


Figure 7.6 Plot for $f'(g)/4$ as a function of the bare continuum coupling $g_c = 0.04g$ with data points obtained from simulations without a WILSON term. The matching is applied for the point at $g = 70$. The continuous and dotted lines represent the predictions coming from the *BES* equation and perturbation theory, respectively.

to a more challenging mass calculation due to the subtraction of non-connected parts of correlators discussed in section 6.3.1. The data in Figure 7.8 is not in very good agreement with the perturbatively predicted mass curve. If we look at the continuum extrapolation in Figure 7.7 we can see that especially for the two smallest g values the deviation between the results of the linear extrapolation and the plateau average for the two finest lattices is quite large. This might be due to cutoff effects, dominating the region of smaller lattices. These effects plague the linear extrapolation and can decrease its quality. In general it would be better to omit smaller lattices like $L = 8, 10$ and increase the statistics on larger lattices like $L = 16, 24, 32$ which is of course more time consuming. Another possibility is to do the fit to a higher order polynomial instead of a linear function to regard the influence of cutoff effects. If we only consider the largest two lattices and assume that cutoff effects can already be neglected there, then we can fit these values to a constant and find the results illustrated in Figure 7.9 which agree much better with the predicted curve, even for the very low amount of statistics available for $r = 0$. This supports our line of constant physics together with the results in Figure 7.5 and indicates that we can handle the symmetry breaking caused by the WILSON term effectively. Further we do not observe any influence of fermion doubling on the considered observables. There might be an effect on measurements of the masses of fermionic fields. Their investigation should be considered as a future aim.

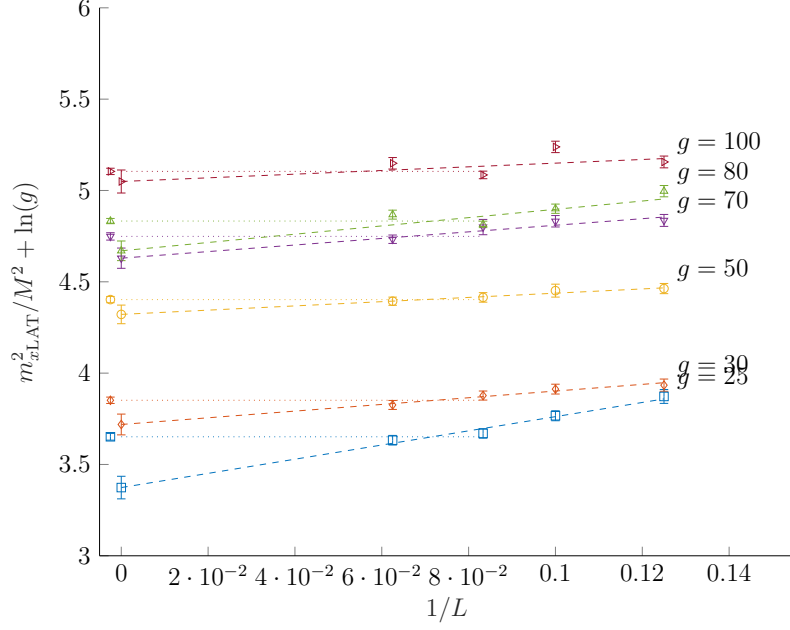


Figure 7.7 Plot of $m_{xLAT}^2(L, g)/M^2 = m_x^2(g)/m^2 + \mathcal{O}(1/L)$ for $LM = 4$ and $r = 0$, as from fits to connected correlators discussed in section 6.3.1. To ensure better visibility of the fits at different g values, $\ln g$ has been added. Dashed lines represent a linear fit to all the data points for one value of g , while for dotted lines the fit is to a constant and only contains the two smallest lattice spacings. Multiple points at the same value of g and L indicate multiple replica.

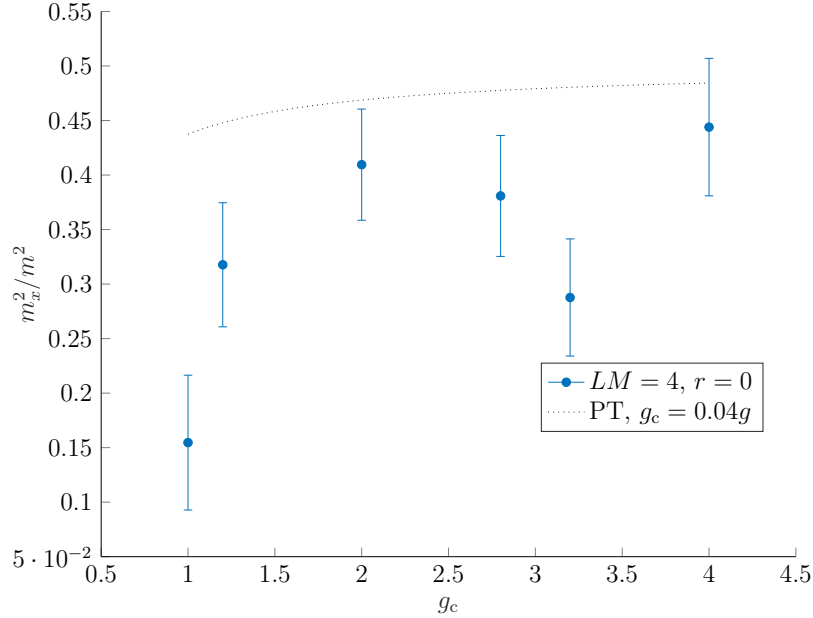


Figure 7.8 Continuum extrapolation for the x field mass as a function of the bare continuum coupling $g_c = 0.04g$ with data points obtained from simulations without a WILSON term. Data points are obtained as continuum extrapolations from the linear fits in Figure 7.7. The dotted line indicates the perturbative prediction according to (6.1.2).

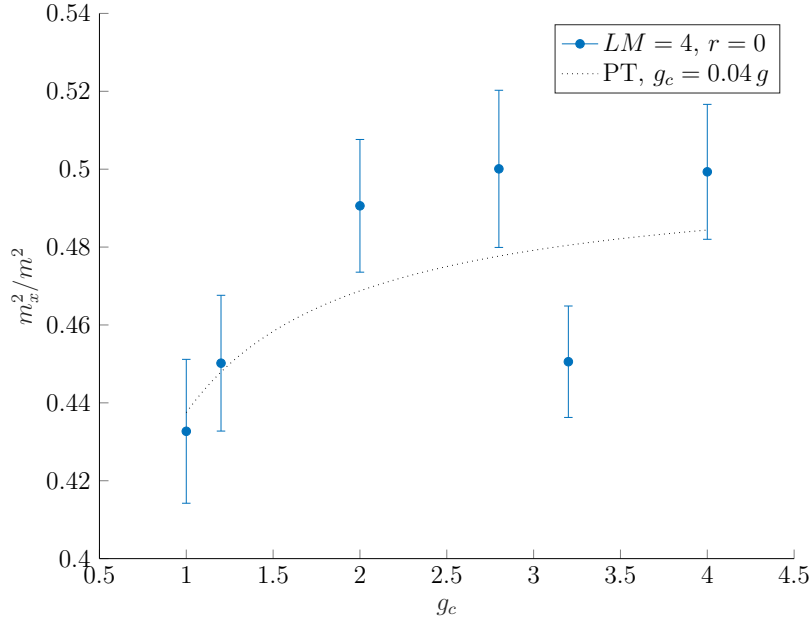


Figure 7.9 Continuum extrapolation for the x field mass as a function of the bare continuum coupling $g_c = 0.04 g$ with data points obtained from simulations without a WILSON term. Data points are obtained as fits to a constant from the two finest lattices where cutoff effects are assumed to be neglectable. The dotted line indicates the perturbative prediction according to (6.1.2).

Pfaffian sign

Throughout the investigations of the properties of the fermion matrix in section 5.1.3 we found that the PFAFFIAN can only change its sign if purely real or imaginary eigenvalues transit through zero. So if we start from a configuration with positive PFAFFIAN and ensure a sufficiently large separation of the smallest eigenvalues from zero, then the PFAFFIAN will remain positive and hence acts as a valid probability density for the RHMC. For a representative amount of configurations we analyse the spectrum of the operator $\hat{\mathcal{O}}_F \hat{\mathcal{O}}_F^\dagger$ (which has eigenvalues $|\lambda_i|^2$, whereas λ_i are eigenvalues of $\hat{\mathcal{O}}_F$) and extract the smallest eigenvalues. Their distribution is shown in Figure 6.1 on the left for $L = 12$ and $g = 5, 10, 30$. For $g = 10, 30$ we plot the mean of such distributions divided by their standard deviation for different values of L in Figure 7.10. This illustrates the separation from zero in units of standard deviations and we observe such a separation by at least 3 standard deviations which (if we assume the distribution in Figure 6.1 to be GAUSSIAN) makes it very unlikely for any eigenvalue to get too close to zero for $g \geq 10$. For finer lattice spacings this separation tends to increase and we thus do not expect any problems in taking the continuum limit. This eliminates sign problems for the regime of $g \geq 10$. For $g = 5$ we basically introduce a lower bound for the eigenvalues with the twisted mass term in the reweighting and if this is adjusted to be high enough then this method should be sufficient to ensure a positive PFAFFIAN. Nonetheless it would be good practice to find a method to check for sign flips also during simulations.

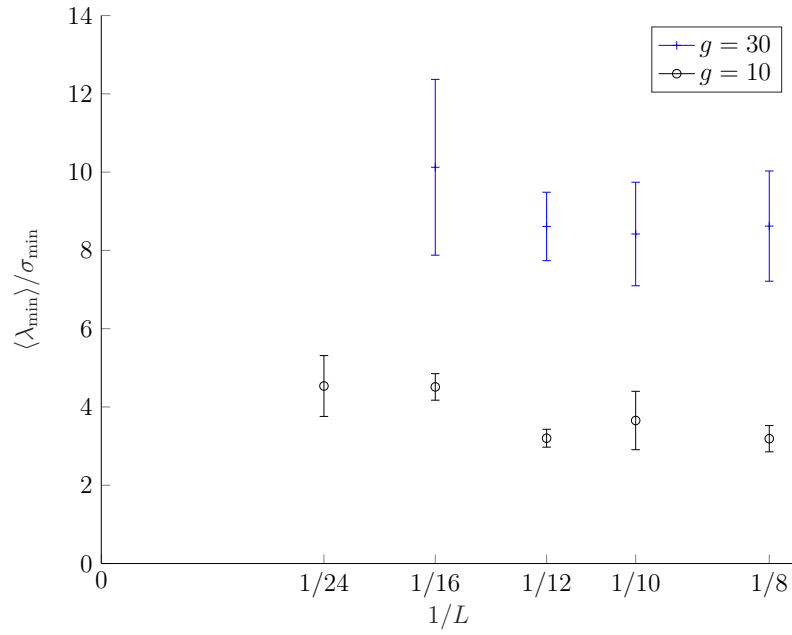


Figure 7.10 In Figure 6.1 on the left we saw the distribution of the minimal eigenvalues of $\hat{\mathcal{O}}_F \hat{\mathcal{O}}_F^\dagger$ for $L = 12$ and multiple g . Here we plot mean over standard deviation of such distributions for $g = 10, 30$ and several values of L . Every point was derived from the minimal eigenvalues of 400 configurations.

8

Conclusion and outlook

In this thesis we studied a discretisation of the AdS -light-cone gauge-fixed action for the Type IIB GREEN-SCHWARZ superstring to investigate the cusp anomalous dimension of $\mathcal{N} = 4$ SYM in a regime of finite 't HOOFT coupling from a string theory perspective via the AdS_5/CFT_4 duality. For the convenience of the reader we reviewed the most essential aspects of superstring theory and AdS/CFT correspondence, and provided a fundamental basis of numerical tools.

We measured the (derivative of the) cusp anomaly of planar $\mathcal{N} = 4$ SYM as derived from string theory and further the masses of two bosonic excitations of the AdS LAGRANGIAN propagating transverse to the relevant, classical solution. The derived data is in good agreement with the perturbative regime of the sigma-model (large $g = \sqrt{\lambda}/4\pi$). For smaller values of g our precision is not high enough and continuum extrapolations do not show the predicted upwards trend, stated by the perturbative prediction for the cusp anomaly. But in turn we can observe quite well a qualitative agreement to the predicted bending down, coming from the integrability of the model.

Lattice simulations were performed utilising a rational hybrid Monte Carlo (RHMC) algorithm and a WILSON term (to avoid fermion doublers) which explicitly breaks the $SO(2)$ symmetry of the model. To perform a well defined continuum extrapolation we employ a line of constant physics that demands physical masses to be kept constant while approaching the continuum limit. Therefore no tuning of the bare mass parameter of the theory (the light-cone momentum p^+ that was later substituted by the mass scale m) is required which is confirmed by our measurement of the masses of the bosonic excitations.

In measuring the action we observe a divergence proportional to the world volume ($\sim 2L^2$) with a coupling dependent coefficient that has to be subtracted by hand. Within lattice regularisation such divergences are expected. In continuum perturbation theory power-divergences arising in this model are set to zero, using dimensional regularisation [13]. In a hard-cutoff regularisation approach on the other hand, like the lattice one, the appearance of power-divergences is inevitable and their further handling is a highly non-trivial task. In our case we proceeded by a non-perturbative subtraction of the divergences which works very well, but in general this method should be treated with caution since potential ambiguities can arise, like errors that diverge in the continuum limit.

To compare our simulation data with the predictions, coming from integrability (Figure 7.3), we employ a matching procedure, based on the hypothesis of a simple scaling relation between the bare couplings on the lattice and in the continuum, respectively. It is possible that this bold assumption is not valid and

the relation between the couplings is of a more complex nature. This could be supported by a further investigation of the model for smaller g which is currently prevented by the instability of the simulations for $g < 5$.

An improvement, that could be achieved compared to a previous status of the project [10], is that there is no appearance of a complex phase in the PFAFFIAN of the fermionic operator $\hat{\mathcal{O}}_F$. We can think of the eigenvalues of $\hat{\mathcal{O}}_F$ as continuous functions of the Monte Carlo time along a RHMC trajectory. In order to change the PFAFFIAN'S sign, some eigenvalues of $\hat{\mathcal{O}}_F$ would need to transit through zero. We checked that for our simulations for $g \geq 10$ the smallest eigenvalues occupy a sufficiently large separation from zero to ensure a stable simulation with positive PFAFFIAN and without the requirement to apply a reweighting. We can therefore say that we eliminated a severe sign problem occurring in [10] in the region of $g \geq 10$ which already tests the non-perturbative regime of the model. Further we did not find any evidence that the results for our considered observables are influenced by finite volume effects or the occurrence of fermion doublers. For small g the simulations are troubled with small eigenvalues, large condition numbers and potential sign flips of the PFAFFIAN that might be correlated.

In the future this problem could be addressed numerically by an improvement of the rational approximation or by the use of a preconditioned conjugate gradient solver, providing a better stability in the regime of small eigenvalues. A reduction of computation time could be achieved by applying a parallelisation, exploiting the outstanding power of modern GPU computing (computations on graphic cards). In four-dimensional gauge theories like QCD the computation on GPUs would not prove very useful since they require a large amount of random-access memory within the parallel framework. GPUs usually have a quite small shared memory, not sufficient for those kinds of memory intense computations. The presented model is much more economic in terms of consuming memory since it only involves scalar fields and two worldsheet coordinates. The saved computation time would allow much higher statistics and therefore improved results on the masses which are derived from highly fluctuating fields.

From a more theoretical point of view one could further try to consider other observables related to the cusp anomaly that do not require a subtraction of divergences, and also measure the masses of fermionic fields in the model to test the validity of the applied line of constant physics.

In the end one can say that the study at hand provides results that are in qualitative agreement with the theoretical predictions, but still contain certain peculiarities, but it is, nonetheless, an interesting approach to investigate *AdS/CFT* in a non-perturbative regime that should be continued.

Appendix

A Grassmann numbers

A.1 Grassmann algebra

When we start considering a QFT including fermions, we have to conclude that our canonical quantisation rules for bosons no longer apply. Instead of a commutation relation

$$[\phi(x), \Pi(y)] = i\hbar\delta(x - y) \quad (\text{A.1})$$

for bosonic fields, one has to introduce anti-commutation relations for fermionic ones [41]

$$\{\psi(x), \pi(y)\} = i\hbar\delta(x - y), \quad (\text{A.2})$$

which in the classical limit $\hbar \rightarrow 0$ is leading to objects that behave like anti-commuting numbers

$$\psi\pi = -\pi\psi, \quad (\text{A.3})$$

which seems rather strange at first. But the concept of anti-commuting numbers, so called GRASSMANN variables, has proved quite useful in the path integral framework to represent the algebra of fermionic position and momentum observables as operators on a space of functions. In the following we want to define these objects and study their properties.

We can identify GRASSMANN numbers with elements of the exterior algebra $\Lambda^1(V)$ over a vector space V over a field K . According to the dimension of V the algebra has a finite collection of generators ξ_1, \dots, ξ_N with $N = \dim V \geq 1$ or infinitely many if the vector space is infinite dimensional. With the exterior product there exists an associative connection on the algebra, which is linear in scalar multiplication and satisfies

$$\xi_i \wedge \xi_i = 0. \quad (\text{A.4})$$

Thereby follows the demanded anti-commutativity for the fermionic GRASSMANN variables

$$\xi_i \wedge \xi_j = -\xi_j \wedge \xi_i. \quad (\text{A.5})$$

In general we can write the exterior algebra as a direct sum of subalgebras

$$\Lambda(V) = \bigoplus_{m=0}^N \Lambda^m(V), \quad (\text{A.6})$$

where $\Lambda^m(V)$ is the quotient algebra of the tensor algebra $T^m(V)$ and the two-sided ideal $I^m(V)$ and $\Lambda^0(V) = K$. For an $a \in \Lambda^k(V)$ and $b \in \Lambda^l(V)$ we have a graded commutative exterior product

$$a \wedge b = (-1)^{kl} b \wedge a. \quad (\text{A.7})$$

Therefore if we have an $a = \xi_i \wedge \xi_j$ and $b = \xi_m \wedge \xi_n$, then we get

$$a \wedge b = b \wedge a \quad (\text{A.8})$$

and a and b behave like bosonic quantities. The highest alternating tensor one can create is

$$\xi_1 \wedge \xi_2 \wedge \dots \wedge \xi_N \in \Lambda^N(V), \quad (\text{A.9})$$

and with (A.4) it applies for all higher tensor spaces that $\Lambda^k(V) = 0$, $\forall k > N$. From now on we want to abbreviate the wedge notation simply by

$$\xi_i \xi_j \equiv \xi_i \wedge \xi_j. \quad (\text{A.10})$$

So any analytic function of some real quantities $x_i \in \mathbb{R}$ and GRASSMANNIAN generators $\xi_j \in \Lambda(V)$ can be represented by finitely many terms

$$f(x_1, \dots, x_n, \xi_1, \dots, \xi_N) = f_0 + f_1 \xi_1 + \dots + f_{12} \xi_1 \xi_2 + \dots + f_{1\dots N} \xi_1 \dots \xi_N, \quad (\text{A.11})$$

where the coefficients are functions of the real quantities. In scope of this thesis we have to deal with vectors of four complex GRASSMANN variables and adapt our notation to the one used in [13]

$$\eta_i = \frac{1}{\sqrt{2}} (\xi_i^{\text{R}} + i \xi_i^{\text{I}}), \quad \text{with } \xi_i^{\text{R}}, \xi_i^{\text{I}} \in \Lambda^1(V), \quad i = (1, \dots, 4). \quad (\text{A.12})$$

We now define the GRASSMANN variables with an upper index as the complex conjugate of the ones with lower index $\eta^i \equiv (\eta_i)^\dagger = (\eta_i)^*$. Complex conjugation of two real GRASSMANN numbers is defined to include a change of position

$$(\xi_1 \xi_2)^* \equiv \xi_2^* \xi_1^* = -\xi_1 \xi_2. \quad (\text{A.13})$$

They therefore behave like a formally purely imaginary quantity, whereas

$$(i \xi_1 \xi_2)^* = i \xi_1 \xi_2 \quad (\text{A.14})$$

behaves like a formally real quantity.

A.2 Grassmann analysis

Now we want to see how we can differentiate and integrate GRASSMANN variables. We define the derivative to obey

$$\frac{\partial \xi_m}{\partial \xi_n} \equiv \delta_{mn}. \quad (\text{A.1})$$

Following [41] and [42] we define the product rule to satisfy

$$\begin{aligned} \frac{\partial}{\partial \xi_n} (\xi_{m_1} \xi_{m_2} \cdots \xi_{m_r}) &\equiv \delta_{m_1 n} \xi_{m_2} \cdots \xi_{m_r} - \delta_{m_2 n} \xi_{m_1} \xi_{m_3} \cdots \xi_{m_r} + \cdots \\ &+ (-1)^{r-1} \delta_{m_r n} \xi_{m_1} \cdots \xi_{m_{r-1}}. \end{aligned} \quad (\text{A.2})$$

The tangent vectors are also elements of the exterior algebra and satisfy the same anti-commutation rules

$$\frac{\partial}{\partial \xi_i} \frac{\partial}{\partial \xi_j} = - \frac{\partial}{\partial \xi_j} \frac{\partial}{\partial \xi_i}. \quad (\text{A.3})$$

So if we perform a coordinate transformation $\xi_i = M_{ij} \theta_j$, an n -form is transforming according to the alternating properties of forms like

$$\frac{\partial}{\partial \xi_1} \cdots \frac{\partial}{\partial \xi_n} = \det(M^{-1}) \frac{\partial}{\partial \theta_1} \cdots \frac{\partial}{\partial \theta_n}, \quad (\text{A.4})$$

where the matrix M is associated with the JACOBIAN

$$M_{ij} = \frac{\partial \xi_i}{\partial \theta_j}. \quad (\text{A.5})$$

For an integral $\mathcal{I}[f]$ of a function $f(\xi)$ it holds true that

$$\frac{\partial}{\partial \xi} \mathcal{I}[f] = 0, \quad (\text{A.6})$$

since the integral is independent of the integration variable. With (A.4) it also follows that

$$\frac{\partial}{\partial \xi} \frac{\partial}{\partial \xi} = 0 \quad (\text{A.7})$$

and therefore one can identify the integration on GRASSMANN numbers with the differentiation up to some normalization constant C

$$\mathcal{I}[f] = \int d\xi f(\xi) = C \frac{\partial}{\partial \xi} f(\xi). \quad (\text{A.8})$$

So we end up with the following integration rules if we define $C \equiv 1$:

$$\int d\xi \xi = \frac{\partial}{\partial \xi} \xi = 1, \quad \int d\xi 1 = \frac{\partial}{\partial \xi} 1 = 0. \quad (\text{A.9})$$

We now want to perform an integration over the complex GRASSMANN variables η and η^\dagger . Therefore we investigate an integration over the function

$$e^{-a\eta\eta^\dagger}. \quad (\text{A.10})$$

With

$$\eta\eta^\dagger = \frac{1}{2} (\xi_R + i\xi_I) (\xi_R - i\xi_I) = -i\xi_R\xi_I \quad (\text{A.11})$$

and (A.4) we can transform the integral using that the determinant of the JACOBIAN is $\det J = i$ and find

$$\begin{aligned} \int d\eta d\eta^\dagger e^{-a\eta\eta^\dagger} &= i \int d\xi_R d\xi_I e^{ia\xi_R\xi_I} \\ &= i \int d\xi_R d\xi_I (1 + i a\xi_R\xi_I) \\ &= a \int d\xi_R d\xi_I \xi_I \xi_R = a \end{aligned} \quad (\text{A.12})$$

We get the same result by integrating over two real GRASSMANN variables ξ_1 and ξ_2

$$\int d\xi_1 d\xi_2 e^{-a\xi_1\xi_2} = a. \quad (\text{A.13})$$

By rewriting it with help of the antisymmetric matrix

$$A = \begin{pmatrix} 0 & a \\ -a & 0 \end{pmatrix} \quad (\text{A.14})$$

we get

$$\int d\xi_1 d\xi_2 e^{-\frac{1}{2}\xi_i A_{ij} \xi_j} = \text{Pf}(A), \quad (\text{A.15})$$

where $\text{Pf}(A)$ is the PFAFFIAN of A , which is defined by the factorisation of the determinant in the following way

$$\text{Pf}(A)^2 = \det(A) \quad (\text{A.16})$$

This relation holds true for an even number of arbitrary many GRASSMANN generators. It is therefore possible to integrate out GRASSMANN variables and be left with calculating a determinant or PFAFFIAN, which comes in quite essential when dealing with GRASSMANN integrals numerically.

A.3 Hubbard-Stratonovich transformation

We have now seen how to deal with bilinear exponentials. But in many cases one also has to deal with higher forms than bilinears. In principle one can expand any function into finitely many terms, like we have seen earlier, and then perform the integration rules, which is but rather ugly and proved not very efficient in numerical simulations. However there is a method to transform an exponential with 4-forms into one with bilinears, by performing an integration over additional bosonic auxiliary fields. This is called a HUBBARD-STRATONOVICH transformation. Assuming that we have a finite number of complex GRASSMANN variables η_i , we can see that the object $\eta^2 \equiv \eta^i \eta_i$ transforms like a formally real quantity

$$(\eta^i \eta_i)^* = (\eta_i)^* (\eta^i)^* = \eta^i \eta_i. \quad (\text{A.1})$$

Therefore $(\eta^2)^2$ is a formally positive real value and we can apply the identity

$$e^{\frac{(\eta^2)^2}{4a}} = \sqrt{\frac{a}{\pi}} \int d\phi e^{-a\phi^2 + \eta^2 \phi}, \quad (\text{A.2})$$

which one can proof simply by square addition and performing a GAUSSIAN integral. If we see this identity in the context of the path integral framework, we can say, that a new bosonic auxiliary field ϕ is introduced for the specific space time point, where the integration took place. Since we can do this transformation at every space time point, this leads to a whole path integral over ϕ . Now we also have to be aware of what happens if the exponent on the left side of (A.2) is negative

$$e^{-\frac{(\eta^2)^2}{4a}} = e^{\frac{(i\eta^2)^2}{4a}} = \sqrt{\frac{a}{\pi}} \int d\phi e^{-a\phi^2 + i\eta^2\phi}. \quad (\text{A.3})$$

We can see that this introduces an imaginary term in the exponent and therefore a highly oscillating function in the integral. Analytically this term would not bother us, but since we want to perform a numerical calculation something like this often results into a numerical sign problem, discussed in section 4.3.4.

B $AdS_5 \times S^5$ spacetime

The $AdS_5 \times S^5$ space is in the central focus of the gauge/gravity duality and should be concerned more deeply. It is a direct product of five-dimensional Anti-de Sitter (AdS) space and a five dimensional compact sphere. Both are maximally symmetric spaces and therefore inherit the isometry groups $SO(2, 4)$ in case of AdS_5 and respectively $SO(6)$ for S^5 [22]. This is an important fact for the AdS/CFT correspondence since the direct product of these groups has the same amount of degrees of freedom as the superconformal group $SO(2, 4) \times SO(6) = SU(2, 2|4)$ as the underlying symmetry group of $\mathcal{N} = 4$ super YANG-MILLS theory in four-dimensional MINKOWSKI space.

B.1 AdS_5 space

Since the construction of a sphere is rather simple, we focus on the Anti-de Sitter space. AdS_5 is a hyperboloid with constant negative curvature, that can be embedded in six-dimensional MINKOWSKI spacetime $X = (X^0, X^1, \dots, X^5) \in \mathbb{R}^{4,2}$, with metric $\tilde{\eta} = \text{diag}(-, +, +, +, +, -)$, so that

$$ds^2 = - (dX^0)^2 + (dX^1)^2 + \dots + (dX^4)^2 - (dX^5)^2 = \tilde{\eta}_{MN} dX^M dX^N, \quad (B.1)$$

where $M, N \in 0, \dots, 5$. AdS_5 is then given by the hypersurface

$$\tilde{\eta}_{MN} X^M X^N = - (X^0)^2 + (X^1)^2 + \dots + (X^4)^2 - (X^5)^2 = -R^2, \quad (B.2)$$

where R is the radius of curvature of the AdS_5 space, see also Figure B.1 for an embedding of AdS_2 in \mathbb{R}^3 . For large X^M the hyperboloid approaches the light-cone of the MINKOWSKI space $\mathbb{R}^{4,2}$, given by

$$\tilde{\eta}_{MN} X^M X^N = 0. \quad (B.3)$$

We therefore can define the ‘boundary’ ∂AdS_5 of Anti-de Sitter space by the set of all lines on the light-cone (B.3) originating from $0 \in \mathbb{R}^{4,2}$. For a point $X \neq 0$ in AdS_5 close to the boundary and therefore satisfying (B.3) we can define (u, v) by

$$u = X^5 + X^4, \quad v = X^5 - X^4, \quad (B.4)$$

so we can rewrite (B.3) as

$$uv = \eta_{\mu\nu} X^\mu X^\nu, \quad (B.5)$$

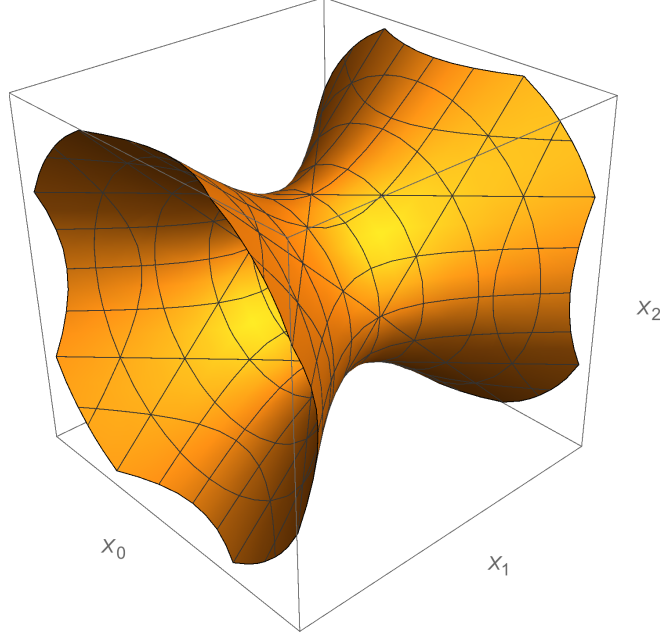


Figure B.1 Embedding of AdS_2 in \mathbb{R}^3 as a hypersurface given by the equation $-(X_0)^2 + (X_1)^2 - (X_3)^2 = -1$.

with $\mu, \nu \in \{0, 1, 2, 3\}$ and $(\eta_{\mu\nu}) = \text{diag}(-, +, +, +)$. Whenever $v \neq 0$ we can rescale the coordinates to set $v = 1$ and solve for u . Therefore one is left with a four dimensional MINKOWSKI space $\mathbb{R}^{3,1}$. Points with $v = 0$ are “points at infinity” added to four dimensional MINKOWSKI space. This makes ∂AdS_5 a conformal compactification of four-dimensional MINKOWSKI space. According to Maldacena [6] the correspondence between a $\mathcal{N} = 4$ theory on $\mathbb{R}^{3,1}$ and Type IIB on $\text{AdS}_5 \times \text{S}^5$ therefore expresses a string theory on $\text{AdS}_5 \times \text{S}^5$ in terms of a theory on the boundary and thus is referred to as “holographic” [43].

B.2 Poincaré patch

Let us now introduce a parametrisation of the hyperboloid (B.2) by the following coordinates $x^\mu \in \mathbb{R}$, for $\mu \in \{0, 1, 2, 3\}$ and $z \in \mathbb{R}_+$. The parametrisation in these coordinates is given by (see e.g. [22, 44])

$$\begin{aligned} X^0 &= \frac{z}{2} \left(1 + \frac{1}{z^2} (x_\mu x^\mu + R^2) \right), \\ X^i &= \frac{R}{z} x^i, \quad i \in 1, 2, 3, \\ X^4 &= \frac{z}{2} \left(1 + \frac{1}{z^2} (x_\mu x^\mu - R^2) \right), \\ X^5 &= \frac{R}{z} x^0, \end{aligned} \tag{B.1}$$

with $x_\mu x^\mu = \eta_{\mu\nu} x^\mu x^\nu$. These local coordinates are called POINCARÉ patch. The metric of AdS_5 in the POINCARÉ patch reads

$$ds^2 = \frac{R^2}{z^2} \left(dz^2 + \eta_{\mu\nu} dx^\mu dx^\nu \right). \quad (B.2)$$

For the whole $AdS_5 \times S^5$ space in POINCARÉ patch we find

$$ds^2 = \frac{R^2}{z^2} \left(dz^2 + \eta_{\mu\nu} dx^\mu dx^\nu \right) + du^I du^I, \quad (B.3)$$

where u^I ($I = 1, \dots, 6$) are coordinates on S^5 that satisfy $u^I u^I = R^2$. For $z \rightarrow 0$ we approach the boundary of $AdS_5 \times S^5$ and we can see from the metric that the contribution of the sphere becomes neglectable close to the boundary. If we include the infinite regime as $\partial(AdS_5 \times S^5)$ where $z = 0$ we can convince ourselves that the metric is conformally equivalent to 4d MINKOWSKI space.

C $SO(6)$ matrices

The matrices ρ_{ij}^M appearing in the action (3.5.13) are the off-diagonal blocks of $SO(6)$ DIRAC matrices γ^M in chiral representation¹

$$\gamma^M \equiv \begin{pmatrix} 0 & \rho_M^\dagger \\ \rho^M & 0 \end{pmatrix} = \begin{pmatrix} 0 & (\rho^M)^{ij} \\ (\rho^M)_{ij} & 0 \end{pmatrix}. \quad (C.1)$$

The ρ_{ij}^M shall all be skew symmetric and we define the ones with the upper indices to satisfy $(\rho^M)^{ij} \equiv (\rho_{ij}^M)^\dagger$. We can therefore state the following properties

$$\rho_{ij}^M = -\rho_{ji}^M, \quad (\rho^M)^{ij} = -(\rho_{ij}^M)^*, \quad (C.2)$$

and we chose to use the following representation

$$\begin{aligned} \rho_{ij}^1 &= \begin{pmatrix} 0 & 1 & 0 & 0 \\ -1 & 0 & 0 & 0 \\ 0 & 0 & 0 & 1 \\ 0 & 0 & -1 & 0 \end{pmatrix}, \quad \rho_{ij}^2 = \begin{pmatrix} 0 & i & 0 & 0 \\ -i & 0 & 0 & 0 \\ 0 & 0 & 0 & -i \\ 0 & 0 & i & 0 \end{pmatrix}, \quad \rho_{ij}^3 = \begin{pmatrix} 0 & 0 & 0 & 1 \\ 0 & 0 & 1 & 0 \\ 0 & -1 & 0 & 0 \\ -1 & 0 & 0 & 0 \end{pmatrix}, \\ \rho_{ij}^4 &= \begin{pmatrix} 0 & 0 & 0 & -i \\ 0 & 0 & i & 0 \\ 0 & -i & 0 & 0 \\ i & 0 & 0 & 0 \end{pmatrix}, \quad \rho_{ij}^5 = \begin{pmatrix} 0 & 0 & i & 0 \\ 0 & 0 & 0 & i \\ -i & 0 & 0 & 0 \\ 0 & -i & 0 & 0 \end{pmatrix}, \quad \rho_{ij}^6 = \begin{pmatrix} 0 & 0 & 1 & 0 \\ 0 & 0 & 0 & -1 \\ -1 & 0 & 0 & 0 \\ 0 & 1 & 0 & 0 \end{pmatrix}. \end{aligned} \quad (C.3)$$

From the CLIFFORD algebra of the DIRAC matrices $\{\gamma^M, \gamma^N\} = 2\delta^{MN}\mathbb{1}_8$ we can derive the relation

$$(\rho^M)^{il}(\rho^N)_{lj} + (\rho^N)^{il}(\rho^M)_{lj} = 2\delta^{MN}\delta_j^i. \quad (C.4)$$

The generators of the $SO(6)$ can be built by

$$(\rho^{MN})^i_j = \frac{1}{2} \left[(\rho^M)^{il} (\rho^N)_{lj} - (\rho^N)^{il} (\rho^M)_{lj} \right]. \quad (C.5)$$

Further relations and identities are

$$(\rho^{MN})^i_j = (\rho^{MN})^{*j}_i, \quad (\rho^{MN})^i_j = (\rho^{NM})^i_j, \quad (C.6)$$

$$(\rho^M)^{im}(\rho^M)^{kn} = 2\epsilon^{imkn}, \quad (\rho^M)^{im}(\rho^M)_{nj} = 2(\delta_j^i \delta_n^m - \delta_n^i \delta_j^m), \quad (C.7)$$

¹The upper or lower placement of the index M on the block matrices has no meaning and is only changed for the purpose of readability.

$$\begin{aligned}
 & \epsilon^{imkn}(\rho^M)_{mj}(\rho^L)_{nl} + \epsilon_{mjnl}(\rho^M)^{im}(\rho^L)^{kn} \\
 &= (\rho^{\{M\})^{ik}(\rho^L\}^{jl} + \delta_j^k(\rho^L)^{im}(\rho^M)_{ml} + \delta_l^i(\rho^M)^{km}(\rho^L)_{mj} \\
 & \quad + \delta^{ML}(-4\delta_l^i\delta_j^k + 2\delta_j^i\delta_l^k) \ ,
 \end{aligned} \tag{C.8}$$

$$-(\rho^{MN})^i{}_j(\rho^{ML})^k{}_ln_Nn_L = -2(\rho^N)^{ik}(\rho^L)_{jl}n_Nn_L - \delta_j^i\delta_l^k + 2\delta_l^i\delta_j^k \ . \tag{C.9}$$

D Discrete Fourier transform

To perform a FOURIER transform on the lattice one needs to discretise it to deal with a finite sequence of N complex numbers x_0, x_1, \dots, x_{N-1} . We define the discrete FOURIER transform X_k to be a vector in the base of roots of unit with components x_n as follows:

$$X_k = \frac{1}{\sqrt{N}} \sum_{n=0}^{N-1} x_n e^{-2\pi i k n / N} \quad k \in \mathbb{Z}. \quad (\text{D.1})$$

We can limit the domain of k to a finite set, because the exponential is periodic in k . In the following we stick to the domain $k \in \left[-\frac{N}{2} + 1, \dots, \frac{N}{2}\right]$ and restrict us to even N . The inverse transform can be defined to be

$$x_n = \frac{1}{\sqrt{N}} \sum_{k=-N/2+1}^{N/2} X_k e^{2\pi i k n / N}, \quad (\text{D.2})$$

where due to periodicity n is in the domain $[0, \dots, N-1]$ like defined in the beginning. If we now insert (D.1) into (D.2) we end up with

$$x_n = \frac{1}{N} \sum_{k=-N/2+1}^{N/2} \left(\sum_{m=0}^{N-1} x_m e^{-2\pi i k m / N} \right) e^{2\pi i k n / N} \quad (\text{D.3})$$

$$= \frac{1}{N} \sum_{k', m=0}^{N-1} x_m e^{2\pi i k' (n-m) / N}, \quad (\text{D.4})$$

where we shifted the summation for k' to be in the same domain as m . This is now only equal to x_n if the following important relation holds true

$$\frac{1}{N} \sum_{k'=0}^{N-1} e^{2\pi i k' (n-m) / N} = \delta_{m,n}. \quad (\text{D.5})$$

We can prove this easily. For $n = m$ this is trivial and for $n \neq m$ we make use of the geometric series

$$\sum_{k'=0}^{N-1} \left(e^{2\pi i c / N} \right)^{k'} = \frac{1 - e^{2\pi i c}}{1 - e^{2\pi i c / N}} = 0, \quad |c| = |n - m| \in [1, \dots, N-1]. \quad (\text{D.6})$$

Now we want to apply the Fourier transform on the two-dimensional lattice used throughout this thesis. We defined the lattice to be

$$\Lambda = \{n = (n_0, n_1) \mid n_0 = 1, \dots, N_0; n_1 = 1, \dots, N_1\}, \quad (\text{D.7})$$

with $N_0 = T$ and $N_1 = L$. Therefore the total number of lattice points is given by

$$|\Lambda| \equiv TL. \quad (\text{D.8})$$

Following [30] we calculate the discrete Fourier transform $\tilde{f}(p)$ of a function $f(n)$. Here for $f(n)$ we impose toroidal boundary conditions

$$f(n + \hat{i}N_i) = e^{2\pi i\theta_i} f(n), \quad (\text{D.9})$$

where \hat{i} is a unit vector in the i -direction and $\theta_i = 0$ corresponds to periodic and $\theta_i = 1/2$ to anti-periodic boundary conditions. The discrete momentum space corresponding to these boundary conditions is given by

$$\tilde{\Lambda} = \left\{ p = (p_0, p_1) \mid p_i = \frac{2\pi}{aN_i}(k_i + \theta_i), k_i = -\frac{N_i}{2} + 1, \dots, \frac{N_i}{2} \right\}. \quad (\text{D.10})$$

With (D.1) and (D.2) we can express the the Fourier transform as

$$\tilde{f}(p) = \frac{1}{\sqrt{|\Lambda|}} \sum_{n \in \Lambda} f(n) e^{-ip \cdot na} \quad (\text{D.11})$$

and for the inverse transform we find

$$f(n) = \frac{1}{\sqrt{|\Lambda|}} \sum_{p \in \tilde{\Lambda}} \tilde{f}(p) e^{ip \cdot na}. \quad (\text{D.12})$$

Here again the important relations hold

$$\frac{1}{|\Lambda|} \sum_{n \in \Lambda} \exp(i(p - p') \cdot na) = \delta(p - p') \equiv \delta_{k_0, k'_0} \delta_{k_1, k'_1} \quad (\text{D.13})$$

$$\frac{1}{|\Lambda|} \sum_{p \in \tilde{\Lambda}} \exp(ip \cdot (n - n')a) = \delta(n - n') \equiv \delta_{n_0, n'_0} \delta_{n_1, n'_1}. \quad (\text{D.14})$$

E Discretised fermion matrix

Here we want to present the details leading to the discretised version (5.2.18) of the operator \mathcal{O}_F . As emphasised in section 5.2.3 $\hat{\mathcal{O}}_F$ is a $16V \times 16V$ matrix and we will continue to use the notation introduced there to write subdivided blocks of size $4V \times 4V$ to result in

$$\hat{\mathcal{O}}_F = \begin{pmatrix} \hat{W}_+ & i\bar{\Delta}_0^A & -i\left(\vec{\Delta}_1^Z + \frac{M}{2}\bar{Z}\right) & 0 \\ i\bar{\Delta}_0^A & -\hat{W}_+^\dagger & 0 & -i\left(\vec{\Delta}_1^{Z^\dagger} + \frac{M}{2}\bar{Z}^\dagger\right) \\ i\left(\vec{\Delta}_1^Z - \frac{M}{2}\bar{Z}\right) & 0 & 2\left(\bar{\Delta}_1^x - \frac{M}{2}\bar{Z}^x\right) + \hat{W}_- & i\bar{\Delta}_0^A - \hat{A}^T \\ 0 & i\left(\vec{\Delta}_1^{Z^\dagger} - \frac{M}{2}\bar{Z}^\dagger\right) & i\bar{\Delta}_0^A + \hat{A} & 2\left(\bar{\Delta}_1^{x*} - \frac{M}{2}\bar{Z}^{x*}\right) - \hat{W}_-^\dagger \end{pmatrix}. \quad (\text{E.1})$$

First of all we should mention that a straightforward discretisation of the operator \mathcal{O}_F would have been of dimension $[a]^{-1}$ which has been absorbed into the fermionic fields to make them dimensionless. Therefore $\hat{\mathcal{O}}_F$ is dimensionless as well, as are now all the bosonic and fermionic fields. Further $\hat{\mathcal{O}}_F$ needs to be anti-symmetric which is why all the discretised derivatives need to be symmetric finite differences. As it is standard in lattice QCD to use anti-periodic boundary conditions in the temporal direction for the fermions [31], we will apply those here as well. For the spatial direction periodic boundary conditions shall be used. So starting from block (1, 2) we make the transition

$$i\partial_t \mathbb{1}_4 \longrightarrow i\bar{\Delta}_0^A, \quad (\text{E.2})$$

where we defined

$$\bar{\Delta}_0^A \equiv \bar{\Delta}_0^a \otimes \mathbb{1}_4, \quad \bar{\Delta}_0^a \equiv \left(\bar{\Delta}_0^a\right)(l, p) = \frac{1}{2} \left(\delta_{l_{+1}, p}^a - \delta_{l_{-1}, p}^a\right). \quad (\text{E.3})$$

Thereby the superscripts A , a refer to the property of the finite differences to respect anti-periodic boundary conditions, whereas p will refer to periodic ones. In the next block (1, 3) we have

$$-i\rho^M \left(\partial_s + \frac{m}{2}\right) \frac{z^M}{z^3} \longrightarrow -i\left(\vec{\Delta}_1^Z + \frac{M}{2}\bar{Z}\right). \quad (\text{E.4})$$

Since z^M/z^3 is on the right, the derivative will also act on this term which we will have to consider in the discretisation. Thus we introduce the definitions

$$Z \equiv Z_{ij}(l) = \rho_{ij}^M \frac{z^M(l)}{z^3(l)}, \quad \bar{Z} \equiv \bar{Z}_{ij}(l, p) = \delta_{l, p} Z_{ij}(l), \quad (\text{E.5})$$

$$\vec{\Delta}_1^Z \equiv \left(\vec{\Delta}_1^Z\right)_{ij}(l, p) = \frac{1}{2} \left[\delta_{l_{+1}, p}^p Z_{ij}(l_{+1}) - \delta_{l_{-1}, p}^p Z_{ij}(l_{-1})\right]. \quad (\text{E.6})$$

The right arrow shall indicate that Z is on the right and respected by the derivative. In block (3, 1) we also have the same operator with arrow to the left which indicates that the derivative will not act on Z

$$\bar{\Delta}_1^Z \equiv (\bar{\Delta}_1^Z)_{ij}(l, p) = \frac{1}{2} [\delta_{l_{+\hat{1}}, p}^p - \delta_{l_{-\hat{1}}, p}^p] Z_{ij}(l). \quad (\text{E.7})$$

In block (3, 3) we observe

$$2 \frac{z^M}{z^4} \rho^M \left(\partial_s x - \frac{m}{2} x \right) \longrightarrow 2 \left(\bar{\Delta}_1^x - \frac{M}{2} \bar{Z}^x \right), \quad (\text{E.8})$$

where

$$\bar{Z}^x \equiv \bar{Z}_{ij}^x(l, p) = \delta_{l, p} \frac{Z_{ij}(l)}{z(l)} x(l), \quad (\text{E.9})$$

$$\bar{\Delta}_1^x \equiv (\bar{\Delta}_1^x)_{ij}(l, p) = \frac{1}{2} \frac{Z_{ij}(l)}{z(l)} [\delta_{l_{+\hat{1}}, p}^p x(l_{+\hat{1}}) - \delta_{l_{-\hat{1}}, p}^p x(l_{-\hat{1}})]. \quad (\text{E.10})$$

The discretised version of A is given by

$$\begin{aligned} \hat{A}_{ij}(l, p) = & -\delta_{ij} \delta_{lp} \frac{\sqrt{6}}{z(l)} \phi(l) + \delta_{lp} \frac{\tilde{\phi}_{ij}(l)}{z(l)} \\ & + i \frac{z^N(l)}{z(l)} (\rho^{MN})_{ij} (\delta_{l_{+\hat{1}}, p}^p z^M(l_{+\hat{1}}) - \delta_{l_{-\hat{1}}, p}^p z^M(l_{-\hat{1}})) \\ & + \frac{1}{z^3(l)} (\rho_N^*)_{ik} \tilde{\phi}_{sk}(l) (\rho^L)_{sj} z^N(l) z^L(l) \delta_{lp}. \end{aligned} \quad (\text{E.11})$$

For the other variations of the finite differences one simply substitutes Z^\dagger or x^* in the associated expressions to derive $\vec{\Delta}_1^{Z^\dagger}$ and $\bar{\Delta}_1^{x^*}$. Since $\hat{\mathcal{O}}_F$ is anti-symmetric we need to meet the condition that $\vec{\Delta}_1^Z = -(\vec{\Delta}_1^Z)^T$ which is easy to check. The same property is needed for the corresponding WILSON term. One can define it to consist of two parts $\hat{W}_\pm^{(1)}$ and $\hat{W}_\pm^{(2)}$ which obey $\hat{W}_\pm^{(1)} = -(\hat{W}_\pm^{(2)})^T$ and vice versa. The resulting WILSON term

$$\hat{W}_\pm = \frac{1}{2} (\hat{W}_\pm^{(1)} + \hat{W}_\pm^{(2)}) \quad (\text{E.12})$$

is therefore skew-symmetric $(\hat{W}_\pm)^T = -\hat{W}_\pm$ which is necessary since it is sitting on the diagonal blocks of $\hat{\mathcal{O}}_F$. The single terms are constructed in the following way

$$\hat{W}_\pm^{(1)} = \frac{r}{2} [\vec{\Lambda}_0^Z \pm i \vec{\Lambda}_1^Z], \quad \hat{W}_\pm^{(2)} = \frac{r}{2} [\tilde{\Lambda}_0^Z \pm i \tilde{\Lambda}_1^Z] \quad (\text{E.13})$$

with

$$\begin{aligned} Z^z &\equiv Z_{ij}^z(l) = Z_{ij}(l) z(l) \\ \vec{\Lambda}_\alpha^Z &\equiv (\vec{\Lambda}_\alpha^Z)_{ij}(l, p) = 2\delta_{l, p} Z^z(l) - \delta_{l_{+\hat{\alpha}}, p} Z^z(l_{+\hat{\alpha}}) - \delta_{l_{-\hat{\alpha}}, p} Z^z(l_{-\hat{\alpha}}) \\ \tilde{\Lambda}_\alpha^Z &\equiv (\tilde{\Lambda}_\alpha^Z)_{ij}(l, p) = (2\delta_{l, p} - \delta_{l_{+\hat{\alpha}}, p} - \delta_{l_{-\hat{\alpha}}, p}) Z^z(l), \end{aligned} \quad (\text{E.14})$$

where again the temporal finite differences need to respect anti-periodic and the spacial ones periodic boundary conditions. The actual implementation nonetheless is slightly different. There we constructed \hat{W}_\pm to have its upper triangular matrix equal to $\hat{W}_\pm^{(1)}$ and the lower triangular matrix equal to $\hat{W}_\pm^{(2)}$ which in the end is leading to the same result.

F Simulation parameters

g	$T \times L$	LM	r	$\tau_{\text{int}}^S(Q)$		$\tau_{\text{int}}^{m_x}(Q)$		R	MDU
10	16×8	4	1	0.6	(0.6)	1.5	(0.5)	4	2826
	20×10	4	1	0.7	(0.5)	1.8	(0.7)	3	2652
	24×12	4	1	0.7	(0.6)	2.2	(1.0)	4	2666
	32×16	4	1	0.7	(0.4)	3.9	(0.6)	4	3802
	48×24	4	1	0.7	(0.3)	10.0	(0.2)	3	2702
	64×32	4	1	0.6	(0.7)	11.9	(0.9)	4	1073
15	16×8	4	1	2.1	(0.6)	1.4	(0.8)	5	4553
	20×10	4	1	2.0	(0.5)	1.5	(0.4)	5	4553
	24×12	4	1	2.1	(0.1)	1.5	(0.0)	5	4553
	32×16	4	1	2.5	(0.7)	2.5	(0.5)	5	4553
	48×24	4	1	2.0	(-)	3.7	(-)	1	925
20	16×8	4	1	35.8	(0.4)	1.4	(0.4)	21	19961
	20×10	4	1	41.6	(0.4)	1.4	(0.6)	21	19961
	24×12	4	1	31.2	(0.1)	1.4	(0.1)	21	19961
	32×16	4	1	42.2	(0.3)	2.0	(0.6)	21	19961
	48×24	4	1	23.3	(0.6)	4.0	(0.8)	4	3602
	64×32	4	1	55.7	(0.3)	6.0	(1.0)	4	1338
25	16×8	4	1	2.3	(0.6)	1.5	(0.8)	19	18060
	20×10	4	1	2.5	(0.2)	1.3	(0.0)	20	19010
	24×12	4	1	2.5	(0.1)	1.3	(0.3)	20	19010
	32×16	4	1	2.6	(0.6)	1.6	(0.2)	20	19010
	48×24	4	1	2.4	(0.3)	2.8	(0.5)	5	4553
	64×32	4	1	2.6	(0.8)	3.9	(0.3)	2	643
30	16×8	4	1	1.0	(0.2)	2.2	(0.0)	17	16159
	20×10	4	1	1.0	(0.2)	1.4	(0.9)	20	18810
	24×12	4	1	1.0	(1.0)	1.4	(0.8)	20	18810
	32×16	4	1	1.1	(0.7)	1.5	(0.4)	20	18810
	48×24	4	1	1.0	(0.7)	2.6	(0.4)	20	18010
	64×32	4	1	1.1	(0.1)	5.3	(0.0)	5	2135
40	16×8	4	1	0.5	(1.0)	3.3	(0.0)	18	17109
	20×10	4	1	0.7	(0.6)	1.7	(0.5)	20	19010
	24×12	4	1	0.6	(1.0)	1.4	(0.4)	20	19010

Appendix F. Simulation parameters

	32×16	4	1	0.6	(0.1)	1.4	(0.1)	20	19010
	48×24	4	1	0.7	(0.8)	1.4	(0.0)	5	5449
50	16×8	4	1	0.7	(0.5)	1.4	(0.5)	20	19010
	20×10	4	1	0.7	(0.9)	6.3	(0.3)	20	19010
	24×12	4	1	0.8	(1.0)	1.4	(0.3)	20	19010
	32×16	4	1	0.8	(0.5)	1.4	(0.7)	20	18852
	48×24	4	1	0.8	(0.0)	1.9	(0.9)	5	4451
100	16×8	4	1	1.1	(0.4)	1.7	(0.0)	2	1701
	20×10	4	1	1.0	(0.9)	1.5	(0.3)	2	1701
	24×12	4	1	1.2	(0.7)	1.5	(0.3)	2	1701
	32×16	4	1	1.1	(0.6)	1.9	(0.5)	2	1701
	48×24	4	1	1.1	(-)	2.0	(-)	1	751
5	16×8	4	1	0.5	(-)	1.9	(-)	1	3591
	24×12	4	1	0.4	(0.1)	4.2	(0.2)	4	3752
	32×16	4	1	0.6	(0.0)	5.0	(0.2)	5	4703
30	16×8	4	1	1.0	(0.9)	2.2	(0.1)	4	9802
	24×12	4	1	1.0	(0.6)	1.3	(0.0)	4	9802
	32×16	4	1	1.0	(0.7)	1.4	(0.8)	2	4901
40	16×8	4	1	0.6	(0.1)	2.5	(0.2)	4	9802
	24×12	4	1	0.6	(0.9)	1.4	(0.7)	4	9802
	32×16	4	1	0.7	(0.5)	1.6	(0.0)	2	4901
50	16×8	4	1	0.8	(0.7)	1.4	(0.4)	4	9802
	24×12	4	1	0.7	(0.0)	1.5	(0.5)	4	9802
	32×16	4	1	0.8	(0.9)	1.6	(0.6)	2	4901
60	16×8	4	1	1.1	(0.9)	1.3	(0.9)	2	19901
	24×12	4	1	1.1	(-)	2.3	(-)	1	9951
	32×16	4	1	0.9	(0.2)	1.5	(0.4)	2	2171
	48×24	4	1	0.9	(-)	1.9	(-)	1	751
70	16×8	4	1	3.0	(0.0)	1.4	(1.0)	2	19901
	24×12	4	1	3.5	(0.9)	12.3	(0.8)	2	19901
	32×16	4	1	3.1	(0.1)	1.6	(0.2)	2	5049
	48×24	4	1	3.5	(-)	1.7	(-)	1	751
100	20×10	6	1	1.2	(0.4)	8.3	(0.7)	3	2652
	24×12	6	1	1.0	(0.3)	1.7	(0.6)	5	4553
	32×16	6	1	1.2	(0.9)	7.9	(0.3)	4	3802
	48×24	6	1	1.4	(0.9)	1.5	(0.8)	5	1541
70	32×16	6	1	3.0	(0.6)	1.6	(0.3)	4	3802
	40×20	6	1	4.4	(0.5)	1.4	(0.8)	4	4002
	48×24	6	1	3.0	(0.3)	1.6	(0.2)	5	1431
50	24×12	6	1	0.6	(0.6)	2.2	(0.4)	5	4553
	32×16	6	1	0.7	(0.9)	1.7	(0.6)	5	4553
	40×20	6	1	0.7	(0.3)	1.5	(0.6)	4	4002

	48×24	6	1	0.6	(0.0)	1.5	(0.7)	5	1333
<hr/>									
30	20×10	6	1	1.0	(0.3)	1.7	(0.7)	5	4553
	24×12	6	1	1.0	(0.2)	1.4	(0.1)	5	4553
	32×16	6	1	1.1	(0.1)	1.4	(0.9)	5	4553
	40×20	6	1	1.0	(0.8)	1.4	(0.7)	4	4002
	48×24	6	1	1.0	(0.9)	1.5	(0.4)	5	1216
<hr/>									
25	20×10	6	0	2.5	(0.4)	1.6	(0.1)	5	4553
	24×12	6	0	2.5	(0.8)	1.3	(0.1)	5	4553
	32×16	6	0	2.6	(0.4)	1.4	(0.3)	5	4553
	40×20	6	0	2.5	(0.7)	1.4	(0.3)	4	4002
<hr/>									
20	20×10	6	1	30.8	(0.3)	1.4	(1.0)	5	4553
	24×12	6	1	41.5	(0.2)	1.3	(0.2)	5	4553
	32×16	6	1	47.9	(0.3)	1.4	(0.8)	5	4553
	40×20	6	1	91.1	(1.0)	1.6	(0.2)	4	4002
<hr/>									
15	20×10	6	1	2.2	(0.1)	1.4	(0.6)	5	4553
	24×12	6	1	2.3	(0.3)	1.5	(0.9)	5	4553
	32×16	6	1	2.0	(0.9)	1.6	(0.3)	5	4553
<hr/>									
10	20×10	6	1	0.6	(0.4)	1.4	(0.7)	5	4553
	24×12	6	1	0.6	(0.1)	1.4	(0.0)	5	4553
	32×16	6	1	0.7	(0.3)	1.8	(0.0)	5	4553
<hr/>									
25	16×8	4	0	2.2	(0.8)	1.4	(0.6)	5	4553
	20×10	4	0	2.0	(0.9)	1.4	(0.3)	5	4553
	24×12	4	0	2.2	(0.0)	1.6	(0.5)	5	4553
	32×16	4	0	1.9	(0.1)	2.1	(0.6)	5	4553
<hr/>									
30	16×8	4	0	0.9	(0.4)	1.9	(0.3)	5	4553
	20×10	4	0	0.8	(0.0)	1.4	(0.5)	5	4553
	24×12	4	0	0.9	(0.7)	1.5	(0.3)	5	4553
	32×16	4	0	1.1	(0.9)	2.0	(0.5)	5	4553
<hr/>									
50	16×8	4	0	0.6	(0.0)	1.3	(0.3)	5	4553
	20×10	4	0	0.7	(0.2)	2.2	(0.2)	5	4553
	24×12	4	0	0.7	(0.4)	1.5	(0.6)	5	4553
	32×16	4	0	0.7	(0.0)	1.4	(0.7)	5	4553
<hr/>									
70	16×8	4	0	2.7	(0.6)	1.4	(0.5)	5	4553
	20×10	4	0	2.7	(0.4)	1.4	(0.2)	5	4553
	24×12	4	0	3.3	(0.7)	4.5	(0.1)	8	6404
	32×16	4	0	3.4	(0.3)	1.5	(0.1)	5	4553
<hr/>									
80	16×8	4	0	24.9	(0.2)	1.4	(0.0)	5	4553
	20×10	4	0	32.4	(0.2)	1.3	(0.5)	5	4553
	24×12	4	0	35.8	(0.6)	1.9	(0.0)	8	6404
	32×16	4	0	13.9	(0.1)	1.6	(0.3)	5	4553
<hr/>									
100	16×8	4	0	1.0	(0.3)	1.6	(0.8)	5	4553
	20×10	4	0	1.1	(0.5)	1.4	(0.6)	5	4553

24×12	4	0	1.0	(0.6)	1.6	(0.0)	5	4553
32×16	4	0	1.2	(0.2)	2.3	(0.2)	5	4553

Table F.1 Parameters of the simulation: the coupling g , the temporal (T) and spacial (L) extent of the lattice, the line of constant physics fixed by LM and the presence of a WILSON term, toggled by r to be included during the simulation (1) or not (0). The size of the statistics after thermalisation is given in the last column in terms of molecular dynamic units (MDU) which equals an HMC trajectory of length one. The number of replica collected for each set of parameters is stated in the column named R. The auto-correlation times τ of our main observables m_x and S are also given in MDU together with the Q-value of the replica in parenthesis.

Bibliography

- [1] Virgo, LIGO Scientific Collaboration, B. P. Abbott et al., “*Observation of Gravitational Waves from a Binary Black Hole Merger*”, Phys. Rev. Lett. 116, 061102 (2016), [arXiv:1602.03837](#).
- [2] Virgo, LIGO Scientific Collaboration, B. P. Abbott et al., “*GW151226: Observation of Gravitational Waves from a 22-Solar-Mass Binary Black Hole Coalescence*”, Phys. Rev. Lett. 116, 241103 (2016), [arXiv:1606.04855](#).
- [3] CMS Collaboration, S. Chatrchyan et al., “*Observation of a new boson at a mass of 125 GeV with the CMS experiment at the LHC*”, Phys. Lett. B716, 30 (2012), [arXiv:1207.7235](#).
- [4] ATLAS Collaboration, G. Aad et al., “*Observation of a new particle in the search for the Standard Model Higgs boson with the ATLAS detector at the LHC*”, Phys. Lett. B716, 1 (2012), [arXiv:1207.7214](#).
- [5] G. Veneziano, “*Construction of a crossing - symmetric, Regge behaved amplitude for linearly rising trajectories*”, Nuovo Cim. A57, 190 (1968).
- [6] J. M. Maldacena, “*The Large N limit of superconformal field theories and supergravity*”, Int. J. Theor. Phys. 38, 1113 (1999), [hep-th/9711200](#), [Adv. Theor. Math. Phys.2,231(1998)].
- [7] S. Catterall, D. B. Kaplan and M. Unsal, “*Exact lattice supersymmetry*”, Phys. Rept. 484, 71 (2009), [arXiv:0903.4881](#).
- [8] G. Bergner and S. Catterall, “*Supersymmetry on the lattice*”, [arXiv:1603.04478](#).
- [9] R. McKeown and R. Roiban, “*The quantum $AdS_5 \times S^5$ superstring at finite coupling*”, [arXiv:1308.4875](#).
- [10] L. Bianchi, M. S. Bianchi, V. Forini, B. Leder and E. Vescovi, “*Green-Schwarz superstring on the lattice*”, JHEP 1607, 014 (2016), [arXiv:1605.01726](#).
- [11] V. Forini, L. Bianchi, M. S. Bianchi, B. Leder and E. Vescovi, “*Lattice and string worldsheet in AdS/CFT : a numerical study*”, PoS LATTICE2015, 244 (2016), [arXiv:1601.04670](#), in: “*Proceedings, 33rd International Symposium on Lattice Field Theory (Lattice 2015): Kobe, Japan, July 14-18, 2015*”, 244p.
- [12] J. M. Maldacena, “*Wilson loops in large N field theories*”, Phys. Rev. Lett. 80, 4859 (1998), [hep-th/9803002](#).
- [13] S. Giombi, R. Ricci, R. Roiban, A. A. Tseytlin and C. Vergu, “*Quantum $AdS(5) \times S^5$ superstring in the AdS light-cone gauge*”, JHEP 1003, 003 (2010), [arXiv:0912.5105](#).
- [14] Z. Bern, M. Czakon, L. J. Dixon, D. A. Kosower and V. A. Smirnov, “*The Four-Loop Planar Amplitude and Cusp Anomalous Dimension in Maximally*

- Supersymmetric Yang-Mills Theory*", Phys. Rev. D75, 085010 (2007), hep-th/0610248.
- [15] S. S. Gubser, I. R. Klebanov and A. M. Polyakov, "A Semiclassical limit of the gauge / string correspondence", Nucl. Phys. B636, 99 (2002), hep-th/0204051.
- [16] S. Frolov and A. A. Tseytlin, "Semiclassical quantization of rotating superstring in $AdS(5) \times S^{*5}$ ", JHEP 0206, 007 (2002), hep-th/0204226.
- [17] N. Beisert, B. Eden and M. Staudacher, "Transcendentality and Crossing", J. Stat. Mech. 0701, P01021 (2007), hep-th/0610251.
- [18] R. R. Metsaev, C. B. Thorn and A. A. Tseytlin, "Light cone superstring in AdS space-time", Nucl. Phys. B596, 151 (2001), hep-th/0009171.
- [19] R. R. Metsaev and A. A. Tseytlin, "Superstring action in $AdS(5) \times S^{*5}$. Kappa symmetry light cone gauge", Phys. Rev. D63, 046002 (2001), hep-th/0007036.
- [20] J. Polchinski, "String theory. Vol. 1: An introduction to the bosonic string", Cambridge University Press (2007).
- [21] J. Polchinski, "String theory. Vol. 2: Superstring theory and beyond", Cambridge University Press (2007).
- [22] M. Ammon and J. Erdmenger, "Gauge/gravity duality", Cambridge Univ. Pr. (2015), Cambridge, UK.
- [23] K. Becker, M. Becker and J. H. Schwarz, "String theory and M-theory: A modern introduction", Cambridge University Press (2006).
- [24] R. R. Metsaev and A. A. Tseytlin, "Type IIB superstring action in $AdS(5) \times S^{*5}$ background", Nucl. Phys. B533, 109 (1998), hep-th/9805028.
- [25] L. Brink, J. H. Schwarz and J. Scherk, "Supersymmetric Yang-Mills theories", Nuclear Physics B 121, 77 (1977).
- [26] M. Kruczenski, "A Note on twist two operators in $N=4$ SYM and Wilson loops in Minkowski signature", JHEP 0212, 024 (2002), hep-th/0210115.
- [27] G. P. Korchemsky and G. Marchesini, "Structure function for large x and renormalization of Wilson loop", Nucl. Phys. B406, 225 (1993), hep-ph/9210281.
- [28] M. Kruczenski, R. Roiban, A. Tirziu and A. A. Tseytlin, "Strong-coupling expansion of cusp anomaly and gluon amplitudes from quantum open strings in $AdS(5) \times S^{*5}$ ", Nucl. Phys. B791, 93 (2008), arXiv:0707.4254.
- [29] N. Beisert et al., "Review of AdS/CFT Integrability: An Overview", Lett. Math. Phys. 99, 3 (2012), arXiv:1012.3982.
- [30] C. Gattringer and C. Lang, "Quantum Chromodynamics on the Lattice: An Introductory Presentation", Springer Berlin Heidelberg (2009).
- [31] I. Montvay and G. Münster, "Quantum fields on a lattice", Cambridge University Press (1994).
- [32] M. E. Peskin and D. V. Schroeder, "An introduction to quantum field theory", Addison-Wesley Pub. Co (1995).
- [33] M. H. Kalos and P. A. Whitlock, "Monte Carlo Methods", 2 edition, Wiley-VCH (2008).
- [34] H. J. Rothe, "Lattice Gauge Theories: An Introduction", 3 edition, World Scientific Publishing Company (2005).

-
- [35] S. Duane, A. Kennedy, B. J. Pendleton and D. Roweth, “*Hybrid Monte Carlo*”, Physics Letters B 195, 216 (1987).
 - [36] S. Giombi, R. Ricci, R. Roiban and A. A. Tseytlin, “*Quantum dispersion relations for excitations of long folded spinning superstring in $AdS_5 \times S^5$* ”, JHEP 1101, 128 (2011), [arXiv:1011.2755](#).
 - [37] ALPHA Collaboration, U. Wolff, “*Monte Carlo errors with less errors*”, Comput. Phys. Commun. 156, 143 (2004), [hep-lat/0306017](#), [Erratum: Comput. Phys. Commun. 176, 383 (2007)].
 - [38] A. M. Ferrenberg and R. H. Swendsen, “*New Monte Carlo Technique for Studying Phase Transitions*”, Phys. Rev. Lett. 61, 2635 (1988).
 - [39] M. Luscher and F. Palombi, “*Fluctuations and reweighting of the quark determinant on large lattices*”, PoS LATTICE2008, 049 (2008), [arXiv:0810.0946](#), in: “*Proceedings, 26th International Symposium on Lattice field theory (Lattice 2008): Williamsburg, USA, July 14-19, 2008*”, 049p.
 - [40] J. Finkenrath, F. Knechtli and B. Leder, “*One flavor mass reweighting in lattice QCD*”, Nucl. Phys. B 877, 441 (2013), [arXiv:1306.3962](#), [Erratum: Nucl. Phys. B 880, 574 (2014)].
 - [41] P. Cartier, C. DeWitt-Morette, M. Ihl and C. Saemann, “*Supermanifolds: Application to supersymmetry*”, [math-ph/0202026](#).
 - [42] F. A. Berezin and A. A. Kirillov (eds.), “*Introduction to Superanalysis*”, 1 edition, Springer Netherlands (1987).
 - [43] E. Witten, “*Anti-de Sitter space and holography*”, Adv. Theor. Math. Phys. 2, 253 (1998), [hep-th/9802150](#).
 - [44] C. A. Bayona and N. R. F. Braga, “*Anti-de Sitter boundary in Poincare coordinates*”, Gen. Rel. Grav. 39, 1367 (2007), [hep-th/0512182](#).

Acknowledgement

First of all I would like to thank my supervisor Dr. Valentina Forini for entrusting me with this topic, for the opportunity to actively participate in her research project and the constructive remarks on my thesis. I am also very grateful for the guidance of Dr. Björn Leder, his patience and willingness to answer all my questions. Furthermore I would like to thank Dr. Edoardo Vescovi, Philipp Krah and Josua Faller for a lot of fruitful discussions and constructive remarks concerning the finalisation of my thesis and the whole Quantum Field and String Theory Group for providing a pleasant and creative atmosphere.

Last but not least I would also like to thank my family and friends for their constant support throughout the last years of study and especially the recent time of finishing this thesis.

Hilfsmittel

Diese Arbeit wurde in \LaTeX unter Verwendung von TexLive-2015 gesetzt. In der Erstellung der Bibliographie wurde BiBTeX mit der von Niklas Beisert verwalteten Stil-Datei „nb.st“ verwendet. Grafiken wurden mit Hilfe der Open-Source Programme Blender und Inkscape und numerische Plots mit Hilfe von MATLAB erstellt. Die Implementierung der für die numerischen Berechnungen verwendeten Programme erfolgte im FORTRAN 95 Standard und wurde mittels eines Intel[®] Fortran Compilers ausführbar gemacht. Für die Erzeugung von Pseudozufallszahlen und das Lösen von Gleichungssystemen wurden die Routinen `ranlux`, `cgne` und `mscg` aus dem Paket `openQCD` adaptiert. Numerische Fehleranalyse erfolgte unter Zuhilfenahme der MATLAB Routine `UWerr` aus [37].

Selbstständigkeitserklärung

Ich erkläre, dass ich die vorliegende Arbeit selbstständig und nur unter Verwendung der angegebenen Quellen und Hilfsmittel angefertigt habe.

Seitens des Verfassers bestehen keine Einwände, die vorliegende Masterarbeit für die öffentliche Benutzung im Universitätsarchiv zur Verfügung zu stellen.

Berlin, den 20. Dezember 2016

Philipp Töpfer